Highly multiplexed in situ protein imaging using DNA-Exchange-Imaging and Immuno-SABER

A Dissertation presented

By

Yu Wang

To

Graduate School Of Arts And Sciences

In Partial Fulfillment of The Requirements

For The Degree of

Doctor of Philosophy

In The Subject of

Biological and Biomedical Science

Harvard University

Cambridge, Massachusetts

March 2019

Thesis advisor: Professor George M. Church and Professor Peng Yin Yu Wang

Highly multiplexed in situ protein imaging using DNA-Exchange-Imaging and Immuno-SABER

Abstract

Mapping the molecular composition of individual cells in their native environment is critical for understanding the cellular and subcellular organization of healthy and diseased tissues. Immunofluorescence (IF) imaging using labeling probes such as antibodies provides an important tool to uncover the spatial distribution of proteins in biological samples. Traditional IF imaging methods suffer from one or more following problems: low multiplexing capability, poor detection sensitivity and limited optical resolution. In this dissertation, I presented my work, in collaboration with others, to develop highly multiplexed *in situ* protein imaging methods that have superior detection sensitivity and are able to perform high/super-resolution imaging. I first developed DNA-antibody conjugation and purification methods to obtain high quality labeling probes. I then developed DNA-Exchange-Imaging, a technique based on Exchange-PAINT, to apply the DNA-Exchange concept to various imaging platforms for highly multiplexed diffraction-limited confocal imaging and super-resolution structure-illumination, STED and PAINT imaging. This technique was further developed to integrate signal amplification capability, by combining with Hybridization Chain Reaction (HCR) and Signal Amplification By Exchange Reaction (SABER), to enable highly multiplexed and high-sensitivity protein detection in tissue samples. Finally, I presented a method that enables highly multiplexed, high-sensitivity and super-resolution imaging *in situ* by conjoining Immuno-SABER and Expansion Microscopy (ExM). I concluded the dissertation with a summary of the evolution of described techniques and a discussion of current challenges in highly multiplexed *in situ* protein detection using DNA-barcoded antibodies.

Table of Contents

Chapter I Introduction 1
1.1. Antibodies 2
1.2. In situ protein detection using immunofluorescence imaging 3
1.3. Challenges for traditional immunofluorescence imaging 4
1.3.1. Multiplexing capability 4
1.3.2. Detection sensitivity and signal amplification strategies 6
1.3.3. Optical resolution and super-resolution imaging 8
1.4. Scope of the thesis 11
Chapter II Development of methods for DNA-antibody conjugation and purification 14
2.1. Abstract 15
2.2. DNA-antibody conjugation chemistry development and validation 15
2.2.1. Conjugation chemistry selection and validation 16
2.2.2. DNA-PAINT imaging with DNA-conjugated secondary antibodies 18
2.2.3. DNA-PAINT imaging with DNA-conjugated primary antibodies 20
2.2.4. DNA-PAINT imaging with DNA-conjugated nanobodies 21
2.2.5. Highly multiplexed Exchange-PAINT imaging using a pool of orthogonally labeled antibodies 23
2.3. DNA-conjugated antibody purification using toehold-displament-mediated DNA affinity pulldown 28
2.4. Methods 30
Chapter III Highly multiplexed *in situ* protein imaging using DNA-Exchange-Imaging 39
3.1. Abstract 40
3.2. Concept of DNA-Exchange-Imaging 41
3.3. DNA-Exchange-Confocal-Imaging in cell culture and tissue samples 42
3.4. DNA-Exchange-SIM- and -STED- Imaging in cell culture samples 51
3.5. DNA-Exchange-PAINT imaging to visualize synaptic structures 53
3.6. Comparison between transient, semi-transient and stable binding of imager/docking DNA duplex 56
3.7. Methods 58

Chapter IV Highly multiplexed *in situ* protein imaging with signal amplification using Immuno-HCR and Immuno-SABER 70
4.1. Abstract 71
4.2. Multiplexed imaging using same species antibodies with signal amplification using immuno-HCR 72
4.2.1. Reduction of non-specific binding of DNA-conjugated antibodies 72
4.2.2. Signal amplification using immuno-HCR 76
4.2.3. Multiplexed imaging with signal amplification using immuno-HCR 76
4.3. Highly multiplexed *in situ* protein detection using immuno-SABER 78
4.3.1. Concept of immuno-SABER 78
4.3.2. Validation and quantification of signal amplification using Immuno-SABER 80
4.3.3. Enhancement of signals through branched-SABER 83
4.3.4. Validating sequences for multiplexing Immuno-SABER 85
4.3.5. Highly multiplexed Immuno-SABER imaging in mouse retina cryosections 87
4.4. Rapid, highly multiplexed super-resolution imaging combining immuno-SABER and Expansion Microscopy 91
4.5. Methods 95
Chapter V Discussion and Conclusion 120

Appendix A Invited Review: From Designing the Molecules of Life to Designing Life: Future Applications Derived from Advances in DNA Technologies 128
Appendix B Open science :Proposal for a "Next-Generation" Scientific Publication System 136
Appendix C List of Publication 148
Reference 151

I dedicate this thesis to my parents and sister, for their love, encouragement and support.

Acknowledgments

My dream has always been working on something that has a significant benefit to the world. I decided to study environmental science when I picked a major in college, with the hope to stop global warming and to save polar bears that were losing their home. At the end of my first year, I started to work in the lab of Professor Liuyan Yang in Nanjing University as a summer student. I am deeply grateful to Professor Yang who brought me into the world of science. I later switched to life science and went to University of Southampton as an exchange student where I learnt how to think and behave like a scientist. I would like to take the oppotunitiy to thank my two mentors in Southampton, Dr. Neil Smith and Dr. Stephen Thirdborough, for their kindness to let a naïve student work in their lab and for training me how to perform basic experiments. At the end of my college, I tried to apply for graduate schools in the US. I received 20 out of 20 rejection letters at the first attempt. I am deeply grateful to Dr. Xiaodong Wang in National Institute of Biological Science for giving me the opportunity to work in his lab as a research assistant in my darkest time, and for supporting me to apply for graduate schools again. I would like to thank my labmates in Dr. Wang's lab (Dr. Jia Guo, Dr. Chenjie Pan, Dr. Xian Jiang, Zeda Zhang) to create an enjoyable environment in NIBS, and particularly thank Dr. Zhirong Shen for supervising me.

I never expected myself to switch from a biologist to a biotechnologist. I would like to express my greatest gratitude to my two PhD advisors: Professor George Church and Professor Peng Yin, who showed me the beauty and power of technology development. Both George and Peng were extremely supportive and gave me the opportunity to freely explore my scientific interest. George is visionary, and always tells me to dream big but also be realistic when it comes to action. George also taught me how important transparency and openness are for science, which shaped my dream for open science. Peng has impressed me with his sharp view and dedication in science and technology, and from him I learnt how to persist in ideas and turn 'impossible' to 'possible'. I would also like to thank Wyss institute and all its staff for introducing me beyond the academia to the industry, where I learnt how business drives the

translation of science in the lab to the daily life of the public. I feel extremely fortunate to have joined George's and Peng's labs.

I am also deeply grateful to the members of my dissertation advisor committee, Professor Connie Cepko, Professor Bernardo Sabatini and Professor Wayne Marasco for taking the time and effort to listen to my project and give valuable feedbacks through the years. I would also like to thank Professor Jeffrey Moffit, Professor Kwanghun Chung and Professor William Shih for serving on my examination committee. I would also like to thank Professor Pascal Kaeser for his guidance in neuroscience during my graduate school.

I would like to thank my colleagues and collaborators, whom I have had immense fortunate to work with. I would like to thank Jonathan Scheiman and Sarit Agasti for being my supervisors in the lab. I am grateful to work with Sinem Saka who is a fantastic collaborator. I would also like to thank Alex Chavez, Su Vora, Mingjie Dai, Evan Daugharthy, Noah Donoghue, Chris Guzman, Eswar Iyer, Kunal Jindal, Fred Vigneault, Yongcheng Wang, Songlei Liu, Tom Schaus, Cherry Fan, Nikhil Gopalkrishnan, Youngeun Kim, Josie Kishi, Di Liu, Ninning Liu, Sinem Saka, Hiroshi Sasaki, Jie Shen, Jesse Silverberg, Sungwook Woo, Feng Xuan, Mike Jin, Weidong Xu, Allen Zhu, Brian Beliveau, Dongran han, Jongmin Kim, Nicolas Garreau de Loubresse, Wei Sun, Rizal Hariadi, Xi Chen, Mael Manesse, Ralf Jungmann, Cameron Myhrvold, Luvena Ong, Maier Avendano for their support in the lab. I am also grateful to Dr. Sylvain Lapan, Shan Shan Wang, Ron Schackmann for being great collaborators. I would also like to thank my intern students, Wenxin Xie, Millicent Lin, Yitian Zeng and Siyuan Yin for their support in research. I would also like to thank the BBS program in Harvard Medical School for providing a great community for science-loving students. I have made so many friends in my classmates, especially Sida Liao, Huiyuan Zhang, Xiaoyi Wang, Yuancheng Lv and Xiaoji Wu.

I would also like to show my great gratitude to my friends, particularly Ye Chen and Justin Granchelli, and they have made my life in Boston a great pleasure. Lastly, I would like to give my special thanks to my families. They create a place called 'home' where I can always go back and find the peace in my heart.

List of Abbreviations

DEI	DNA exchange imaging
ExM	Expansion Microscopy
FWHM	Full width at half maximum
HCR	Hybridization chain reaction
IF	Immunofluorescence
MALDI-MS	Matrix-assisted laser desorption/ionization-mass spectrometry
NA	Numerical aperture
NHS	N-hydroxysuccinimide
PAINT	Point accumulation for imaging in nanoscale topography
PER	Primer exchange reaction
PFA	Paraformaldehyde
PSF	Point spread function
SABER	Signal amplification by exchange reaction
SIM	Structured illumination microscopy
$SM(PEG)_2$	PEGylated succinimidyl 4-(N-maleimidomethyl) cyclohexane-1-carboxylate
STED	Stimulated emission depletion (microscopy)

Chapter I

Introduction

1.1. Antibodies

Antibodies are proteins naturally produced by B cells to initiate an immune response against target antigens such as DNA, proteins and carbohydrates[1]. They are able to bind targets selectively with an affinity as low as in the sub-nanomolar range (measured as equilibrium dissociation constant)[2]. The most characterized type of antibodies is IgG, which resembles the shape of a letter Y and is formed by two light chains and two heavy chains (**Figure 1**). It contains two domains, a variable domain and a constant domain. The variable domain varies between antibodies and provides the antigen recognition specificity, whereas the constant domain is conserved within a species and mediates downstream functions, such as receptor binding and complement activation[1].

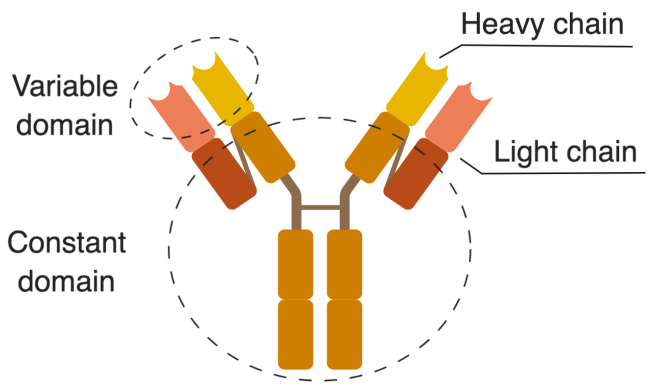

Figure 1. Schematic of an IgG antibody molecule.

Other probes, such as nanobodies and aptamers, also have the specific antigen recognition capability. Nanobodies are engineered from the variable domains of heavy chain only antibodies found in camelids[3], and aptamers are synthetic oligonucleotides that display antigen binding motifs[4]. Compared with antibodies, nanobodies and aptamers are smaller in size (antibodies are ~150 kDa, nanobidies are 12~15 kDa and aptamers are 5~15 kDa)[4,5]. However, they are much

less developed and fewer high quality reagents are available. Therefore, this thesis will focus on antibodies.

1.2. *In situ* protein detection using immunofluorescence imaging

The history of immunofluorescence imaging (i.e. using dye-modified antibodies to label specific targets in tissues and cells followed by fluorescence microscopy imaging) can be traced back to 1930s[6,7]. At that point in time, Dr. John Marrack first showed the use of red dye-labeled anti-typhus and anti-cholera antibodies to visualize their reactions with antigens[8]. Later, Dr. Albert Coons, in collaboration with his colleagues, used fluorescein isocyanate-conjugated antipneumococcal antiserum to detect *Streptococcus pneumoniae* in formalin-fixed tissues harvested from infected mice[9]. It was critical that they showed antibodies could retain antigen detection specificity after chemical modification. It paved the way for a variety of techniques and therapeutics using chemically modified antibodies, including the method developed in this thesis in which single stranded DNA oligonucleotides are attached to antibodies.

The technique of IF imaging has since been further developed with better fluorophores that has higher brightness and greater resistance to photobleaching. IF imaging has now become a standard technique that is widely used in research and clinical laboratories for *in situ* protein detection. One important development that is worth noting is the indirect immunostaining method. It takes advantage of the conserved protein sequences in the constant domain of antibodies. In the method, primary antibodies are used to label specific targets followed by fluorophore-conjugated secondary antibodies that target the constant domain of primary antibodies. Advantages of the indirect immunostaining method include: 1) signal amplification because each primary antibodies can be bound by multiple secondary antibodies targeting

different regions of the constant domain; 2) avoidance of antigenecity loss caused by direct modification of primary antibodies.

1.3. Challenges for traditional immunofluorescence imaging

Despite of being a robust technique, traditional IF imaging with fluorophore-conjugated antibodies has a few limitations, including low multiplexing capability, poor detection senstivity and limited optical resolution.

1.3.1. Multiplexing capability

The multiplexing capability of IF imaging refers to the number of targets visualized in one sample. The multiplexing capability of traditional IF methods is limited by the intrinsic properties of fluorophores that are used for imaging. Fluorophores absorb energy from light within a range of wavelengths (termed as excitation spectrum) and re-emit the energy as light at a longer range of wavelengths (termed as emission spectrum)[10] (**Figure 2a**). Fluorophores with distinct excitation and emission spectra have been developed so as to antibodies conjugated with different fluorphores can be used in one sample to visualize multiple targets. However, the spetra of fluorophores are broad enough so that fluophores with heavily overlapped spetra are not distinguishable and, as a result, cannot be used in the same sample. For example, Alexa Fluor 647 and Alexa Fluor 635 cannot be used together, but either of them can work with Alexa Fluor 488 (**Figure 2b**). In general practice, only 3~4 targets are imaged in one sample[11]. This low multiplexing capability limits the information obtained from a single experiment, which may be inconclusive or misleading in some cases.

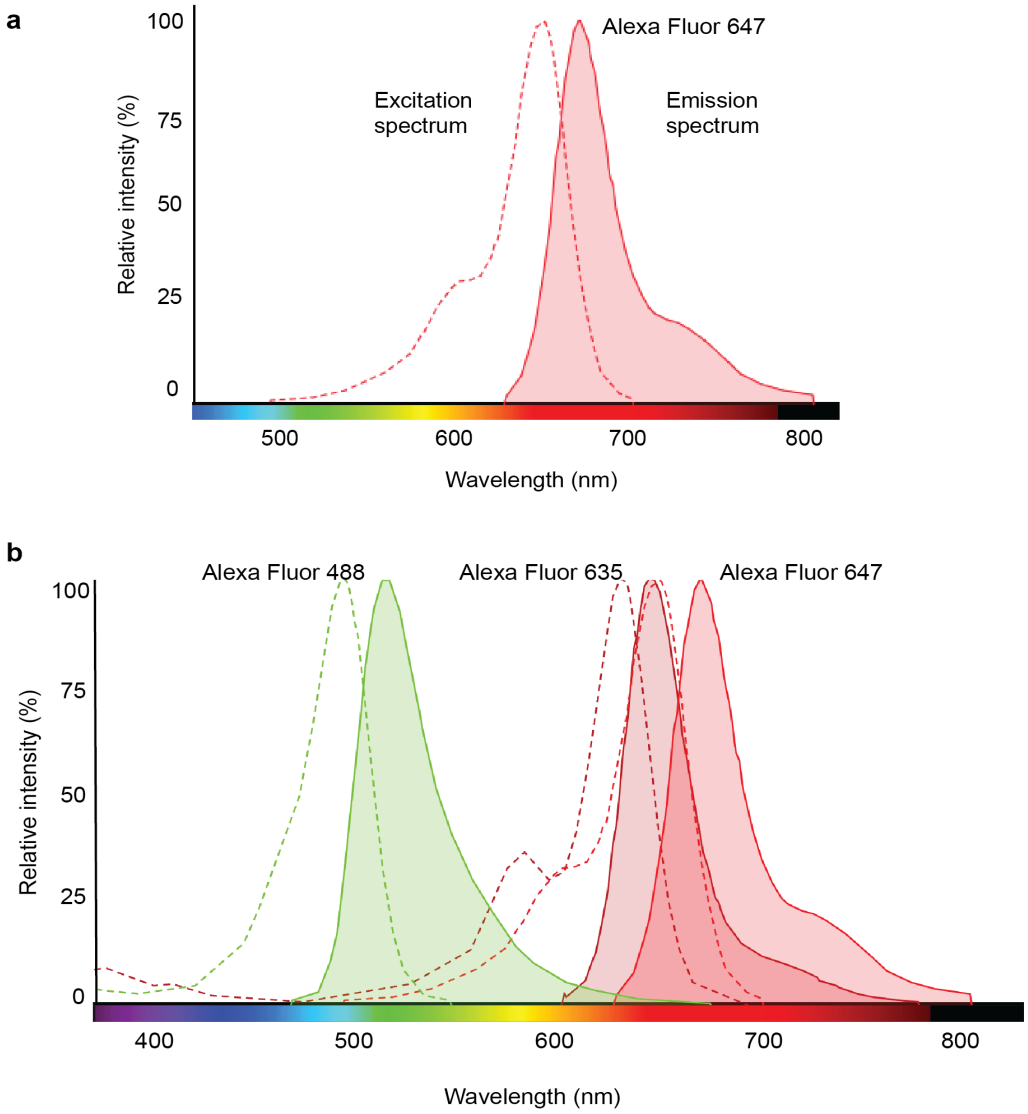

Figure 2. Multiplexing capability of immunofluorescence imaging is restricted by the excitation and emission spectra overlapping between fluorophores. a) Excitation and emission spectra of Alexa Fluor 647. **b)** Excitation and emission spectra of Alexa Fluor 488, 635 and 647. The spectra of Alexa Fluor 647 and 635 are heavily overlapped and therefore cannot be used simultaneously in a typical IF experiment. Both of their spectra are sufficiently separated from that of Alexa Fluor 488, and hence either of them can be combined with Alexa Fluor 488.

Different methods have been developed to address this limitation, including multiplexed detection via unconventional probes and specialized instruments (as applied in multiplexed ion beam imaging [12,13], imaging mass cytometry [14-16], or multiplexed vibrational imaging[17]), iterative sequential antibody labeling and imaging (MxIF[18] and CycIF[19,20]). These techniques

can achieve higher multiplexing (i.e. ≥5-targets), but typically at an expense of decreased sensitivity, throughput, or accessibility (specialized instruments). MIBI, IMC and vibrational imaging requires specialized instruments and typically operate by point-scanning small fields of view (~2-5 min per 50 μm × 50 μm field of view); hence are exceedingly slow for large areas like centimeter scale tissue sections[12,17]. In contrast, fluorescence methods utilizing sequential antibody staining (MxIF and CycIF) offer high accessibility and relatively fast image acquisition; however, they require multiple cycles of slow primary antibody incubation steps (typically hours to overnight per staining cycle), and can result in total experimental time of weeks to months (scaling with the number of targets)[18-20].

1.3.2. Detection sensitivity and signal amplification strategies

Ideally, a digital image formed on the fluorescent microscopy camera only contains signals from the target, enabling qualitively and quantitively analysis of the molecules. In practice, a digital image comprises signals from the target, background and noise. There are multiple sources for background and noise, such as autofluorescence of specimens and poise noise due to measurement of number of photons *et cetera*[21,22]. Unfortunately, background and noise cannot be completely eliminated. Therefore, maximizing signals from the targets using signal amplification strategies, especially for low copy number targets, is necessary to achieve high signal-to-background and signal-to-noise, enabling accurate target visualization and quantification.

Indirect immunostaining using primary antibodies followed by polyclonal secondary antibodies provides a simple method for signal amplification as each primary antibody molecule can be bound by multiple secondary antibodies. However, this method further restricts the multiplexing capability because primary antibodies raised from different species have to used in

the same sample to avoid secondary antibody crosstalk, and most commercially available antibodies are raised in mice or rabbit. In addition, the signal amplification capability of indirect immunostaining is limited to 5~30 folds in our practice[23,24]. Tyramide signal amplification (TSA)[25,26] is an effective way for amplification of the signal through covalent binding of the diffusive tyramide molecules in the vicinity of the target. But, due to lack of orthogonal chemistries, TSA is restricted to labeling of one target at a time. Labeling multiple targets requires sequential antibody labeling and signal amplification with different fluorophores needs to be performed sequentially with microwave-based removal of antibodies after each round (up to 7-color multispectral imaging has been demonstrated this way)[27-29]. Relying on the orthogonal sequence design, DNA-mediated methods offer a promising route for simultaneous signal amplification. DNA-tagged antibodies allows for signal amplification through either DNA template copying or component self-assembly. In rolling circle amplification (RCA)[30], a processive polymerase acts on a circular template to synthesize long concatenated repeats, generating micron-diameter balls of DNA. RCA offers high levels of amplification and potential for multiplexing, but *in situ* enzymatic reaction is hard to control or tunable for individual targets[31]. Both TSA and RCA may also lead to blurring of signals and decreased resolution, respectively due to spreading of the tyramide molecules or the large size of the amplicons (reaching from 250 nm to over ~1 μm radius[32,33]). Branched DNA assemblies[34-36], such as RNAscope[37,38], generate complex tree structures for stable binding of fluorescent DNA strands, whereas HCR utilizes the triggered assembly of metastable fluorophore-conjugated hairpins[39-41]. The structural complexities of these existing DNA-assembly based platforms present potential challenges for designing highly multiplexed orthogonal systems (e.g. each HCR design entails working with the complex kinetic pathway of triggered assembly of two meta-stable hairpins[42-

[44]). In practice, simultaneous signal amplification for proteins beyond spectral multiplexing (3-5 targets) remain to be developed[45,46].

1.3.3. Optical resolution and super-resolution imaging

The optical resolution of a light microscopy does not refer to the ability to detect small objects but denotes to the ability to distinguish two adjacent objects as separate ones instead of a single structure[47]. The optical resolution of a far-field light microscopy is fundamentally limited by the diffraction of light as first described by Ernst Abbe in 1837, which causes a sharp point on the object to blur into a finite-sized spot in the image (**Figure 3**)[47,48]. The 3D intensity distribution of the spot is termed as point-spread-function (PSF). When two points on the object are closer than the full-width-at-half-maximum (FWHM) of their PSFs, their images will substantially overlap so that individual spots cannot be resolved[48]. Pratically speaking, the FWHM of a PSF is determined by two main factors: the wavelength of light (λ) and the numerical aperture (NA) of the objective lens. The FWHM in the lateral direction (i.e. xy) approximitely equals to 0.61λ / NA, and the axial width is about 2~3 times as large as the lateral width for an ordinary objective with high NA[47,48]. When imaging using light of 550 nm wavelength and objective NA of 1.515, the lateral and axial width is ~220 nm and ~520 nm, respectively[48]. Many subcelluar structures in biolgical samples are below the optical resolution of a regular fluorescence microscopy, restraining the detailed studies of those structures.

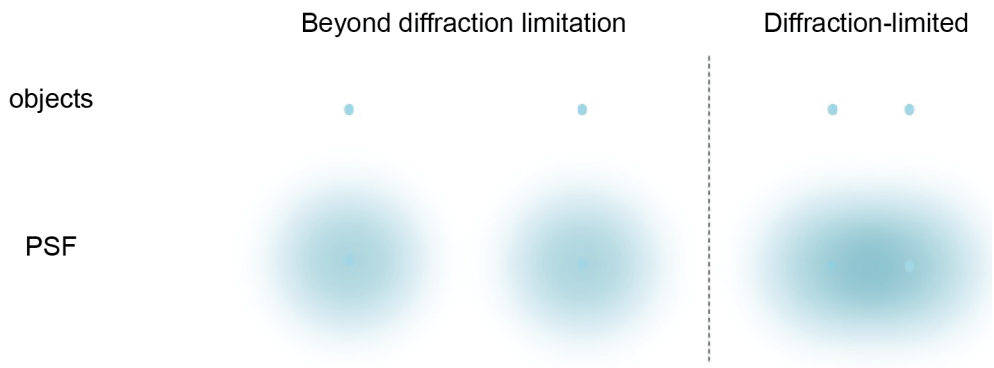

Figure 3. Optical resolution of microscopy is limited by the diffraction of light that turns a sharp object into a finite-sized spot, referred to as point spread function (PSF). Two objects cannot be distinguished if they are within a certain distance.

The diffraction limit has been surpassed by the development of super-resolution imaging and molecules can be resolved as close as a few nanometers[47-50]. Commercially available microscopy platforms, including Strctured Illumination Microscopy (SIM), Stimulated Emission Depletion Microscopy (STED) and Single Molecule Localization nanoscopy, have been introduced into biological laboratories to visualize fine subcelluar structures. In SIM, an illumination pattern is projected to the sample, interfering with sample features to produce Moiré patterns that contain high frequency spatial information. Final images can be reconstructed using specialized algorithms with doubled spatial resolution[47,48]. STED achieves super-resolution by using a second laser to suppress the fluoresence from the fluorophore located off the center, enabling imaging with a lateral resolution of ~30 nm[48]. Single molecule localization nanoscopy, relies on stochastically activating fluorophores within a diffraction-limited region at different

time points, that is, only one molecule is in bright state at a time (**Figure 4a**).

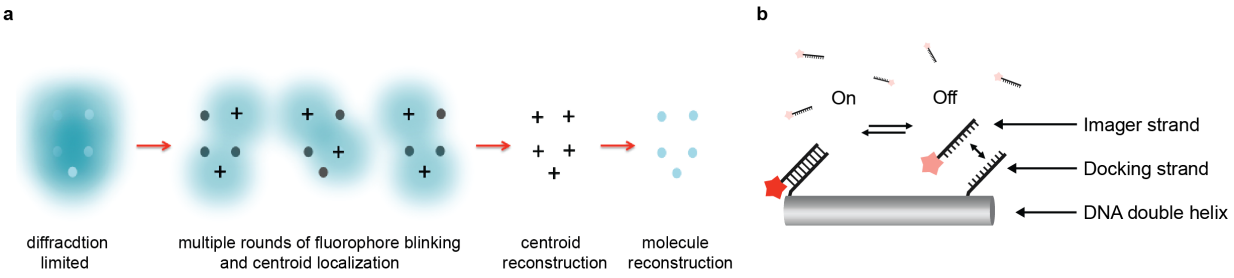

Figure 4. Mechanisms of **a)** single molecule localization nanoscopy and **b)** DNA-PAINT. Detailed description can be found in the main text.

A super-resolved image can be reconstructed afterward by mapping the localization of each molecule with high precision. This category includes photoactivated localization microscopy (PALM) and stochastic optical reconstruction microscopy (STORM) and PAINT (Point Accumulation for Imaging in Nanoscale Topography)[48,51,52]. With single molecule localization nanoscopy, as low as 5 nm resolution has been demonstrated[49]. Previously, our lab has developed a new single molecule localization nanoscopy, named as DNA-PAINT[51]. In this method, the stochastic switching of fluorescence between on- and off- state is achieved by repetitive, transient binding of fluorophore-tagged DNA probes (named as Imager Strands) to complementary DNA docking strands attached to the targets (e.g. DNA nanogrids or antibodies) (**Figure 4b**). In the unbound state, only background fluorescence signal from imager strands is observed. Once imager strands bind to docking strands, the fluorescence signal get temporarily immobilized, allowing sufficient photon collection for precise single molecule localization. Importantly, the transient binding properties of these short DNA strands enables the facile removal of imager strands. Hence, orthogonal imager strands can be used to sequentially visualize multiple targets of interest. More recently, Boyden et al. developed a new super-resolution imaging method, termed as Expansion Microscopy, in which samples are incorporated

in swellable hydrogels and can be physically expanded to pull molecules further apart[53]. This method does not reply on specialized microscopy platforms and a conventional confocal microscope can be used to achieve high speed and deep tissue imaging[54].

1.4. Scope of the thesis

Despite of the methods that have been developed to address individual abovementioned challenges, there is no such method that can simultaneously provide high multiplexing, high sensitivity and high/super optical resolution imaging. In this thesis, I presented the development of a series of techniques that utilize DNA-barcoded antibodies for highly multiplexed, highly sensitive and high/super-resolution imaging. The general concept of the techniques is illustrated in **Figure 5**.

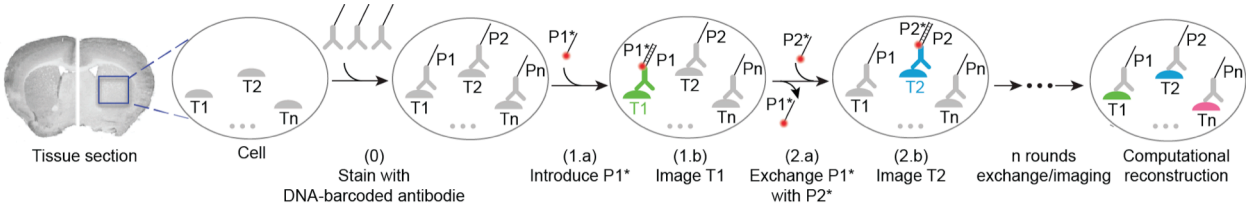

Figure 5. General concept of highly multiplexed *in situ* protein detection using DNA-barcoded antibodies. Distinct targets (T1, T2, … ,Tn) are labeled using corresponding antibodies conjugated to orthogonal DNA docking strands (P1, P2, …, Pn) in a single step. Imager strands (P1*, P2*, …, Pn*) are sequentially introduced to visualize target signals. The imager strands are washed away rapidly using washing buffer after each round of imaging. After imaging, all images are computationally registered and a final merged image is reconstructed by assigning pseudo-colors to each target image.

The techniques have evolved significantly throughout my thesis, as illustrated in **Figure 6**, and are described in detail from chapter 2 to 4.

In chapter 2, I presented methods to generate DNA-conjugated antibodies, including chemical modification and purification, and demonstrated the use of those modified probes for *in situ* DNA-PAINT imaging.

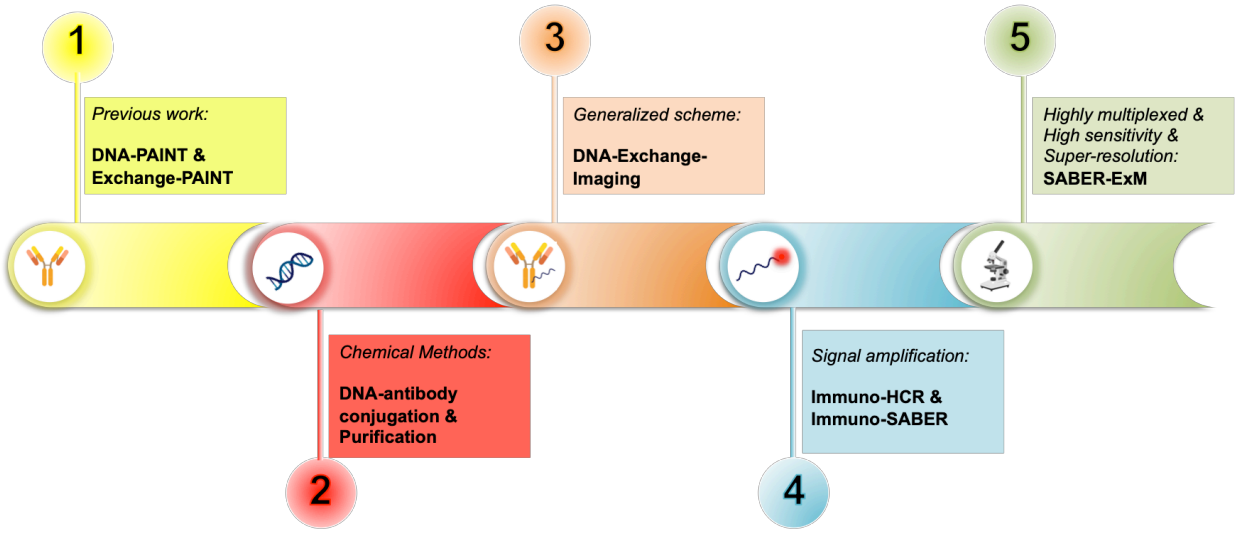

Figure 6. Evolution of highly multiplexed *in situ* protein detection using DNA-barcoded antibodies. It started from previous published lab work DNA-PAINT and Exchange-PAINT. I first developed chemical methods for covalent DNA-antibody conjugation followed by purification. Using improved DNA-conjugated antibodies, we generalized the DNA-Exchange scheme to various imaging platforms and developed an umbrella technique termed as DNA-Exchange-Imaging. We later integrated signal amplification capability by combining DNA-Exchange-Imaging with Hybridization chain reaction (HCR) or Signal amplification by exchange reaction (SABER). We finally developed highly multiplexed, high sensitivity and super-resolution imaging by using immuno-SABER and Expansion Microscopy (ExM).

In chapter 3, I presented a generalized scheme of using DNA-barcoded antibodies for highly multiplexed imaging, called DNA-Exchange-Imaging, and demonstrated its compatibility with various imaging platforms, including confocal, SIM, STED and PAINT, and imaged both cell culture and tissue sections samples.

In chapter 4, I presented an augmented version of DNA-Exchange-Imaging with signal amplification to achieve high sensitivity *in situ* protein detection. I simultaneously explored two DNA-based signal amplification methods, Hybridization chain reaction (HCR) and Signal amplification by exchange reaction (SABER), and was able to achieve over 50-fold signal amplification using both methods.

In this chapter, I also integrated the techniques with super-resolution Expansion Microscopy (ExM) to present a highly multiplexed, highly sensitive and super-resolution imaging method, called SABER-ExM.

Finally, I concluded the thesis with a summary of the evolution of the techniques and discussed the remaining challenges.

In the appendix, I provided a published review article describing in situ 'omics' analysis using DNA barcodes. In addition, I portrayed an open science community that would take advantage of the fast-developing internet technologies to build a massively connected network. The goal of the community is to facilitate openly sharing resources, skills and knowledge, and to promote collaboration between researchers. Its ultimate goal is to accelerate scientific and drug discovery, and to decrease drug pricing by reducing R&D cost.

Chapter II

Development of methods for DNA-antibody conjugation and purification

This chapter contains contents from publication:

1. Agasti, S.S., Wang, Y.*, Schueder, F., Sukumar, A., Jungmann, R.§ and Yin, P. § (2017). DNA-barcoded labeling probes for highly multiplexed Exchange-PAINT imaging. Chemical science, 8(4), pp.3080-3091.*

*2. Saka, S.K.**, § , Wang, Y., **, § Kishi, J.Y., Zhu, A., Zeng, Y., Xie, W., Kirli, K., Yapp, C., Cicconet, M., Beliveau, B.J., Lapan, S.W., Yin, S., Lin, M., Boyden, E.S., Kaeser, P.S., Pihan, G., Church, G.M. and Yin, P. § (2018). Highly multiplexed in situ protein imaging with signal amplification by Immuno-SABER. bioRxiv, p.507566.*

2.1. Abstract

In situ protein detection utilizes affnity probes such as antibodies to label specific targets. In order to implement DNA-Exchange-based protein detection, high quality DNA-conjugated labeling probes are required. In this chapter, I described a method to covalently attach single stranded DNA oligonucleotides onto antibodies through amine-N-hydroxysuccinimide ester crosslinkers. In addition, I presented a method to purify DNA-conjugated products from unconjugated antibodies using toehold displacement-mediated DNA affinity pulldown.

2.2. DNA-antibody conjugation chemistry development and validation

Previously, we have attached biotinylated single stranded DNA oligonucleotides to biotinylated antibodies via streptavidin to form an 'antibody-streptavidin-DNA' sandwich. While successful, this labeling procedure has a few drawbacks: firstly, the reaction is not covalent conjugation. Slow dissociation of DNA oligonucleotides from antibodies may cause loss of signals and cross-reassociation between different antibodies. Secondly, the 'linkage-error', that is,

the distance between the true target and labeled DNA docking sites is increased due to the addition of streptavidin, which ultimately leads to a localization offset from the true target position[55]. Thirdly, the large size of these complexes leads to sterical hindrance in the labeling process, which impedes the achievable labeling density and efficiency.

2.2.1. Conjugation chemistry selection and validation

To develop a covalent chemistry for DNA-antibody conjugation, we chose a few criteria. Firstly, the conjugation chemistry should be versatile such that it is applicable to various antibody isotypes. Secondly, the method should work for commercially available antibodies. Hence, conjugation techniques involving genetic engineering of antibodies, such as unnatural amino acid incorporation, is not favored. Lastly, the method should be simple, economical, high yield and easily accessible to researchers. Based on these criteria, we chose to conjugate thiol-modified DNA oligonucleotides to lysine residues on antibodies via $SM(PEG)_2$ (PEGylated succinimidyl 4-(N-maleimidomethyl) cyclohexane-1-carboxylate) crosslinkers (**Figure 7a**). In this strategy, the small 'footprint' of $SM(PEG)_2$ ensures minimum steric hindrance for antigen binding while placing the DNA label in close proximity to the antibody for achieving high-resolution. In addition, the use of the PEG spacer helps to reduce nonspecific binding[56]. For conjugation, the phosphate-buffered solution of antibody was first incubated with $SM(PEG)_2$ crosslinkers. In this step, the N-hydroxysuccinimide (NHS) ester group of $SM(PEG)_2$ reacts with the amine groups present on the lysine residues and anchors the maleimide group on the antibody surface. After removing the excess cross-linker using size-exclusion chromatography, maleimide-functionalized antibodies were reacted with thiol-modified DNA oligonucleotides to

form stable DNA-antibody conjugates. The antibody conjugates were purified using molecular weight cut-off filter (50 or 100 kDa).

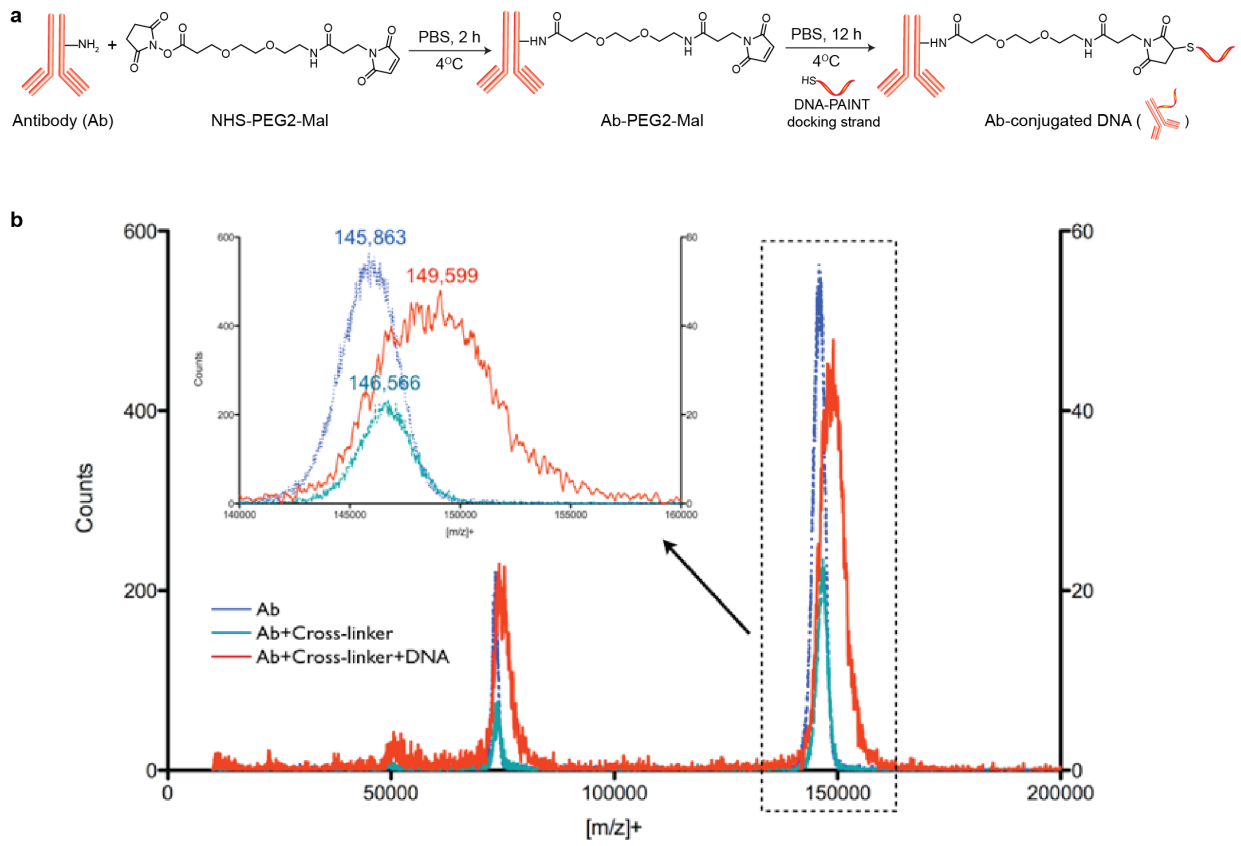

Figure 7. DNA-antibody conjugation and validation. a) Description of the conjugation chemistry using NHS-PEG2-Maleimide crosslinker. The NHS ester group reacts with the amine group of lysine residues and the maleimide group reacts with the thiol group of DNA oligonucleotides. **b)** MALDI-MS validation of DNA antibody conjuation. Based on the mass shift bwtween DNA-modified and unmodidifed antibody (~3700 Da), on average of 1 DNA oligos was conjugated to the antibodies.

The successful conjugation of DNA strands to antibodies was verified using matrix-assisted laser desorption/ionization-mass spectrometry (MALDI-MS). We have optimized protocols to yield conjugates with close to 1 DNA label/Ab (**Figure 7b**). Limiting the number of conjugated DNA oligonucleotides per antibody has two advantages: first, it helps to decrease nonspecific binding, which is potentially mediated by interactions of conjugated DNA with other cellular

compartments; secondly it reduces the probability that lysine residues in the antigen recognition sites are labeled with DNA, which otherwise jeopardizes the antigen binding affinity.

2.2.2. DNA-PAINT imaging with DNA-conjugated secondary antibodies

To test the super-resolution imaging capability of the directly conjugated antibody probes, we first used DNA-conjugated secondary antibody and performed single-color DNA-PAINT imaging of the microtubule network in BSC-1 cells. Among various fibrous cytoskeleton protein networks, microtubules were selected as a model system to evaluate imaging performance due to their well-defined structure, shape and importantly their nanoscale, sub-diffraction dimensions (diameter ~25 nm)[55]. To perform DNA-PAINT imaging, at first we fixed the microtubule network in BSC-1 cells using methanol and stained with primary antibodies against alpha-tubulin followed by DNA-conjugated secondary antibody (**Figure 8a and b**). Next, DNA-PAINT imaging was performed using ATTO655-conjugated imager strands using highly inclined and laminated optical sheet (HILO) illumination. Afterwards, a super-resolved DNA-PAINT image was reconstructed using a custom spot-finding and 2D-Gaussian fitting algorithm[51]. In addition, fiducial-based drift correction was performed using gold nanoparticles to compensate for any sample movement during image acquisition.

As shown in the **Figure 8b**, the resulting DNA-PAINT image showed a significant resolution increase compared to the diffraction-limited representation. The increased resolution could be easily observed by visualizing a dense region of microtubule network where individual microtubule filaments could be clearly distinguished. This was impossible in the standard diffraction-limited micrograph. More importantly, when a single microtubule fiber was magnified, DNA-PAINT was able to resolve the hollow tubular structure[57]. This underlines

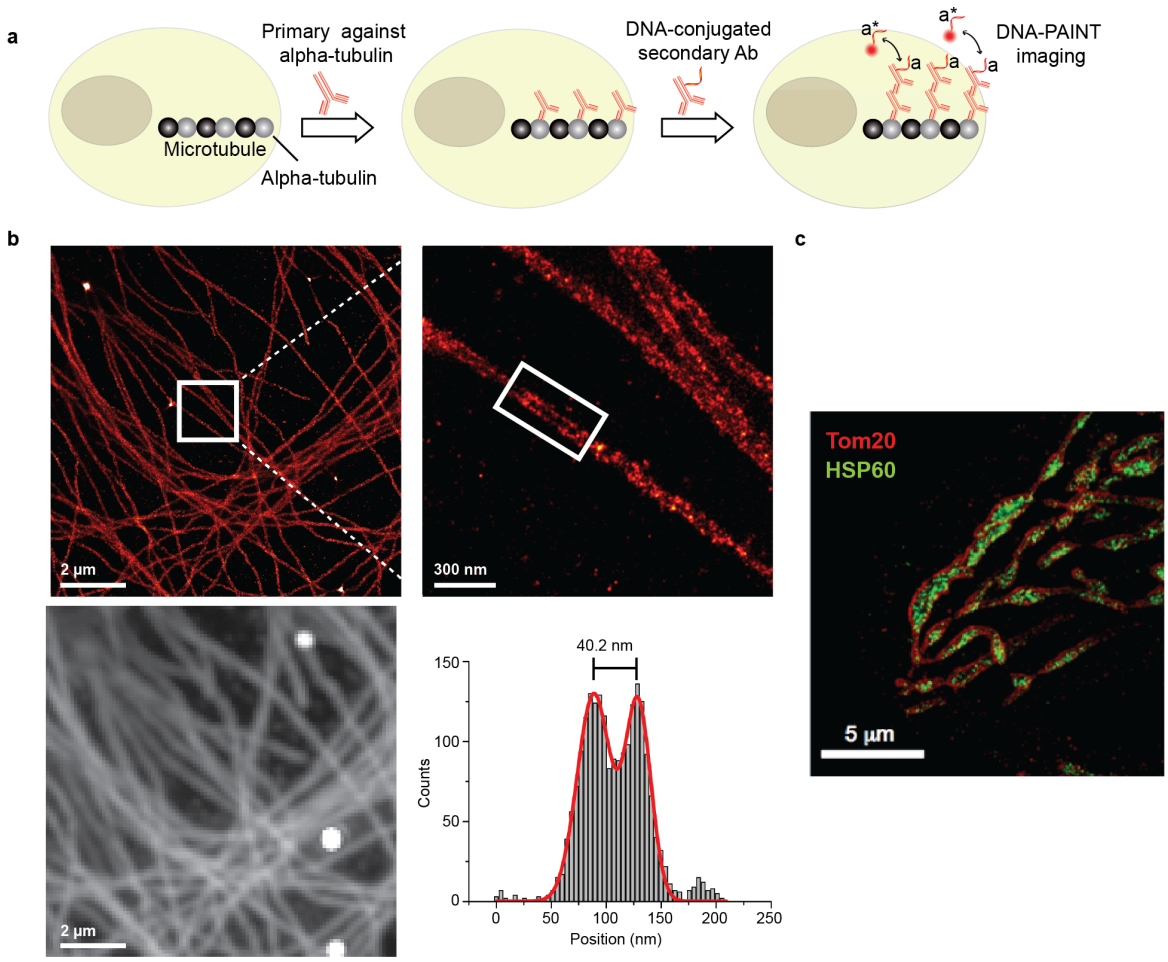

Figure 8. DNA-PAINT imaging with DNA-conjugated secondary antibodies. a) Labeling strategy with DNA-conjugated secondary antibody. **b)** Secondary antibody-based DNA-PAINT super-resolution imaging of microtubules inside a fixed BSC-1 cell. Zoom-in of the highlighted area shows the resolution improvement compared to the diffraction-limited micrographs of the same area. The cross-sectional histogram of a hollow microtubule structure clearly shows two distinct lines with a separation of ~40 nm. **c)** Two color imaging for mitochondrial markers, Tom20 and HSP60. Tom20 is on the outer membrane of mitochondria whereas HSP60 is inside mitochondria.

substantial improvement of labeling density and size over previously published DNA-PAINT cell data[51], where biotin-streptavidin-mediated DNA conjugated antibodies failed to resolve this hollow tubular structure. To semi-quantitatively assess the achievable resolution, we measured the cross-sectional profile of localizations of a "hollow" microtubule structure. As depicted in **Figure 8b**, the cross-sectional profiles showed two well-resolved peaks with a separation of ~40 nm between them, which was in good agreement with the previous reports[58]. We also tested our

direct DNA-conjugated antibodies for dual-color super-resolution imaging (**Figure 8c**). Here, we co-stained Tom20, a mitochondrial outer membrane protein, and HSP60, a mitochondrial matrix protein in fixed HeLa cells. The image was taken using ATTO655- and Cy3B-conjugated imager strands for Tom20 and HSP60, respectively. This dual-color DNA-PAINT image showed Tom20 localizing on the outer mitochondrial membrane, while HSP60 localizes on the inside of the mitochondria.

2.2.3. DNA-PAINT imaging with DNA-conjugated primary antibodies

Although secondary antibodies are widely used as indirect immunostaining approaches, they are not the ideal choice for highly multiplexed super-resolution imaging for primarily two reasons: on one hand, the limited availability of primary antibodies from different species; on the other hand, due to the increased size of the primary-secondary antibody sandwich, the resulting larger 'linkage-error' could lead to lower spatial accuracy. Therefore, we next turned to more direct immunostaining approaches, involving only primary antibodies.

To test primary antibody-based DNA-PAINT imaging, we used two model systems: microtubules and mitochondria. The microtubule network was stained with DNA-conjugated primary antibodies against alpha-tubulin, whereas the mitochondria were stained for Tom20 (**Figure 9a**). **Figure 9b and c** show the resulting DNA-PAINT images of directly-labeled microtubules and mitochondria structures, respectively. Individual microtubules as revealed by alpha-tubulin staining and the outer mitochondrial membrane as revealed by Tom20 are clearly visible from the super-resolved image, similar to the secondary antibody-based staining.

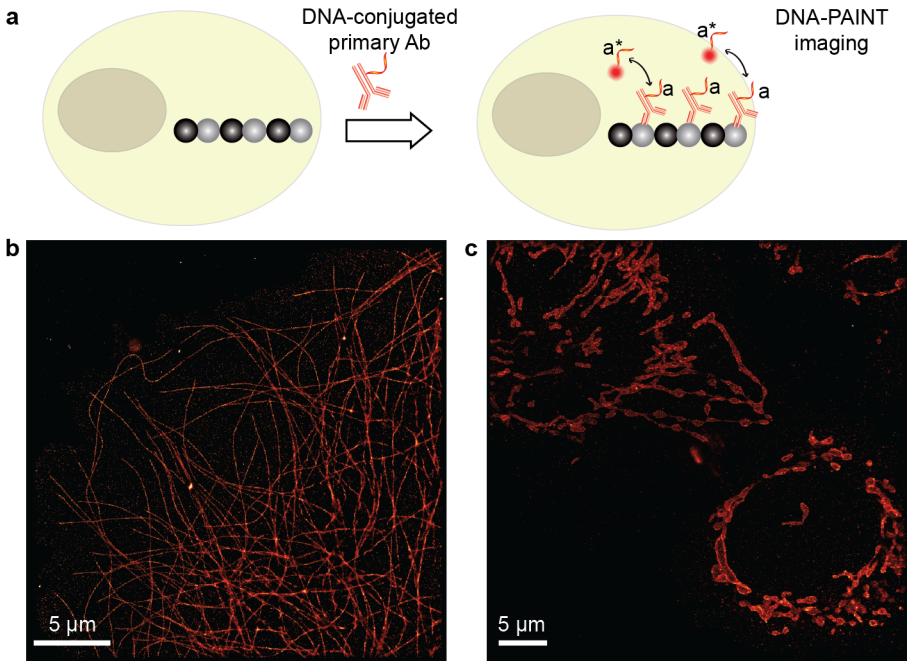

Figure 9. DNA-PAINT imaging using DNA-conjugated primary antibodies. a) Labeling scheme with DNA-conjugated primary antibody. **b)** Primary antibody-based DNA-PAINT imaging of microtubules inside a fixed BSC-1 cell. **c)** Primary antibody-based DNA-PAINT imaging of Tom20 in mitochondria. Tom20 localized to the mitochondrial membrane, which was clearly resolved.

2.2.4. DNA-PAINT imaging with DNA-conjugated nanobodies

IgG antibodies, typically used in immunofluorescence studies, are ~150 kDa in molecular weight and ~10 nm in size. Although the large commercial available repertoire of antibodies is advantageous for their use in highly multiplexed imaging, their rather large size is ultimately a concern when highly accurate localization of the target is necessary or high density labeling is required for molecular counting[55,59]. To address this issue, we used nanobiodies, antibody-like affinity molecules with smaller sizes. Nanobodies are derived from heavy chain-only antibodies generated by camelids[3]. They are small in size (~1.5 nm × 2.5 nm) with only ~13 kDa in MW and have high affinity for their target molecule[3,55,59]. Previous reports have demonstrated the enhanced resolving power of nanobodies for super-resolution imaging of microtubules[55,60].

We began with optimizing the conjugation chemistry for DNA-labeled nanobodies. We used a cycloaddition reaction between 1,2,4,5-tetrazine (Tz) and trans-cyclooctene (TCO) to couple DNA-PAINT docking strands to a model anti-GFP nanobody (**Figure 10a**). The strain-promoted {4+2} cycloaddition reaction between Tz and TCO is fast with a rate constant of up to 10^6 $(Ms)^{-1}$, quantitative and can proceed in physiological condition, which helps to rapidly and efficiently conjugate DNA while preserving the functionality of the nanobodies[61]. In brief, TCO-NHS ester was used to react with primary amine groups from Lysine residues on nanobodies in PBS (pH = 8) for 3 hours. On the other hand, amine-modified DNA-PAINT docking strands were reacted with Tz and subsequently purified using HPLC. TCO-modified nanobodies were then coupled with Tz-modified DNA-PAINT docking strands under reaction in PBS (pH = 7.4) for 3 hours.

Next, we tested the performance of our DNA-conjugated nanobodies for DNA-PAINT super-resolution imaging in HeLa cells expressing mitochondria-green fluorescent protein (GFP). HeLa cells were transfected with a baculoviral vector containing mitochondrial leader sequence-fused GFP (BacMam2.0)[62], and the expression of GFP was detected after 2 days of transfection (**Figure 10b and c**). The transfected cells were stained with DNA-conjugated anti-GFP nanobodies after PFA fixation. The DNA-PAINT image shows a specific signal and clear resolution increase when resolving mitochondrial structures (**Figure 10d**). The shape of mitochondria as detected with DNA-PAINT in **Figure 10d** correlated well with their corresponding GFP signals detected using the conventional fluorescence microscopy in **Figure 10c**. We note that some mitochondria in **Figure 10c** did not show up in **Figure 10d**. These "missing" mitochondria were actually out-of-focus when imaged in HILO mode, and hence did not generate enough localization events for super-resolution image reconstruction.

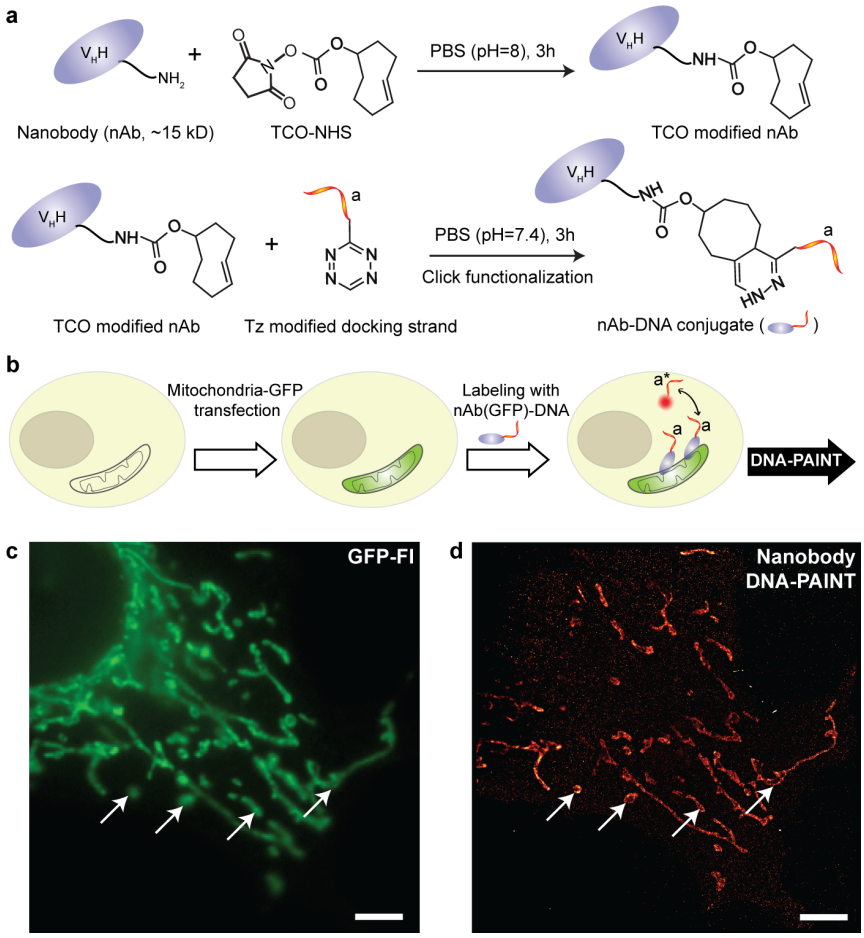

Figure 10. DNA-PAINT imaging using DNA-conjugated nanobodies. a) Synthesis scheme for DNA-conjugated nanobody preparation. **b)** Labeling scheme with DNA-conjugated nanobody. **c and d)** Nanobody-based DNA-PAINT super-resolution imaging of the mitochondrial network inside a fixed HeLa cell. The comparison of the diffraction-limited image (**c**) to the DNA-PAINT image (**d**) underlines the achievable resolution increase. Scale bars: 5 μm.

2.2.5. Highly multiplexed Exchange-PAINT imaging using a pool of orthogonally labeled antibodies

Protein interaction networks mediate cellular responses to various environmental stimuli. It is increasingly evident that the spatial heterogeneity of protein distribution in cells leads to intracellular functionality differences among distinct compartments and intercellular variance among cells located in different regions. Mapping the heterogeneity of protein networks is challenging for three reasons: (1) the location information of proteins need to be well preserved;

(2) comprehensive studies probing multiple protein targets need to be performed in order to understand the whole network; (3) high spatial accuracy is required to achieve subcellular mapping, rendering conventional diffraction-limited fluorescence imaging unsuitable.

The development of Exchange-PAINT imaging enables highly multiplexed super-resolution detection in single cells and is hence desirable for protein network mapping directly *in situ*. By synergistically combining optimized DNA probes design and improved DNA-antibody conjugation, we here report thus far unprecedented nine-target super-resolution imaging in biological samples.

Given indirect immunostaining approaches are most widely used and present a cost-effective method for labeling protein targets, we firstly tested multiplexed super-resolution imaging using DNA-conjugated secondary antibodies. Here, we stained fixed HeLa cells with phalloidin[63] and primary antibodies from seven different species followed by DNA-conjugated secondary antibodies from donkey species. Eight rounds of probe exchange were performed to image all targets. The results showed that eight cellular structures could be clearly visualized with Exchange-PAINT, and there was minimal-to-no crosstalk of signals among different antibodies (**Figure 11**). It can be seen that Paxillin localized at the tip of actin filaments, which is consistent with the fact that Paxillin is an actin regulation protein in focal adhesions[64]. The nuclear pore complex signal was present specifically in the nucleus which was indicated by DAPI staining of the nucleus.

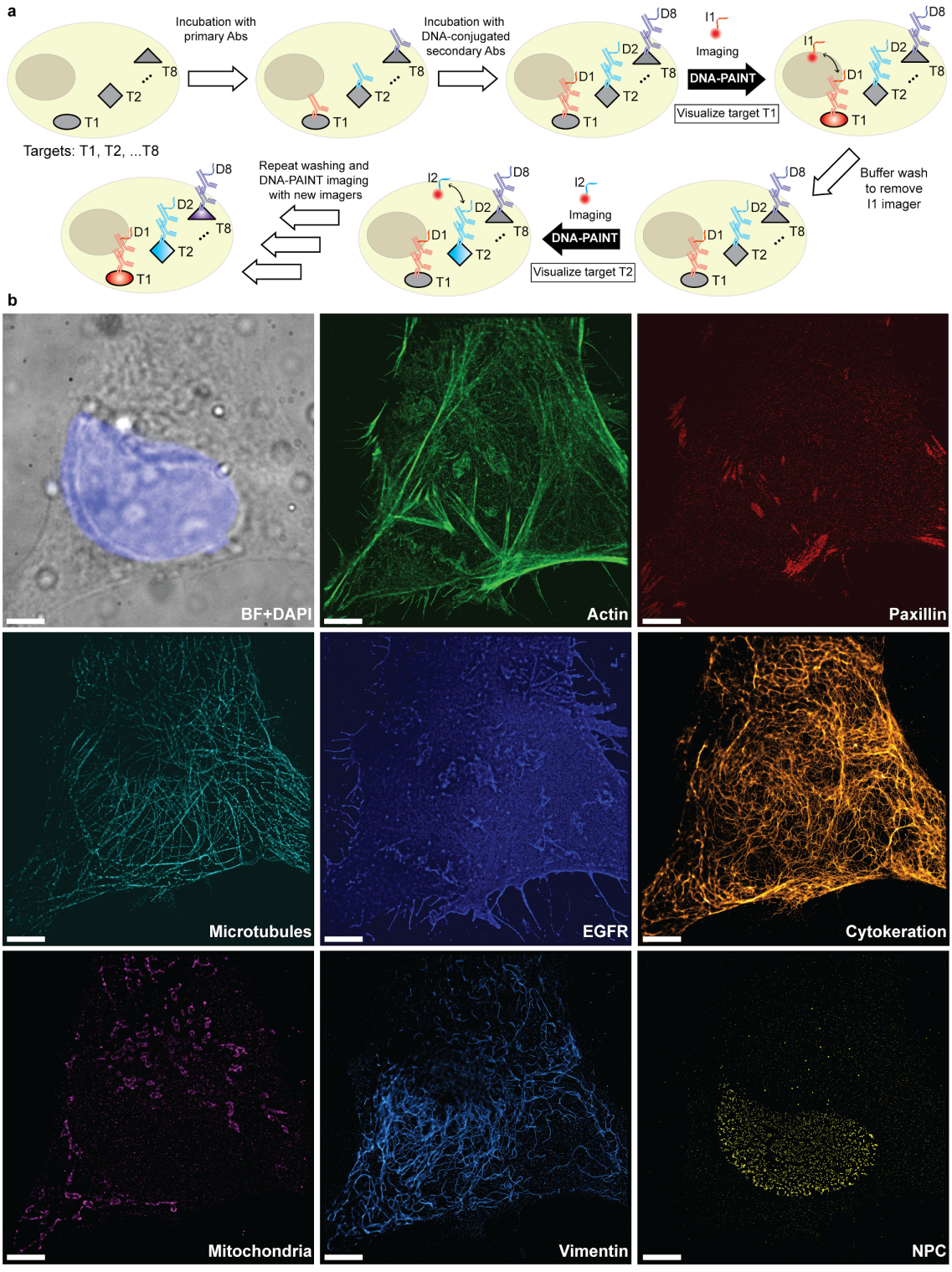

Figure 11. Secondary antibody-based labeling for multiplexing with Exchange-PAINT. a) Schematic representation of Exchange-PAINT using DNA-conjugated secondary antibodies. **(b)** Eight-target DNA-PAINT image of fixed HeLa cells acquired in eight sequential rounds. Scale bars: 5 μm.

The use of secondary antibodies for multiplexed detection, however, is limited by the availability of primary antibodies from different species. Therefore, we next used directly DNA-labeled primary antibodies and small molecule binders, and achieved nine-target super-resolution visualization (**Figure 12**). Nuclear protein Ki67 signals were mostly located in the nucleus while Lamin and Nuclear Pore Complex (NPC) marked the nuclear membrane. Clathrin signals indicated the distribution of coated-vesicles in the cytoplasm. We note that the super-resolution signal in the reconstructed images obtained using primary antibodies was lower compared to indirect labeling using secondary antibodies, which is expected due to lack of signal amplification in the primary antibody only case. We anticipate that this fact can be improved by increasing the imaging time to obtain more localization events. This, again, is unique to Exchange-PAINT, due to its resistance to photobleaching and replenishable imaging probes.

The PAINT DNA sequences are listed in **Table 1**, and the antibodies used for the experiments are listed in **Table 2 and 3**.

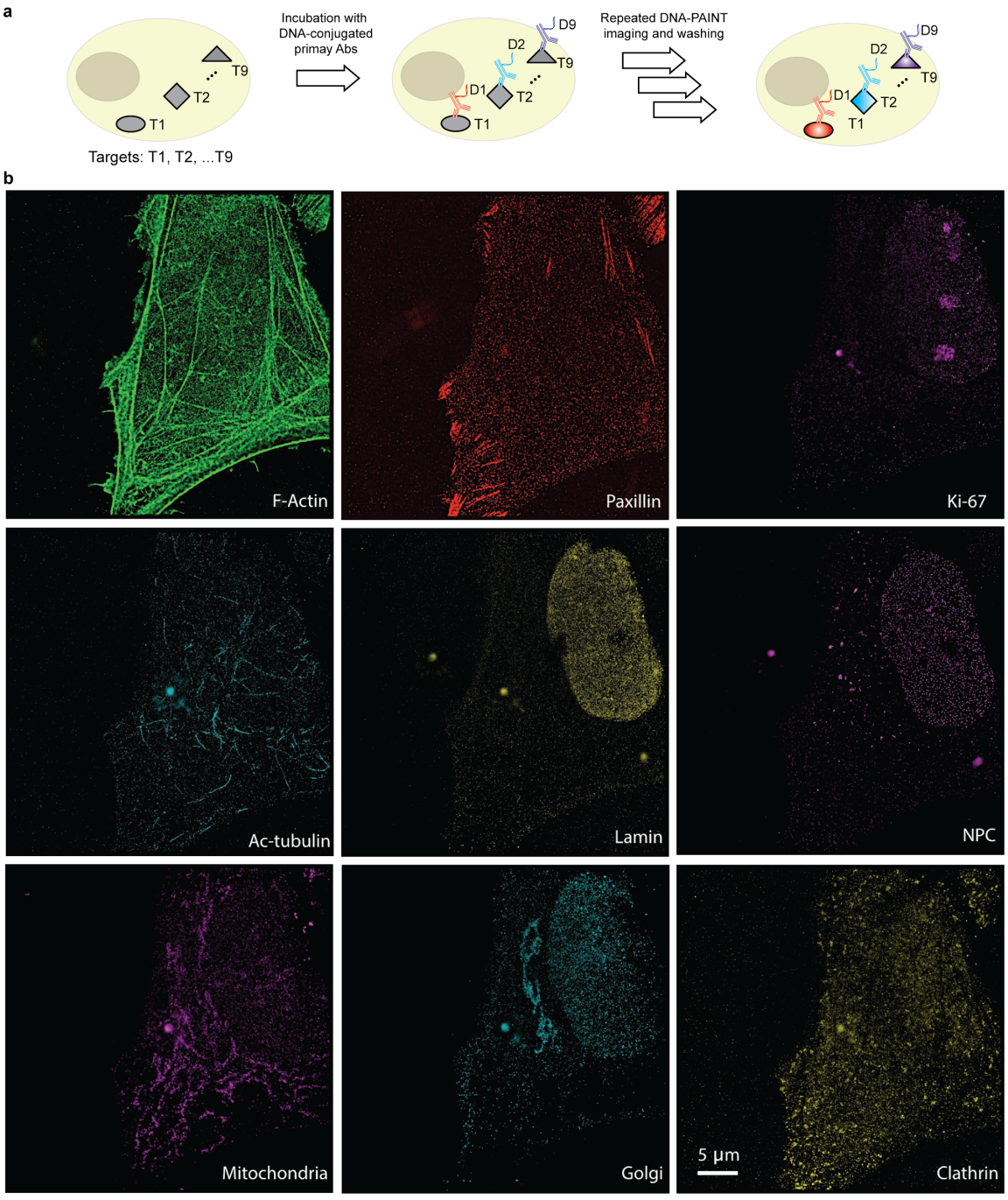

Figure 12. Primary antibody-based labeling for multiplexing with Exchange-PAINT. (a) Labeling strategy for primary antibody-based Exchange-PAINT imaging. **(b)** Nine-target super-resolution image of proteins in fixed HeLa cells acquired using nine rounds of Exchange-PAINT.

2.3. DNA-conjugated antibody purification using toehold-displament-mediated DNA affinity pulldown

In order to ensure high quality imaging, relatively pure solution of DNA-conjugated antibodies without contamination from unconjugated products is preferred. Ion exchange chromatography can be used to separate molecules with charge differences, such as unconjugated antibodies and antibodies with negatively charged DNA oligonucleotides. However, in the case of antibodies used for DNA-PAINT, the DNA sequence contains only 12 nucleotides, which is challenging for ion exchange chromatography to resolve the charge differences. In addition, different antibodies have distinct isoelectronic points (PI), which means the purification process has to be optimized for different antibodies. To address the issue, I developed a toehold-displacement[65]-mediated DNA affnity pulldown method for DNA-conjugated antibody purification (**Figure 13**).

In the method, a capture DNA sequence (b*c) that is partially or fully complement to the conjugated docking DNA sequence (ab) can be designed using NUPACK[66] to introduce a toehold displacement sequence (c). The capture DNA sequence is modified with biotin so that it can be attached to streptavidin agarose beads. After mixing antibody conjugation products with capture sequence-coated streptavidin beads, DNA-conjugated antibodies are bound to the beads while unconjugated antibodies remain in the solution. The binding affinity between docking sequences and capture sequences can be tuned with solution salt concentration (Mg^{2+} or Na^{+}) and reaction temperature. The higher salt concentration or the lower reaction temperature is, the stronger the binding is. With 1x PBS and 4 °C, the binding of 12-nucleotide DNA duplex is sufficiently strong for antibody pulldown. After the DNA affinity pulldown, DNA-conjugated antibodies are recovered by introducing excessive amount of toehold displacment sequences

(b*c). The displacement sequence is fully complement to the capture sequence and hence has higher affinity than the docking sequence on antibodies has. It will drives the reaction towards displacement of the docking sequence from the capture sequence, releasing the antibody from the beads. Size cut-off filtering columns are then used to buffer exchange and concentrate DNA-conjugated antibodies. As shown in **Figure 13 b and c**, unconjugated antibodies are mostly removed from the solution after purification.

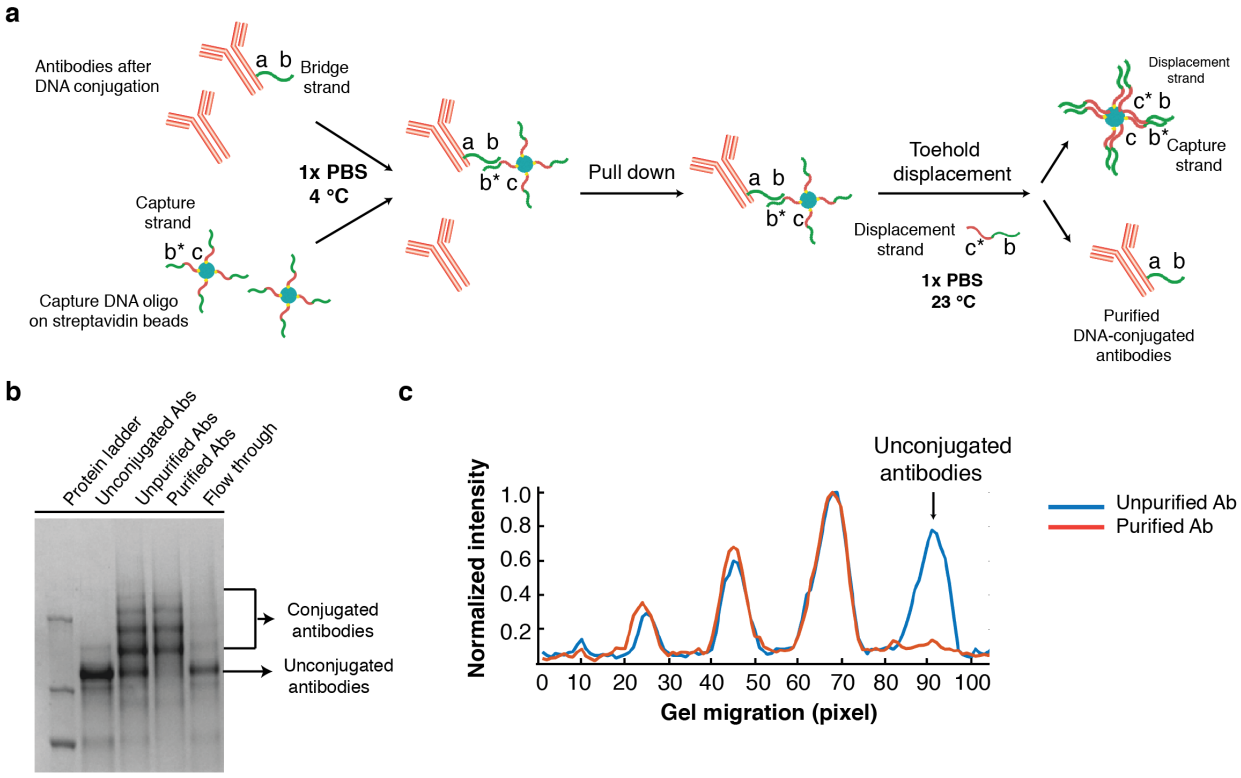

Figure 13. Purification of DNA-conjugated antibodies using a toehold displacement-mediated DNA affinity pull-down. (a) Schematic of the pull down assay. Biotin-modified capture DNA strands (biotin-*c*-*b**, where *c* is 15-nucleotides and *b** is 16-nucleotides; a+b can be as low as 12-nucleotides as used in DNA-PAINT) are attached to streptavidin beads, and used to pull down DNA-conjugated antibodies after antibody-bridge DNA conjugation (bridge strand sequence: *a*-*b*, where *b* is 16 nucleotide*s*). The attached antibodies are dissociated from the beads using toehold displacement strands (*c**-*b*) that compete with capture strandson antibodies. While optional for Immuno-SABER, we found that purifying the DNA-conjugated antibodies via pull-down and toehold-mediated displacement may be helpful to improve the signal for select antibodies. **(b)** Visualization of purification products using an SDS-PAGE gel assay. After DNA conjugation, the majority of antibodies were conjugated with 0, 1 or 2 DNA oligos per antibody. After purification, antibodies without DNA were removed. **(c)** Plot of protein densities for the bands in **b**. The band corresponding to removed unconjugated antibodies is marked with an arrow.

2.4. Methods

Materials

Unless otherwise stated, all chemicals and solvents were purchased from commercial suppliers and used as received. PEGylated SMCC (succinimidyl 4-(N-maleimidomethyl)cyclohexane-1-carboxylate) cross-linker (SM(PEG)$_2$), trans-4-Cycloocten-1-yl 2,5-dioxo-1-pyrrolidinyl carbonate (TCO-NHS) and benzylamino tetrazine N-hydroxysuccinimidyl ester (Tz-NHS) were purchased from Sigma-Aldrich. GFP nanobodies were purchased from ChromoTek. Amicon Ultra Centrifugal Filter (100 kDa MWCO) was purchased from Merck Millipore. Zeba spin desalting column (7000 MWCO) was purchased from Thermo Fisher Scientific. NAP-5 columns were purchased from GE Healthcare. Dulbecco's Phosphate-Buffered Saline (PBS, pH 7.4) without calcium and magnesium was purchased from Life Technologies. Unmodified, dye-labeled and biotinylated DNA oligonucleotides were purchased from Integrated DNA Technologies (IDT). Streptavidin was purchased from Invitrogen (catalog number: S-888). BSA-biotin was obtained from Sigma-Aldrich (catalog number: A8549). Coverslips were purchased from VWR (coverslips 18 × 18 mm, #1.5). The glass slides were purchased from VWR (25 × 75 × 1 mm). M13mp18 scaffold was obtained from New England BioLabs (N4040s). Freeze 'N Squeeze columns were ordered from Bio-Rad (catalog number: 7326165).

Microscope setup

Fluorescence imaging was carried out on an inverted Nikon Eclipse Ti microscope (Nikon Instruments) with the Perfect Focus System, applying an objective-type TIRF configuration with an oil-immersion objective (CFI Apo TIRF 100×, NA 1.49, Oil). For excitation of ATTO655 fluorophores, a 639 nm laser (150 mW nominal, Toptica iBeam Smart) was used. The laser beam

was passed through a cleanup filter (ZET 642/20x, Chroma Technology, Bellows Falls, VT) and coupled into the microscope objective using a single-band beam splitter (ZT647rdc, Chroma Technology). Fluorescence light was spectrally filtered with an emission filter (ET6651p, ET705lp, Chroma Technology).

For excitation of Cy3B fluorophores, a 561 nm laser (200 mW nominal, Coherent Sapphire) was used. The laser beam was passed through a cleanup filter (ZET 561/10x, Chroma Technology, Bellows Falls, VT) and coupled into the microscope objective using a single-band beam splitter (ZT561rdc, Chroma Technology). Fluorescence light was spectrally filtered with an emission filter (ET600/50n, Chroma Technology). Single molecule fluorescence signals were imaged on an EMCCD camera (iXon Ultra 897 EMCCD, Andor Technology). Data acquisition was performed without additional magnification in the detection path and yielding a pixel size of 160 nm.

Cell Culture

Cells (HeLa, BSC-1 and U2OS) were cultured in Dulbecco's Modified Eagle Medium (DMEM), supplemented with fetal bovine serum (FBS; 10%), penicillin and streptomycin (1%), and L-glutamine (1%). Cell lines were maintained at 37 °C in a humidified atmosphere containing 5% CO_2.

EGFR Transfection

At confluence, before plating, cells were washed, trypsinized and suspended in culture media. Cells were counted. In a typical experiment, ~50000 cells/well were plated in 8-well Nunc™ Lab-Tek™ Chamber Slides. 24 h post plating, when the cells achieved ~70% confluency, 2 μg or

4 µg of EGFR plasmid DNA along with P3000 were mixed together in 5 µl of Opti-MEM for each well in the chamber. At the same time, Lipofectamine 3000 transfection agent was mixed separately in 10 µl of Opti-MEM. The Lipofectamine and the DNA reagents were mixed in a 1:1 ratio and incubated at room temperature for 5 minutes to form complexes. This was added dropwise to cells and the cells were incubated at 37 °C in a humidified atmosphere containing 5% CO2. After 24 h, the media was replaced with Dulbecco's Modified Eagle Medium (DMEM), supplemented with fetal bovine serum (FBS; 10%), penicillin and streptomycin (1%), and L-glutamine (1%). Typically 48 h following transfection cells were used in the indicated assays.

CellLight Mitochondria-GFP, BacMam 2.0 Transfection

At confluence, before plating, HeLa cells were washed, trypsinized and suspended in culture medium. Cells were counted and ~50000 cells were plated in a Labtek Chamber. After 24 h, 10 µl of CellLight Mitochondria-GFP, BacMam 2.0 Transfection reagent was added to each well in the chamber and cells were incubated at 37 °C in a humidified atmosphere containing 5% CO_2. The transfection efficiency was checked 24 h after transfection and the cells were used typically 48h after transfection.

MALDI-TOF mass spectrometry

The DNA-modified antibody (DNA-Ab, conc. of ~1 mg/ml) was transferred to Milli-Q water using Zeba spin columns (7000 MWCO). A matrix solution was prepared by dissolving sinapinic acid (1 mg) in acetonitrile (70 µl) and water with 0.1% trifluoroacetic acid (30 µl). 1 µl of the DNA-antibody solution was deposited onto the MALDI plate and then mixed with 1 µl of

MALDI matrix. The plate was allowed to dry at room temperature for ~4-5 h. The MALDI-TOF mass data was collected using the AB SCIEX 4800 MALDI-TOF/TOF analyzer.

Preparation of DNA-antibody conjugates

Antibodies were purchased from commercial vendors and initially concentrated to ~2.5 mg/ml using Amicon Ultra Centrifugal Filters (100 kDa MWCO). Azide or any other preservatives were removed, and the antibody was buffer-exchanged to phosphate buffered saline (PBS, pH 7.4) using Zeba spin columns (7000 MWCO). The concentration of the antibody was adjusted and in a typical conjugation experiment 200 μg of antibody in 95 μl of PBS was used in the next step. 200 μg antibody in 95 μl PBS was mixed with 7.5 eq of PEGylated SMCC (succinimidyl 4-(N-maleimidomethyl)cyclohexane-1-carboxylate) cross-linker ($SM(PEG)_2$) in 5 μl of DMF (dimethyl formamide). The solution was then incubated at 4 °C for 1.5 h. Excess PEGylated SMCC cross-linker was removed from maleimide-activated antibodies using Zeba spin columns (7000 MWCO, eluent: PBS, pH 7.4). In parallel, thiol-modified DNA oligos (20 nmole) were reduced using dithiothreitol (DTT, 100 mM) in 0.1 ml PBS (1 mM EDTA, pH 8.0) for 2 h at room temperature. The reduced DNA oligos were purified using NAP-5 columns (GE Healthcare). Deionized water was used as eluent. The maleimide-activated antibodies were mixed with the reduced form of their respective DNA oligos (15 eq) in PBS solution. The reaction was allowed to proceed for 12 h at 4 °C. DNA-antibody conjugates were purified and concentrated using Amicon Ultra Centrifugal Filters (100 kDa MWCO).

Preparation of TCO conjugated GFP nanobody

GFP nanobody (250 µl, 1 mg/ml) was first buffer-exchanged to PBS (pH7.4) containing 10% 1 M $NaHCO_3$ (v/v) using Zeba spin columns (7000 MWCO). 25 eq TCO-NHS in 12.5 µl was added into the GFP nanobody solution. The reaction was incubated at room temperature for 3 h. Excess TCO-NHS was removed from nanobodies using Zeba spin columns (7000 MWCO, eluent: PBS, pH 7.4). TCO-GFP was incubated with 3 eq of tetrazine (Tz) modified DNA. The reaction mixture was incubated at room temperature for 3 h. Excess Tz modified DNA was removed from DNA conjugated nanobodies using Zeba spin columns (7000 MWCO, eluent: PBS, pH 7.4). DNA modified nanobodies were further purified using Amicon Ultra Centrifugal Filter (10 kDa MWCO).

Immunostaining protocol with only PFA

~25,000 cells/well was plated in a Lab-Tek chamber. Culture medium was removed and proceed to fixation. Fixation for 10 min with 4% paraformaldehyde in PBS. Washing with PBS for three times. Permeabilization with 0.25% v/v Triton X-100 in PBS for 10 min. Washing with PBS for three times. Blocking for 2 h with 3% bovine serum albumin and 0.1% v/v Triton X-100 in PBS. Staining for overnight at 4C with primary antibody (10 µg/ml) diluted in 3% bovine serum albumin and 0.1% v/v Triton X-100 in PBS. Washing with PBS (3×) with 5 min incubation each time. Incubation for 1 h with secondary antibodies (10 µg/ml) in 3% bovine serum albumin and 0.1% v/v Triton X-100 in PBS to a concentration. Washing with PBS (3×) with 5 min incubation each time. Proceed to DNA-PAINT imaging.

Immunostaining protocol with PFA+glutaraldehyde

~25,000 cells/well was plated in a Lab-Tek chamber. Culture media was removed and proceed to fixation. Fixation for 10 min with 3% paraformaldehyde and 0.1% glutaraldehyde in PBS. Washing with PBS for three times. Reduction for 7 min with 0.1% sodium borohydride in PBS to reduce background fluorescence. Washing with PBS for three times with 5 min incubation each time. The rest is same as above.

Immunostaining protocol with methanol

~25,000 cells/well was plated in a Lab-Tek chamber. Culture media was removed and proceed to fixation. Fixation for 15 min with 100% methanol at -20°C. Washing with PBS for three times with 5 min incubation each time. The rest is same as above.

Antibody purification using toehold displacement-mediated DNA affinity pull down

200 μl of high capacity streptavidin agarose (ThermoFisher #20357) was centrifuged down, washed 3 times using 500 μl PBS, and incubated with 10 μl 1 mM of biotin-labeled binding sequences in 300 μl PBS with 0.1% Triton X-100 for 30 min at room temperature. The agarose was then washed twice with PBS with 0.1% Triton X-100, followed by blocking with 250 μl blocking buffer (2% BSA + 0.1% Triton in PBS) for 1 h at room temperature with rotation. The agarose was then centrifuged and resuspended with 200 μl incubation buffer (1% BSA + 0.1% Triton in PBS) containing the DNA-conjugated antibodies, followed by rotation at 4°C for 1 h. The sample was centrifuged at 4°C and washed twice with 200 μl incubation buffer. The bound antibodies were recovered by adding 20 μl of 1 mM toehold strands in 200 μl incubation buffer. After centrifugation, the supernatant was collected and the agarose was washed three times with 300 μl washing buffer (PBS + 0.1% Triton), collecting supernatant for each time. The

supernatant was pooled together and buffer exchanged using 2 ml 50 kDa Amicon Ultra Filters six times to remove toehold DNA oligonucleotides.

Table 1. *52 orthogonal DNA-PAINT imager and corresponding docking sequences*.

Name	Imager DNA sequence	Docking DNA sequence
P1	CTAGATGTAT-dye	TTATACATCTA
P2	TATGTAGATC-dye	TTGATCTACAT
P3	GTAATGAAGA-dye	TTTCTTCATTA
P4	GTAGATTCAT-dye	TTATGAATCTA
P5	CATACATTGA-dye	TTTCAATGTAT
P6	CTTTACCTAA-dye	TTTTAGGTAAA
P7	GTACTCAATT-dye	TTAATTGAGTA
P8	CCATTAACAT-dye	TTATGTTAATG
P9	CATCCTAATT-dye	TTAATTAGGAT
P10	GATCCATTAT-dye	TTATAATGGAT
P11	CACCTTATTA-dye	TTTAATAAGGT
P12	GCTCTAACTA-dye	TTTAGTTAGAG
P13	CCTTCTCTAT-dye	TTATAGAGAAG
P14	GTATCATCAA-dye	TTTTGATGATA
P15	CAACAAACTA-dye	TTTAGTTTGTT
P16	CAATTAAACG-dye	TTCGTTTAATT
P17	CAATTTTAGG-dye	TTCCTAAAATT
P18	CACACTTTAT-dye	TTATAAAGTGT
P19	CAGATCATAT-dye	TTATATGATCT
P20	CAGCTTAATA-dye	TTTATTAAGCT
P21	CATTCTATGT-dye	TTACATAGAAT

P22	CATTTCACAT-dye	TTATGTGAAAT
P23	CCAAAGTATT-dye	TTAATACTTTG
P24	CCATGATTAT-dye	TTATAATCATG
P25	CCTGTTTTAA-dye	TTTTAAAACAG
P26	CGAACTTTTT-dye	TTAAAAAGTTC
P27	CGAGTTATAT-dye	TTATATAACTC
P28	CGGTATAATT-dye	TTAATTATACC
P29	CGTCAATATA-dye	TTTATATTGAC
P30	CTATGCTTTA-dye	TTTAAAGCATA
P31	CTGTAAATTC-dye	TTGAATTTACA
P32	CTGTTGAAAA-dye	TTTTTTCAACA
P33	CTTAGTTGAT-dye	TTATCAACTAA
P34	CTTATAGTTC-dye	TTGAACTATAA
P35	CTTCTGTTAT-dye	TTATAACAGAA
P36	CTTTGAGATT-dye	TTAATCTCAAA
P37	GACACTAAAT-dye	TTATTTAGTGT
P38	GAGAACATAA-dye	TTTTATGTTCT
P39	GATAAGATAG-dye	TTCTATCTTAT
P40	GATACACATA-dye	TTTATGTGTAT
P41	GATTTATCCA-dye	TTTGGATAAAT
P42	GCAAGATTAA-dye	TTTTAATCTTG
P43	GCATTCAAAA-dye	TTTTTTGAATG
P44	GCTTTTCTTT-dye	TTAAAGAAAAG
P45	GGTTTTTATG-dye	TTCATAAAAAC
P46	GTATATCACA-dye	TTTGTGATATA
P47	GTATGACTTT-dye	TTAAAGTCATA

P48	GTCGATTTTT-dye	TTAAAAATCGA
P49	GTGTACTATT-dye	TTAATAGTACA
P50	GTTAAGGAAA-dye	TTTTTCCTTAA
P51	GTTTACGATT-dye	TTAATCGTAAA
P52	GTTTCGTATA-dye	TTTATACGAAA

Table 2. *Primary antibodies used in indirect immunostaining multiplexing*

Target	**Antibody commercial source**	**Species**
Tubulin (alpha)	Thermo-Scientific (MA1-80017)	Rat
Nuclear Pore Complex	abcam (ab24609)	Mouse
Mitochondria (Tom20)	Santa Cruz (sc-11415)	Rabbit
EGFR	ImClone Systems (Cetuximab)	Human
Paxillin	R&D systems (AF4259)	Sheep
Vimentin	abcam (ab24525)	Chicken
Pan Cytokeratin	Acris Antibodies (BP5069)	Guinea pig

Table3. *Secondary antibodies used in indirect immunostaining multiplexing*

Target	**Host**	**Specification and commercial source**
Rat	Donkey	Donkey Anti-Rat IgG (H+L) (min X Bov, Ck, Gt, GP, SyHms, Hrs, Hu, Ms, Rb, Shp Sr Prot) Jackson ImmunoResearch Laboratories, INC. (712-005-153)
Mouse	Donkey	Donkey Anti-Mouse IgG (H+L) (min X Bov, Ck, Gt, GP, Sy Hms, Hrs, Hu, Rb, Rat, Shp SrProt) Jackson ImmunoResearch Laboratories, INC. (715-005-151)
Rabbit	Donkey	Donkey Anti-Rabbit IgG (H+L) (min X Bov, Ck, Gt, GP, Sy Hms, Hrs, Hu, Ms, Rat, Shp Sr Prot) Jackson ImmunoResearch Laboratories, INC. (711-005-152)

Human	Donkey	Donkey Anti-Human IgG (H+L) (min X Bov, Ck, Gt, GP, Sy Hms, Hrs, Ms, Rb, Rat, Shp Sr Prot) Jackson ImmunoResearch Laboratories, INC. (709-005-149)
Sheep	Donkey	Donkey Anti-Sheep IgG (H+L) (min X Ck, GP, Sy Hms, Hrs, Hu, Ms, Rb, Rat Sr Prot) Jackson ImmunoResearch Laboratories, INC. (713-005-147)
Chicken	Donkey	Donkey Anti-Chicken IgY (IgG) (H+L) (min X Bov, Gt, GP, Sy Hms, Hrs, Hu, Ms, Rb, Rat, Shp Sr Prot) Jackson ImmunoResearch Laboratories, INC. (703-005-155)
Guinea pig	Donkey	Donkey Anti-Guinea Pig IgG (H+L) (min X Bov, Ck, Gt, Sy Hms, Hrs, Hu, Ms, Rb, Rat, Shp Sr Prot) Jackson ImmunoResearch Laboratories, INC. (706-005-148)

Chapter III

Highly multiplexed *in situ* protein imaging using DNA-Exchange-Imaging

This chapter contains contents from publication:

1. Wang, Y., Woehrstein, J.B., Donoghue, N., Dai, M., Avendaño, M.S., Schackmann, R.C.J., Zoeller, J.J., Wang, S.S.H., Tillberg, P.W., Park, D., Lapan, S.W., Boyden, E.S., Brugge, J.S., Kaeser, P.S., Church, G.M., Agasti, S.S. §, Jungmann, R. § and Yin, P. § (2017). Rapid sequential in situ multiplexing with DNA exchange imaging in neuronal cells and tissues. Nano letters, 17(10), pp.6131-6139.

3.1. Abstract

I present here a practical and robust method, DNA-Exchange-Imaging (DEI), for rapid *in situ* spectrally-unlimited multiplexing. This technique overcomes speed restrictions by allowing for single-round immunostaining with DNA-barcoded antibodies, followed by rapid (less than 10 minutes) buffer exchange of fluorophore-bearing DNA imager strands. The programmability of DNA-Exchange-Imaging allows us to apply it to diverse microscopy platforms (with Exchange-Confocal, Exchange-SIM, Exchange-STED, and Exchange-PAINT demonstrated here) at multiple desired resolution scales (from ~300 nm down to sub-20-nm). I optimized and validated the use of DEI in complex biological samples, including primary neuron cultures and tissue sections. These results collectively suggest DNA-Exchange as a versatile, practical platform for rapid, highly multiplexed *in situ* imaging, potentially enabling new applications ranging from basic science, to drug discovery, and to clinical pathology.

3.2. Concept of DNA-Exchange-Imaging

In DEI, we employ DNA-barcoded antibodies, instead of dye-labeled antibodies, that are conjugated with short DNA oligonucleotides (from 9 to 21 nucleotides) called docking strands. Multiplexed protein target labeling is performed efficiently by single-step simultaneous immunostaining with antibodies carrying orthogonal DNA docking strands, followed by image acquisition where dye-labeled complementary imager strands are applied sequentially via rapid buffer exchange (**Figure 14**). The washing buffer condition varies depending on the length of imager strands. Lowering salt concentration is sufficient to remove short imager strands (9 to 11 nucleotides). Chemical reagents, such as formamide, can be used to break imager and docking strands binding if longer strands are used. Cleavable groups, such as disulfide bonds[67], can also be introduced between fluorophores and imager strands, allowing signal removal through incubation in reducing environment (e.g. TCEP).

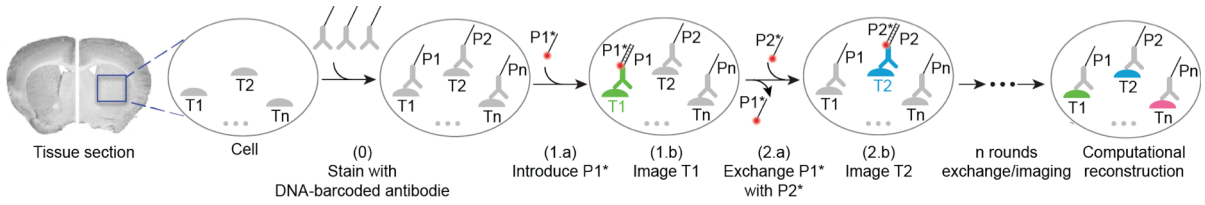

Figure 14. Concept of DNA-Exchange-Imaging Distinct targets (T1, T2, … ,Tn) are labeled using corresponding antibodies conjugated to orthogonal DNA docking strands (P1, P2, …, Pn) in a single step. Imager strands (P1*, P2*, …, Pn*) are sequentially introduced to visualize target signals. The imager strands are washed away rapidly using washing buffer after each round of imaging. After imaging, all images are computationally registered and a final merged image is reconstructed by assigning pseudo-colors to each target image.

DEI is a generalized platform that is based on Exchange-PAINT and applies the DNA-Exchange scheme to various imaging methods to enable both diffraction-limited and super-resolution highly multiplexed imaging. In this chapter, I demonstrated a series of DNA-Exchange-Imaging techniques with progressively increased optical resolutions, including Exchange-Confocal, Exchange-SIM, Exchange-STED and Exchange-PAINT.

3.3. DNA-Exchange-Confocal-Imaging in cell culture and tissue samples

Despite the superior resolution of Exchange-PAINT, its utility is restricted due to its imaging time and depth tradeoff. It requires recording a time-lapse movie of single molecule blinking events for final SR image reconstruction, which typically takes minutes to even hours for a single reconstructed image. In addition, the high signal-to-noise ratio requirement for PAINT imaging, single-molecule-compatible microscopes (usually Total Internal Reflection Fluorescence microscopes) are necessary, limiting the imaging depth to typically a few hundred nanometers above the coverslip. Moreover, diffraction-limited imaging is often sufficient for experiments that only require single-cell resolution (*e.g.* pathological analysis). In super-resolution PAINT imaging, sparse labeling of targets with transiently binding imager strands is required for single-molecule localization. In contrast, diffraction-limited Exchange-Confocal imaging shown here aims to capture signals from all the molecules of a certain target in a single image frame, which requires pseudo-permanent and dense target labeling with imager strands. To achieve this, we tuned three parameters: imager/docking strand association time, imager strand concentration and camera exposure time. First, we designed imager/docking strand duplexes with higher binding affinity to attain a relatively slow dissociation rate (0.2 s^{-1} for a 10 base-pair duplex on average[68]) by increasing the length of the DNA duplex (**Figure 15a**). To minimize the number of unoccupied docking sites, we used a high concentration of imager strand (*e.g.* 10 nM as compared to 1 nM in single-molecule PAINT applications) to densely label the docking sites for the corresponding target (**Figure 15b**). Furthermore, we used longer camera exposure times

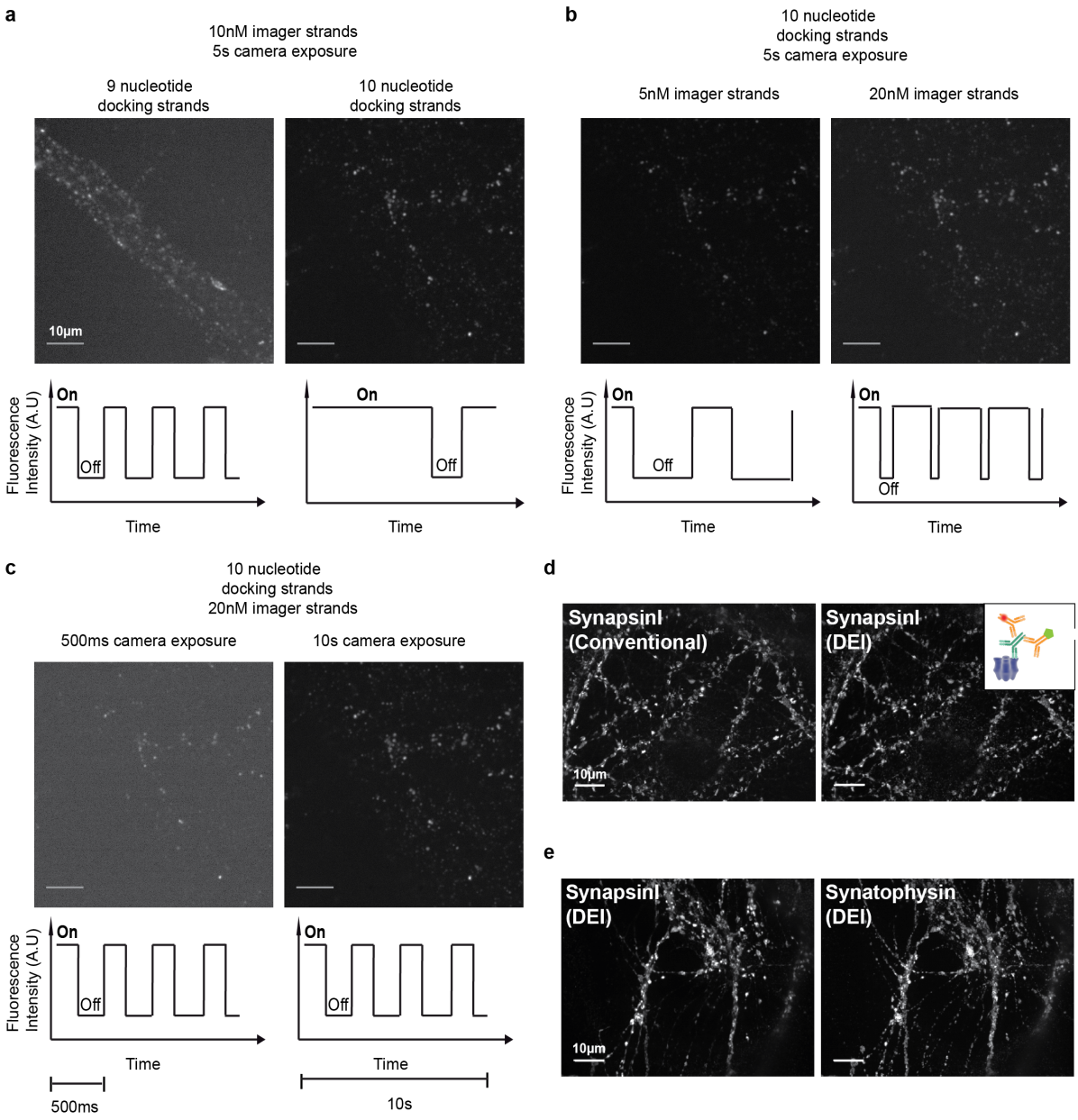

Figure 15. Adaption of DNA-PAINT for diffraction-limited imaging by using semi-stable binding imager/docking DNA duplex. a) Comparison of imaging quality using 9 nucleotide- and 10 nucleotide- docking strands conjugated antibodies targeting Bassoon that is a presynaptic active zone protein. The lower panel is a schematic fluorescence 'blinking' trace plot. The change of docking strand from 9 nucleotides to 10 nucleotides increases the duration of fluorescence 'on' state. **b)** Comparison of imaging quality of Bassoon using 5nM and 20nM imager strands. Increasing of imager strand concentration shortens the duration of fluorescence 'off; state. **c)** Comparison of imaging quality of Bassoon with 500ms and 10s camera exposure. Increased camera exposure time encompasses multiple 'blinking' events and enhances signal-to-noise ratio. **d)** Comparison of conventional staining using dye-conjugated antibodies and DEI using DNA-conjugated antibodies. Fixed neurons were stained with primary antibodies targeting SynapsinI, followed by both Alexa647-conjugated and DNA-conjugated antibodies, as shown in the schematic. DNA-conjugated antibody signals were visualized using Cy3b-imager strands. The correlation coefficient of the two images was 0.96. **e)** Co-localization of SynapsinI and Synaptophysin in neurons visualized using two rounds of

(typically 50 to 300 ms for a widefield microscope and 500 ms to 5 s for a spinning disk confocal microscope) to minimize unoccupied docking sites and enhance the signal-to-noise ratio (**Figure 15c**).

As a result, we achieved diffraction-limited Exchange-Confocal imaging with a quality comparable to that of conventional IF methods. To examine signal specificity of Exchange-Confocal, we compared the Exchange-Confocal images with those attained by conventional IF methods using fluorophore-conjugated antibodies (**Figure 15d**). We labeled synapses with the marker protein SynapsinI using primary antibodies followed by secondary antibodies conjugated either with DNA docking strands or with Alexa488 dye. The SynapsinI signals from Exchange-Confocal and from conventional IF were obtained with 561 nm and with 488 nm excitation, respectively. We observed co-localization of fluorescence signals from these two methods with a correlation coefficient of 0.96. We also performed Exchange-Confocal based co-localization analysis of SynapsinI and Synaptophysin, both of which are present in synaptic vesicles (**Figure 15e**). We obtained a correlation coefficient of 0.80, which is similar to values that have been reported using array tomography[69].

As Exchange-Confocal requires sequential application of imager strands labeled with the same fluorophore, efficient imager strand removal is critical. We tested changes in fluorescence intensity between each cycle of imager strand exchange (**Figure 16**). DIV14 mouse hippocampal neurons were fixed and stained with antibodies against glial fibrillary acidic protein (GFAP, a marker protein for astrocytes) and beta3Tubulin (a marker protein for neurons). P1* and P2* imager strands were sequentially applied to visualize GFAP and beta3Tubulin, respectively. The fluorescence intensity after washing with PBS decreased to the background level and thus was

negligible compared to signal levels in the other images, confirming sufficiently efficient removal of imager strands from the solution.

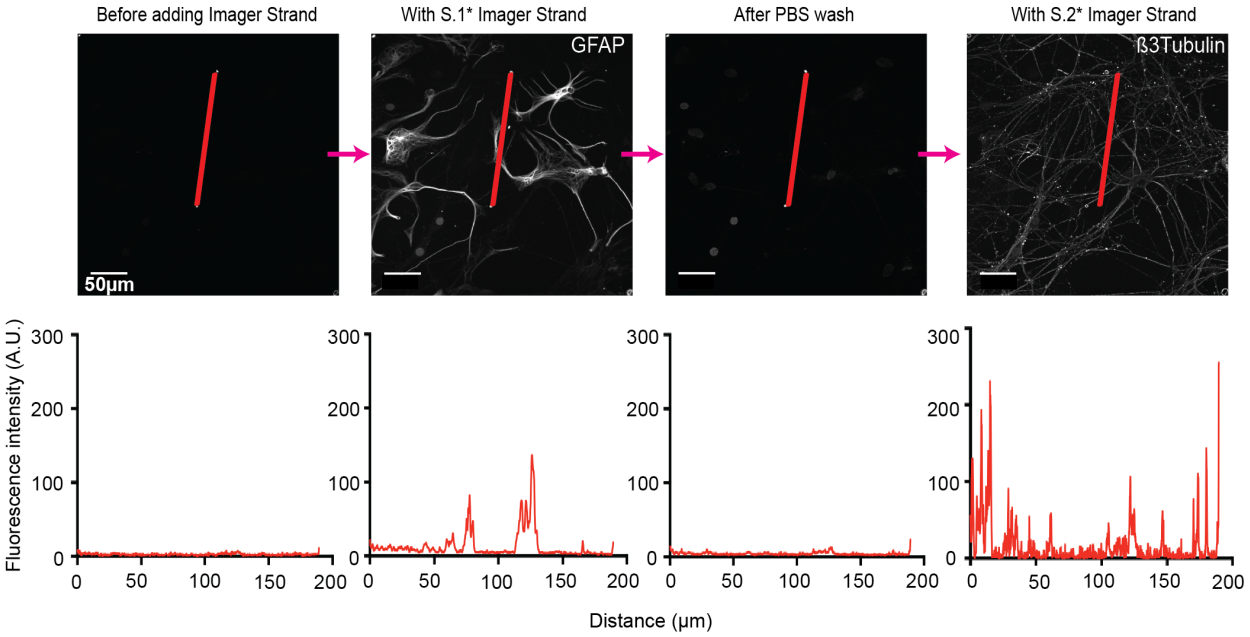

Figure 16. Demonstration of sequential application of imager strands for Diffraction limited DNA-Exchange-confocal imaging on neuron culture samples. The upper panels show the process of sequential application of imager strands to visualize GFAP and Beta3-Tubulin. All images were adjusted to the same scale. The fluorescence intensities along the red lines are shown in the lower panel, as measured using FIJI.

To demonstrate multiplexed Exchange-Confocal, we next imaged eight targets in a fixed primary mouse hippocampal neuron culture (**Figure 17**). SynapsinI antibodies were used to mark all synapses, and Vesicular GABA transporter (vGAT) antibodies labeled inhibitory synapses. Five other structural proteins were also labeled, including Microtubule associated protein2 (MAP2) (a dendritic marker), phosphorylated neurofilament heavy chain (pNFH) (in neurites), AlphaTubulin (a microtubule component), AcetylTubulin (a microtubule component) and GFAP (an astrocyte marker). DAPI was used to stain nuclei. For the eight protein targets, we performed dual-color imaging (using Cy3b- and Atto655-conjugated imager strands) to reduce probe exchange cycles. Sample drift was monitored by signals from the 488 nm channel, and images

were registered accordingly (**Figure 17b and c**). Three-dimensional (3D) images were taken for each target using a spinning disk confocal microscope and the color-coded 2D maximum

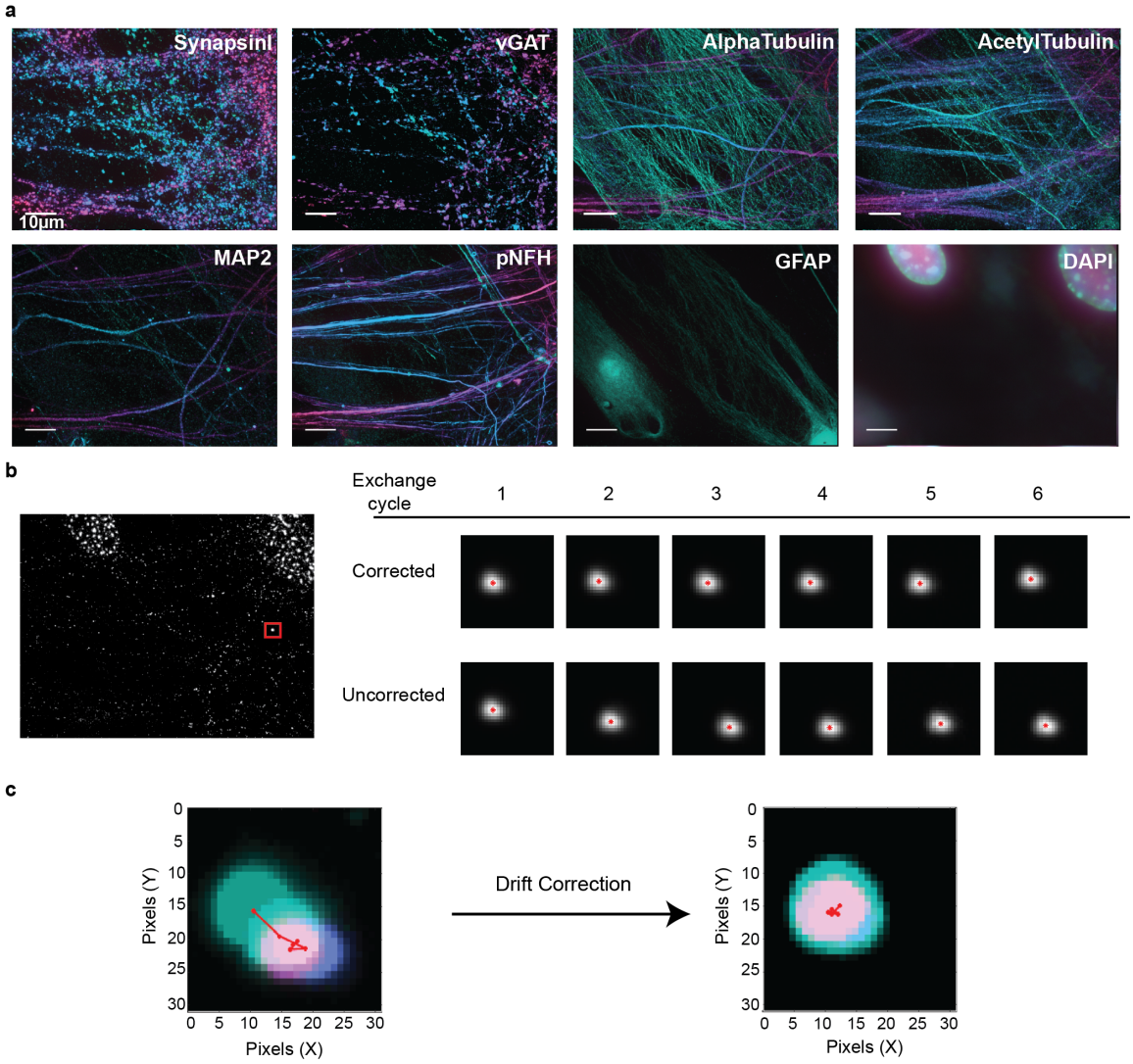

Figure 17. Highly multiplexed DNA-Exchange-confocal imaging on primary neuron culture. a) Multiplexed eight-target imaging in neurons. Fixed DIV (Days *in vitro*) 14 mouse hippocampal neurons were stained with DNA-conjugated antibodies against SynapsinI, vGAT, MAP2, pNFH, GFAP, AlphaTubulin and AcetylTubulin. A 3D image stack of 14 µm thickness in z-axis was taken for each target and displayed as 2D color-coded maximum intensity projection (bottom to top: green to red). **b)** Drift correction of images from multiple rounds of buffer exchange and imaging. Images on 488 nm laser channel (stained using gephyrin primary antibodies followed by Alexa488-labeled secondary antibodies in this experiment) were imaged on every cycle of imaging along with other targets. The bright signal indicated in the red box region was used for demonstration. The centroids of the selected spot were marked as red asterisks, and demonstrated in drift-corrected and uncorrected. **c)** Track of centroid positions of the selected marker in merged images from (b). The x- and y- axis indicted the pixel value, and the whole image is 31 × 31 pixels with a pixel size of ~ 64 × 64 nm^2.

projection images were displayed for each target (**Figure 17a**). We used green and red colors to represent the signals from the bottom and top focal planes respectively. A color gradient from green to red was used to represent the signals from intermediate focal planes. Astrocytes, labeled with GFAP, were mostly shown in green, consistent with the fact that astrocytes grew beneath neurons. SynapsinI labeled both excitatory and inhibitory synapses, while vGAT only labeled inhibitory synapses. As expected, SynapsinI signals were more abundant than those of vGAT. AlphaTubulin was observed in both astrocytes and neurons across the whole z-stack, and acetyl-Tubulin was highly expressed in neurons.

To test the applicability of Exchange-Confocal to tissue samples, we performed eight-target Exchange-Confocal in formaldehyde-fixed mouse retina tissue sections (**Figure 18a** and **b**). We chose retina samples because the tissue organization has been intensively studied and different cell types can be distinguished using protein markers[70,71]. A 40 μm thick retina section was stained using DNA-conjugated antibodies against SV2, GFAP, Cone arrestin, Chx10, Vimentin, and Synapsin, and imaged with six rounds of exchange using Cy3b-conjugated imager strands. Lectin-Alexa488 was used to stain blood vessels and imaged for every exchange cycle for image registration. DAPI was used to stain the nucleus. As expected, every protein species was truthfully detected using Exchange-Confocal with the distribution of each target being with previous reports[70-72]. SV2 and Synapsin are both located in synapses. SV2 exists in both Outer Plexiform Layer (OPL) and Inner Plexiform Layer (IPL), whereas Synapsin is only located in the IPL, similar to what has been reported in Salamander retina[73] (**Figure 18b**). It should be noted that SynapsinI antibody was used to stain the sample and the lack of Synapsin signal in the OPL only reflects the absence of SynapsionI, which could be replaced by alternative forms of Synapsin, such as Synapsin II or III. GFAP marks astrocytes that are located close to the

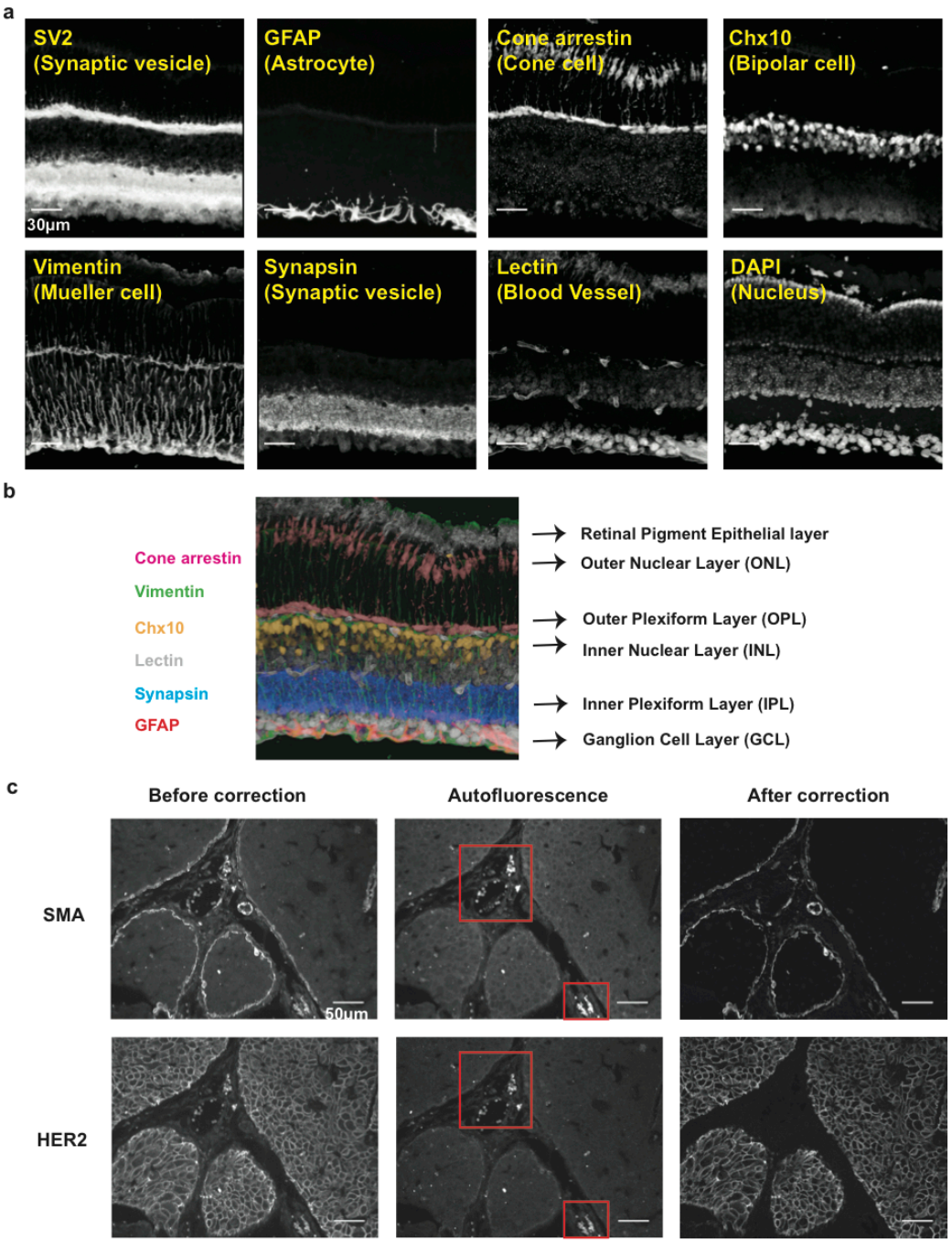

Figure 18. Highly Multiplexed DNA-Exchange-Confocal-Imaging in tissue samples. a) A 40 μm thick PFA-fixed mouse retina section was stained with antibodies targeting SV2, GFAP, Cone arrestin, Chx10, Vimentin, Synapsin. 3D images were taken with six rounds of exchange of Cy3b-labeled imager strands. Blood vessels were stained with Alexa488-conjugated lectin probes and imaged in every exchange cycle for image registration. The nucleus was stained with DAPI. **b)** Merged six-target image reveals different layers of cells in the retina. **c)** Autofluorescence correction with DEI on a paraffin-embedded breast tumor section. Autofluorescence images were taken before adding imager strands with the same laser intensity and camera exposure time, and then subtracted from the corresponding target images to obtain autofluorescence-corrected images. Note that the strong autofluorescence (presumably from blood cells, labeled with red square) was eliminated in the corrected images.

Ganglion Cell Layer (GCL) and Muller glial endfeet. Cone arrestin marks the cone photoreceptor cells in the Outer Nuclear Layer (ONL). Vimentin labels Muller cells that spread across multiple layers. Chx10 is a pan-bipolar cell marker[72] located in the Inner Nuclear Layer (INL).

We also tested Exchange-Confocal in paraffin-embedded tissue samples, and performed two rounds of probe exchange to visualize HER2 and smooth muscle actin (SMA) in a 4 μm formalin-fixed and paraffin-embedded intraductal breast tumor carcinoma tissue from a HER2+ xenograft of SUM225 tumor cells[74] (**Figure 18c**). SMA stains the myoepithelial cells surrounding the intraductal tumor as well as stromal fibroblasts. We also note that Exchange-Confocal permits simple autofluorescence correction, an additional advantage over conventional fluorescence imaging for tissue samples. Autofluorescence, caused by the presence of various endogenous molecules (e.g. reduced NAD(P)H, flavins, reticulin fibers, lipofuscins, elastin and collagen) can mask true target signals[75]. Although a few approaches have been developed, such as autofluorescence quenching using Sudan Black B, photobleaching with high intensity lasers and post-measurement image correction using complex mathematical models, they require optimization specific for each type of sample and/or may cause sample damage if harsh treatment is performed[75]. When performing DEI – as fluorophore-tagged imager strands are not added until the sample is ready to be imaged on the microscope – an image exhibiting only autofluorescence can be acquired immediately before the addition of imager strands, and subsequently subtracted from the true target image. In **Figure 18c**, autofluorescence signals were captured before addition of imager strands in the same field of view. Compared with images before correction, the 'false' signals indicated by the red arrows were significantly reduced in the corrected images. It should be noted that the laser intensity and camera exposure time for

autofluorescence images should be identical to those used for the real target image to ensure accurate correction.

Another feature of DNA-Exchange-imaging using semi-transient binding strands is photobleaching resistance (**Figure 19**). Fluophores can be typically photobleached upon

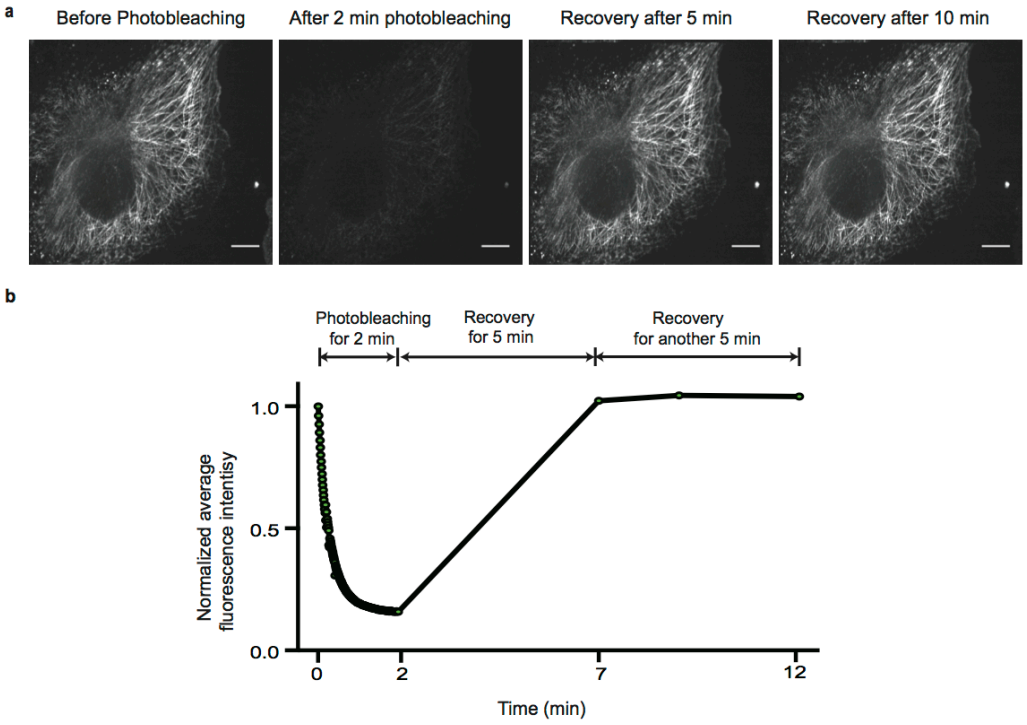

Figure 19. **Fluorescent signal recovery after photobleaching in DNA-Exchange-Imaging**. **a**) BSC1 cells were stained for Beta-tubulin and imaged using Cy3b-conjugated imager strands. Photobleaching was performed using a 561 nm laser with 30 mW excitation power. Fluorescence signal decreased after photobleaching. A series of 200 images were taken in 2 min with 600 ms camera exposure time for each image. Fluorescence was then allowed to recover for 10 min. Scale bars: 10 μm. **b**) Quantification of average fluorescence intensity of the images. The average fluorescence intensity dropped to 16% after 2 min of photobleaching and returned to ~100% after 5 minutes and remained the same afterwards.

sufficient long exposure to excitation lasers, and the rate of photobleaching depends on fluorophore species, the intensity of illuminating lasers and the buffer environment. Initial focusing and scanning of the specimen to locate the regions of interest often results in photobleaching of the fluorophores and hence undesired loss of fluorescent signals. Using conventional imaging methods with dye-conjugated antibodies, photobleaching is irreversible

and leads to permanent loss of fluorescence signals. However, in DEI, due to the semi-transient nature of the binding interaction between the imager strand and docking strand, a photobleached imager strand will be eventually replenished by an unbleached one in the solution, allowing the full recovery of transiently bleached fluorescence signals at the target site.

3.4. DNA-Exchange-SIM- and -STED- Imaging in cell culture samples

Although diffraction-limited Exchange-Confocal enables faster and deeper sample imaging, its resolution may not be sufficient to address certain biological questions that require subcellular resolution. To achieve this, we applied DNA-Exchange-Imaging to various fast super-resolution imaging microscopy platforms. First, we performed DEI using structured illumination microscopy (SIM), which doubles the achievable resolution[76]. Here in Exchange-SIM, we stained BSC-1 cells with antibodies against AlphaTubulin followed by DNA-conjugated secondary antibodies (**Figure 20a and b**). We measured the full width at half maximum (FWHM) of microtubules by Gaussian fitting the intensity plot of 20 microtubule cross-sections, and obtained an average of ~2-fold reduction in FWHM, consistent with the theoretical resolution enhancement for commercial SIM microscopes (**Figure 20c and d**). While improving spatial resolution helps to resolve fine molecular structures, it also renders the experiment more sensitive to sample drift during buffer exchange process. To reduce drift-induced errors, we adapted a phase correlation-based algorithm[77] to perform subpixel registration (see Methods for more details). The algorithm correctly identified sample drift between different exchange cycles and registered images accordingly (**Figure 20e**). Multiplexed SIM imaging was performed with four rounds of exchange with Cy3b-conjugated imager strands targeting alphaTubulin, Vimentin, Tom20, and betaTubulin (**Figure 20f**). An upsampling factor of 5 in x- and y-axis and a factor of

2 in z-axis were used to perform subpixel image registration, resulting in a subpixel precision of 5 nm in x and y-axis and 75 nm in z-axis.

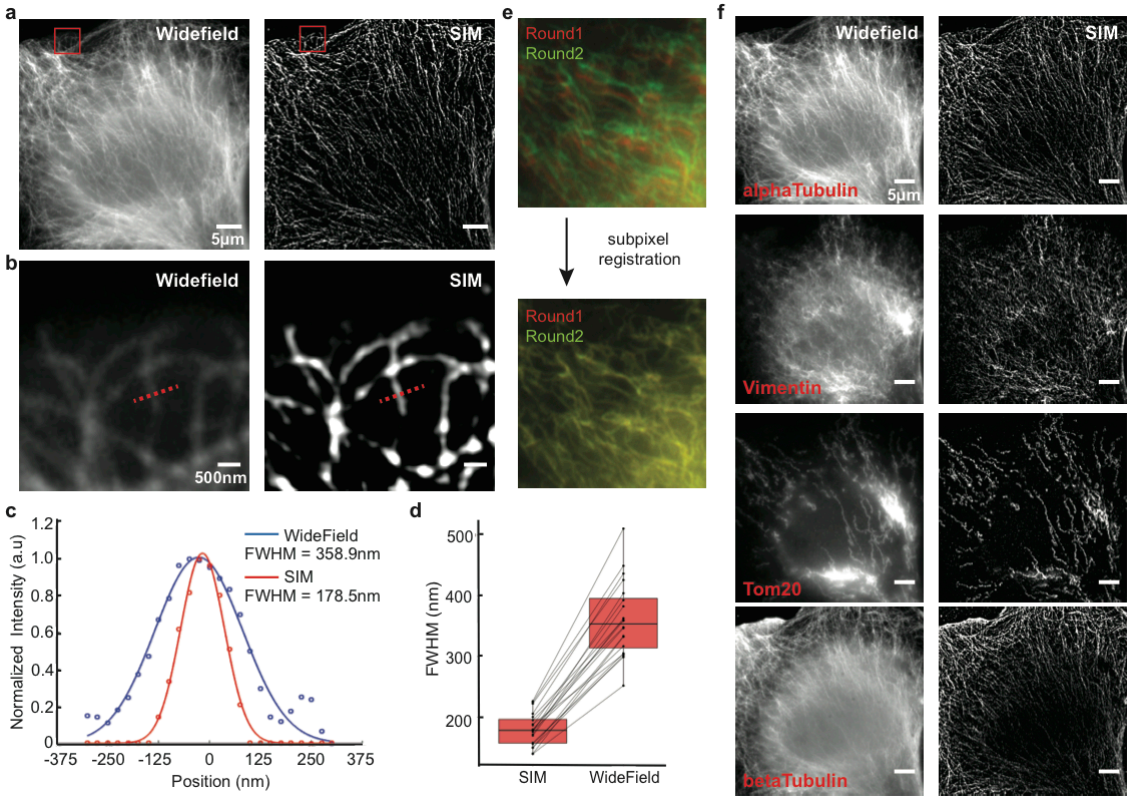

Figure 20. Multiplexed DNA-Exchange-SIM-imaging in BSC-1 cells. a) Comparison of widefield and SIM images on alphaTubulin. Scale bars: 5 µm. **b)** Zoom-in views of the microtubules highlighted by red square in **a**. **c)** Measurement of the apparent width of microtubules using Full width at half maximum (FWHM) criterion. The intensity plot of the cross-section highlighted in **b** was fitted using a Gaussian. **d)** FWHM measurement of 20 microtubule cross-sections revealed 2.014 ± 0.045 fold reduction of FWHM (the error range is SEM; boxes denote median values ± quartiles). **(e)** Subpixel registration of images in different exchange rounds. Vimentin was stained with both DNA-conjugated and Alexa488-labeled antibodies, and the 488 nm channel used for image registration. **(f)** Multiplexed 3D Exchange-SIM imaging in BSC-1 cells. The 2D maximum intensity projections are presented here. Scale bars: 5 µm.

A similar multiplexed experiment was performed using a STED microscope (**Figure 21**). Together with previous related Exchange-STED work applied to synthetic DNA nanostructures[78], our results show that DEI is generally compatible with SIM and STED microscopy and can be used for rapid multiplexed super-resolution imaging.

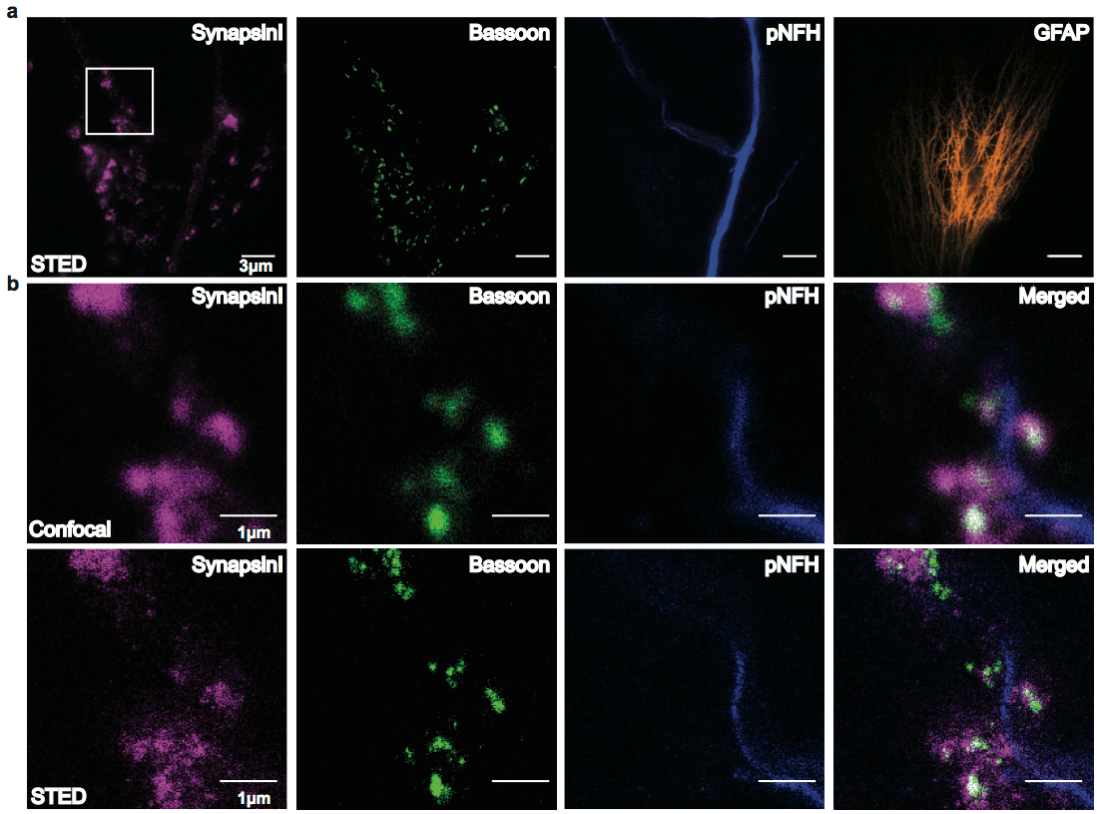

Figure 21. Multiplexed chromatic aberration-free Stimulated emission depletion (STED) imaging using DNA-Exchange-imaging. (a) Fixed DIV14 mouse hippocampal neurons were stained for GFAP, pNFH, SynapsinI and Bassoon. Four-round exchanges of Cy3b-conjugated imager strands were performed to acquire a 2D image for each target. It should be noted that GFAP was imaged in a region slightly under the other three targets because of the missing GFAP signal in the original region. Scale bar: 3 µm. **(b)** Magnified view of SynapsinI, Bassoon and pNFH from the white square region in (a). Confocal images of the same region are also presented for comparison. Scale bar 1 µm.

3.5. DNA-Exchange-PAINT imaging to visualize synaptic structures

For even higher spatial resolutions, we turned to our previous Exchange-PAINT method and demonstrated eight-target super-resolution imaging in cultured neurons. DIV14 mouse hippocampal neurons were fixed and stained with antibodies against AcetylTubulin, AlphaTubulin, Vimentin, Tom20, SynapsinI, Bassoon, vGAT, and Gephyrin. While synapsin1 and vGAT antibodies label all and inhibitory synaptic vesicle clusters, respectively, Bassoon is a marker for the presynaptic active zone and gephyrin marks postsynaptic scaffolds at inhibitory synapses. AcetylTubulin and AlphaTubulin are both microtubule components. Vimentin is a

protein component in intermediate filaments, and Tom20 is located in the mitochondria. Eight rounds of Exchange-PAINT imaging with Atto655-conjugated imager strands were performed to visualize each target (**Figure 22**).

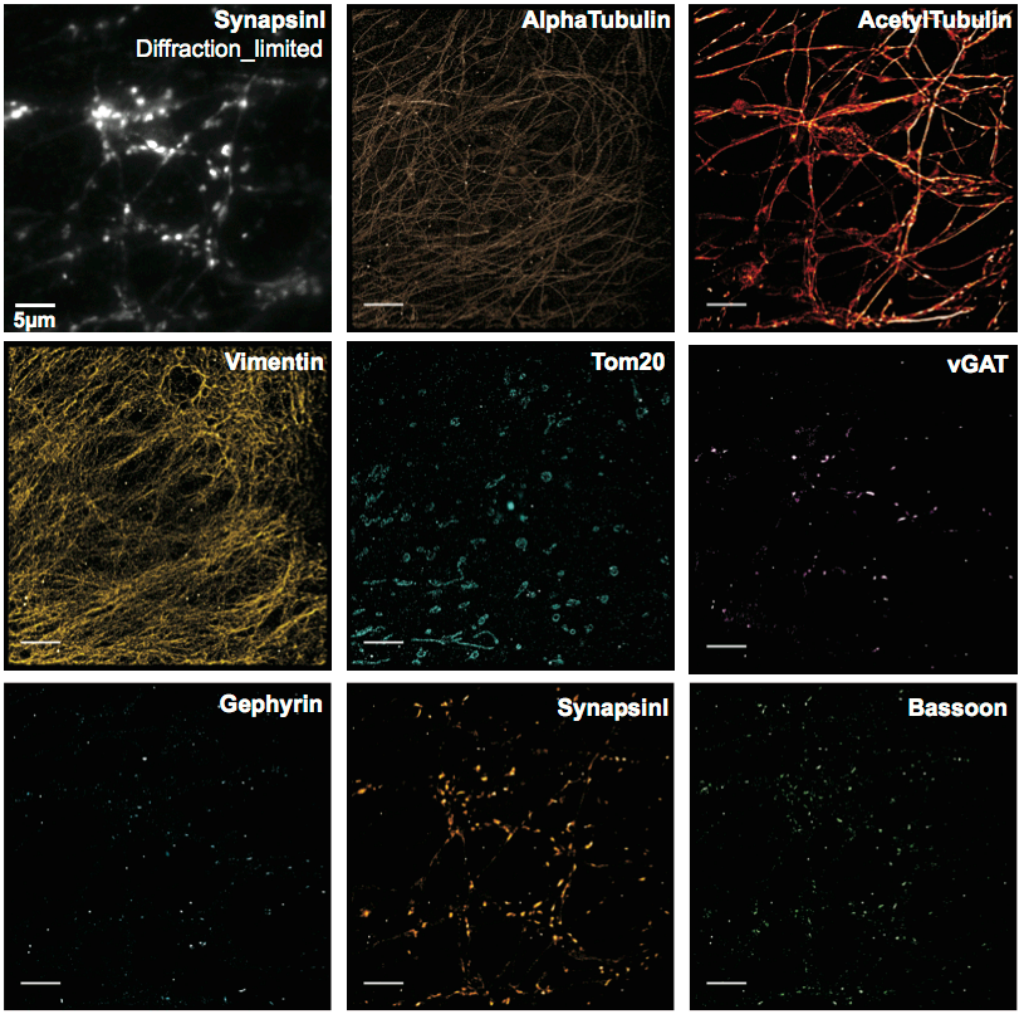

Figure 22. Eight-target chromatic aberration-free Exchange-PAINT imaging in primary neurons. Fixed DIV14 mouse hippocampal neurons were stained with DNA-conjugated antibodies targeting AlphaTubulin, Vimentin, vGAT, Gephyrin, SynapsinI, Bassoon, AcetylTubulin, and Tom20. SynapsinI was additionally labeled with Alex488-conjugated secondary antibodies for selecting regions of interest. In total, eight rounds of Exchange-PAINT imaging with Atto655-conjugated imager strands were performed to visualize all targets. Scale bar: 5 μm.

One unique application of multiplexed imaging is to detect protein-protein co-localization. To test the applicability of Exchange-PAINT for such studies, we merged the four synaptic protein images from **Figure 22** to assay co-localization of these proteins (**Figure 23a**). We first compared the diffraction-limited and super-resolution images. Individual synapses are difficult to

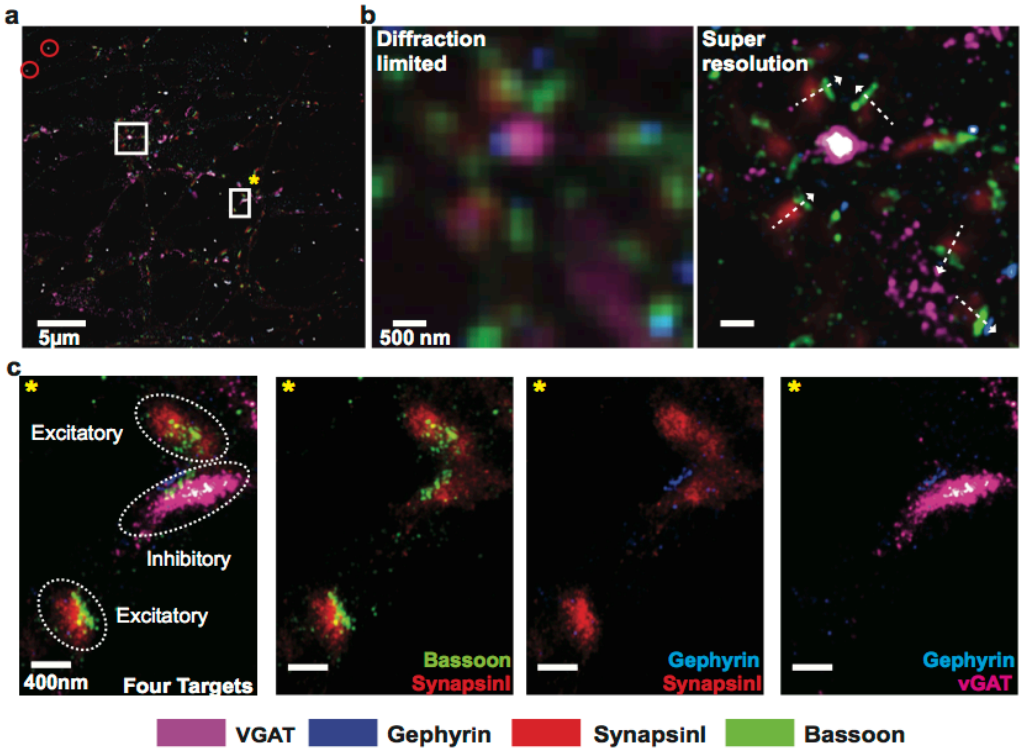

Figure 23. Co-localization of synaptic proteins detected using multiplexed Exchange-PAINT imaging. a) The images of synaptic proteins from **Figure 22** were merged using gold nanoparticles as registration markers (highlighted with red circles). Scale bar: 5 µm. **b)** Comparison of diffraction-limited and super-resolution images of four synaptic proteins from the region highlighted with a white square without *. The orientation of synapses could be visualized in the super-resolved image as indicated by the white dashed arrows. Scale bar: 500 nm. **c)** One region from **a** was selected for a magnified view (highlighted with a white square with *). Scale bars: 400 nm.

distinguish from each other in the diffraction-limited images but can be clearly visualized in the super-resolution images (**Figure 23b**). Particularly, the synapse orientation can be detected by lining synapsin (synaptic vesicle marker that is further from the presynaptic membrane), Bassoon (active zone marker that is closer to the presynaptic membrane) and gephryin (postsynaptic

density marker on the postsynaptic sites) (**Figure 23b**). We also selected one region for a magnified view (**Figure 23c**). SynapsinI and Bassoon are known to be present in both excitatory synapses and inhibitory synapses, whereas vGAT and Gephyrin selectively label inhibitory synapses[69]. Three synapses were included in this region. Two of them contained only SynapsinI and Bassoon signals, suggesting they were excitatory synapses, whereas the middle synapse contained all four targets, indicating that it was an inhibitory synapse (**Figure 23c**). SynapsinI, Bassoon and vGAT were present in the presynaptic site and therefore well separated from the signal from Gephyrin that existed in the postsynaptic site. The distribution patterns of SynapsinI and vGAT, both of which were localized on synaptic vesicles, correlated well with each other. The result indicates Exchange-PAINT is well suited for high-resolution visualization of protein-protein co-localization *in situ*.

3.6. Comparison between transient, semi-transient and stable binding of imager/docking DNA duplex

DNA-PAINT utilizes transient binding of imager DNA sequence to docking DNA sequence on antibodies to enable fast blinking of fluorescence signals. Exchange-confocal/SIM/STED described above employs semi-transient binding, aiming to capture the signal from targets in a signal frame image. Stable binding can also be used as shown in Schueder et al. and Kishi et al.[79,80]. We compared these three schemes and listed the pros and cons in **Table 4**.

Table 4. Comparison of transient, semi-transient and stable binding of imager/docking DNA duplex.

Binding scheme	Transient	Semi-transient	Stable
Pros	• Fast blinking frequency that allows DNA-PAINT imaging • Easy removal of signal from the previous cycle • Resistant to photobleaching • Faster imaging as no need to remove excessive imager strands	• Longer binding duration on docking sites enables confocal and other platform imaging • Easy removal of signal from the previous cycle • Resistant to photobleaching • Faster imaging as no need to remove excessive imager strands	• Superior signal-to-background ratio • Suitable for widefield and STORM imaging
Cons	• Only suitable for DNA-PAINT imaging • Requires high signal-to-background ratio microscopy (e.g. TIRF, light sheet, spinning disc confocal) for imaging	• Not suitable for STORM imaging. • Widefield imaging requires post-imaging deconvolution processing. • Lower signal-to-background compared with stable binding; requires experimental adjustment of imager strand concentration and laser intensity to get optimal imaging setting	• Requires long incubation time and additional wash to remove excessive imager strands prior to imaging. • Requires harsher washing condition (e.g. 30% formamide for 12mer) to remove signal from the previous cycle. • Sensitive to photobleaching
Application	DNA-PAINT	Confocal, SIM, STED, Expansion microscopy	Widefield, Confocal, SIM, STED, STORM, Expansion microscopy

The DNA sequences and antibodies used in this study are listed in **Table 5 to 12**.

3.7. Methods

Cultured cells preparation and staining

All animal procedures were in accordance with the National Institute for Laboratory Animal Research Guide for the Care and Use of Laboratory Animals and approved by the Harvard Medical School Committee on Animal Care and the Massachusetts Institute of Technology Committee on Animal Care.

Hippocampal neuron cultures were prepared from postnatal day 0 or 1 mice and plated on eight-well Lab-Tek II chambers with a density of 10,000 ~ 15,000 cells per well. Cells were grown for 14 days before fixation. Neurons used in Figure 18 were fixed using precooled methanol at -80 °C followed by three 5 minute PBS washes. Neurons used in other figures were fixed using 4% formaldehyde for 15 minutes at 37 °C, followed by quenching in 50 mM NH_4Cl for 10 minutes. HeLa cell and BSC-1 cells were plated on eight-well Lab-Tek II chambers (15,000 cells per well) and grown for 24 hours. BSC-1 cells used in SIM experiments were fixed using 3% Paraformaldehyde (PFA), 0.1% Glutaraldehyde, and 0.1% Triton X-100 for 12 minutes. Cells used in other experiments were fixed with 4% PFA.

Cells were then permeabilized and blocked in 0.1% Triton X-100, 0.1% Tween20, 3% Acetyl-BSA and 5% normal donkey serum for 2 hours. Specimens were incubated with primary antibodies diluted in incubation buffer (0.1% Triton X-100, 0.1% Tween20, 3% IgG-free BSA) overnight at 4 °C, and then washed with washing buffer (0.1% Tween20, 1% IgG-free BSA) for five times (brief wash for the first two washes and 10 minute incubation for the other three washes). DNA-labeled secondary antibodies (Jackson ImmunoResearch, conjugated in house) diluted in incubation buffer were incubated with samples for 2 hours at room temperature and then washed as for primary antibodies. In multiplexed detection experiment in which primary

antibody-DNA docking strand conjugates were used, the sample was left on the microscope to maintain the position for imaging. Conjugated primary antibodies were diluted in incubation buffer and incubated with samples for 2 hours at room temperature, followed by PBS wash as described above. Post-staining fixation using 4% paraformaldehyde for 10 minutes followed by 5 minute quenching is recommended but optional.

Mouse retina section preparation and staining

Animals were given a lethal dose of sodium pentobarbital (120 mg/kg) (MWI, 710101) and enucleated immediately. Eyes were removed and fixed in PFA for 15-30 min. Following dissection, retinas were immersed in 30% sucrose overnight prior to freezing in TFM (EMS, 72592) and cryosectioning at 40 μm. Coverslips were treated with poly-D-Lysine overnight, followed by PBS washes. Retina sections were washed with PBS + 0.3% Triton X-100 for three times with five minutes per wash. They were then blocked and stained as above. Note that SV2 was stained using DNA-primary antibody conjugates whereas other targets were stained using primary antibodies followed by DNA-secondary antibody conjugates.

Breast tumor section preparation and staining

Ductal carcinoma *in-situ* tumors were generated using the SUM225 cell line as described previously[81]. Tumor tissues were formalin fixed and paraffin embedded 4 μm sections were mounted onto coverslips (24 × 50 mm no.1.5 VWR #48393.241) pre-treated with Silane solution (Leica Biosystems #3803120) to prevent tissue detachment during processing. Slides were baked for 1 hour at 60 °C, followed by deparaffinization in 100% xylene (Sigma 534056) for 5 minutes twice, and rehydrated by ethanol series (2 time for 2 minutes each 100% with EtOH, 1 time for 2

minutes with 70% EtOH, 1 time for 2 minutes with 50% EtOH, 1 time for 2 minutes with 25% EtOH, 1 time for 5 minutes with ddH_2O). The coverslips were incubated in antigen retrieval solution (IHCworld Cat# IW-1100) and placed in a steamer (Black & Decker HS1050) for 40 minutes (cold start). Slides were allowed to cool to room temperature for 20 minutes, followed by two washes of 5 minutes in ddH_2O. Blocking was performed using 5% goat serum (Invitrogen #16210) in 1× Tris-buffered saline (TBS) for 30 minutes at room temperature. Tissue sections were incubated in TBS with 2.5% goat serum containing anti-HER2 and anti-SMA primary antibodies for 1 hour at room temperature. Slides were incubated with DNA-conjugated secondary antibodies for 1 hour at room temperature and stored in TBS until imaging.

Diffraction-limited image acquisition

The diffraction-limited images for cell cultures and breast tumor samples were acquired with a Yokogawa spinning disk confocal CSU-X1 unit on a Nikon Ti inverted microscope. Cell culture images were acquired using a 100× Plan Apo NA1.4 oil-immersion objective whereas tumor samples images were acquired using a 20× / 0.75 NA dry objective with additional 1.5× magnification. Alexa488 was visualized using the 488 nm laser (1.74 mW, out of objective) and 525/50 emission filter; YFP was visualized using the 515 nm laser (1.89 mW) and 535/30 emission filter; Cy3b was visualized using 561 nm laser (4.02 mW) and 620/60 emission filter; Atto655 was visualized by the 647 nm laser (7.2 mW) and 700/75 emission filter. Images were collected with an ORCA-AG cooled CCD camera from Hamamatsu and Metamorph software.

In multiplexed imaging in neuron cultures, SynapsinI, vGAT, MAP2, pNFH and AlphaTubulin were stained using primary antibodies from five species, followed by DNA-conjugated secondary antibodies. After imaging, two primary antibodies that are directly

conjugated with DNA docking strands were introduced to target AcetylTubulin and GFAP, surpassing the limitation of available antibody species. Sequential imager strand application was performed manually with gel-loading tips. Imager strands were diluted in 1× PBS/ 500 mM NaCl with a concentration of 10 nM. 1× PBS with 0.1% Tween 20 was used as washing buffer to remove imager strands.

The images for mouse retina tissue samples were acquired using a Zeiss Axio Observer with LSM 710 scanning confocal system. The images were 1024*1024 pixels and acquired at acquisition speed 7. Each image was acquired by averaging 4 images. The retina multiplexing experiment was performed by six rounds of buffer exchange of Cy3b-tagged imager strands. The scale was adjusted to the same range using FIJI for comparison. To facilitate imager strand removal in thick tissue sample, 0.1× PBS with 0.1% Tween 20 was used as washing buffer in the exchange tissue imaging experiment.

Multiplexed Structured Illumination image acquisition

BSC1 cells grown in Lab-Tek chambers were fixed and stained with primary antibodies targeting alphaTubulin, betaTubulin, Tom20 and Vimentin, followed by DNA-conjugated secondary antibodies. Alexa488-conjugated anti-chicken (Vimentin) secondary antibodies was added along with DNA-conjugated secondary antibodies in about 1:10 ratio (dye conjugated and DNA-conjugated anti-chicken antibodies). Antibodies were fixed using 4% PFA after staining. The multiplexed images were acquired by four rounds of buffer exchange of Cy3b-tagged imager strands. All 3D-SIM data was collected on a Zeiss ELYRA system with a 63×/1.40 N.A Plan Apo oil immersion objective lens. Image stacks were acquired with a z-step of 150 nm and with 25 raw images per plane (five phases and five angles). Super-resolution images were

computationally reconstructed from the raw data set with a built-in algorithm in the Zeiss software. Buffer exchange was performed using flow cell chambers described in Jungmann et al.[51]. Glox oxygen scavenger system was added to the imaging buffer to prevent photobleaching. 0.1× PBS was used as washing buffer to facilitate imager strand removal.

Multiplexed STED image acquisition

Images were acquired using Leica SP8 X with STED 3X microscope system. Leica 100X/1.4 oil objective specialized for STED imaging is used. Green and Red channel laser/detection were set up as 488 nm/(500-540 nm) and 561 nm/(570-630 nm). Imaging was performed at zoom 5 with 1024 × 1024 format, yielding 23 nm pixel size to match STED imaging resolution requirement. Multiple line accumulation and frame average were used to increase STED image Signal-to-Noise quality. SynapsinI was stained also with Alexa488-conjugated secondary antibodies and its signal from 488 nm laser channels were used for image registration.

Super-resolution Exchange-PAINT image acquisition

Images were acquired using an inverted Nikon Eclipse Ti microscope, applying an objective-type TIRF configuration using a Nikon TIRF illuminator with a 100×, NA1.49 oil-immersion objective (CFI Apo TIRF). Two sets of lasers and emission filters were used: 488 nm (200 mW nominal, Coherent Sapphire) / ET525/50 nm and 647 nm (300 mW nominal, MBP Communications) / ET700/75 nm. Images were captured on an electron-multiplying (EM) CCD camera (iXon X3 DU-897, Andor Technologies). The CCD readout rate was set to 3 MHz at 16 bit and 5.1 pre-amp gain. No EM gain was used. 30,000 frames with 100 ms integration time were acquired for each target. 80 nm gold nanospheres (Microspheres-Nanospheres) were used

as fiducial markers for drift and alignment markers. The z-axis focal planes were kept constant for all the synaptic proteins, SynapsinI, Bassoon, vGAT and Gephyrin, while the focal planes were adjusted for four other structural proteins to obtain images of optimal quality. Sequential imager strand application was performed manually with gel-loading tips. Imager strands were diluted in 1× PBS/ 500 mM NaCl with a concentration of 3 nM. 1× PBS with 0.1% Tween 20 was used as washing buffer to remove imager strands.

Image processing and analysis

For super-resolution PAINT images, the time-lapse imaging movies were saved as Raw Data using FIJI and imported into custom-written program in MATLAB. The final images were reconstructed using spot-finding and 2D-Gaussian fitting algorithms. A simplified version of this software is available for download at http://molecular.systems/software or http://www.dna-paint.net. The image alignment for the merged synaptic protein image was performed by overlaying gold nanoparticles manually.

Image registration for diffraction-limited data acquired by the spinning disk confocal microscope was performed as follows: since samples were maintained on the stage and all microscope settings were kept the same during the entire experiment, only rigid transformation (translation and rotation) will be considered and corrected. The spinning disk confocal microscope contained the Nikon perfect focus system to maintain z-position. Therefore, drifts in only x- and y-axis were corrected. Signals from 488 nm laser channel were captured in every exchange cycle and served as the reference for sample drift. Images were first corrected for translation using a Fast Fourier Transformation (FFT)-based phase correlation algorithm, and

then corrected for rotation using a Harris feature extraction and matching algorithm with Matlab built-in functions. The transformation matrices were applied to target images.

Image registration for 3D diffraction-limited retina imaging was performed using an algorithm developed by Hunter Elliott from Harvard Medical School Image and Data analysis core. The images were first filtered with a gradient filter and the intensity was then normalized. 3D FFT- based phase correlation was performed to calculate the image shift.

Subpixel Image registration for SIM and STED was performed based on an algorithm developed by Guizar-Siciros M, et al.[77] (the Matlab code is available from Mathworks and the detailed algorithm was described in the original paper). The initial code was written for 2D image registration but it can be extended to 3D by adding one dimension. For 3D SIM data, the reference image f and target image g were first converted to frequency domain F and G using FFT. The normalized cross-spectrum is defined as $R = F \times G^*/|F \times G^*|$, where G^* denotes the complex conjugate of G. To have an upsampling factor of 2, R was zero padded into a larger array of dimension (2x, 2y, 2z). This number can be further increased. However, it can be very computationally expensive. Further upsampling was achieved in the 1.5x1.5 pixel region of the estimated peak of cross-correlation using matrix multiplication discrete Fourier Transformation. For STED data, only 2D image registration was performed using the same method.

Cross correlation studies for were performed using normxcorr2 function in Matlab.

Antibody-DNA conjugation

The conjugation involves crosslinking of thiol-modified DNA oligonucleotidess to Lysine residues on antibodies described in Chapter 2. In brief, 250 uM 5' thiol-modified DNA oligonucleotides (Integrated DNA Technologies) were activated by 100 mM DTT for 2 hours

and then purified using NAP5 columns (GE Healthcare Life Sciences, 17-0853-02) to remove excessive DTT. Antibodies formulated in PBS only were concentrated using 100KDa Ambicon Ultra Filters (EMDMillipore, UFC510096) to 2 mg/ml and reacted with maleimide-PEG2-succinimidyl ester crosslinkers (Singma 746223) for 2 hours. Antibodies were then purified using 0.5ml 7kDA Zeba desalting columns (LifeTechnologies, 89883) to remove excessive crosslinkers. Activated DNA oligonucleotides were incubated with antibodies (11:1 DNA: Antibody ratio) overnight at 4 °C. Final conjugated antibodies were washed using PBS/BSA (100ug/ml) in Ambicon Ultra Filters four times to remove nonreacted DNA oligonucleotides. Conjugated antibodies were kept at 4 °C. The SV2 antibody used in Figure 3 was conjugated using the SiteClick kit from ThermoFisher (S10467). The DBCO-modified DNA oligos were purchased from Boston Open Labs.

Table 5. *DNA-Exchange-Imaging docking and imager strand sequences used in this study*

Description	Docking Strand Sequence	Imager Strand Sequence
P1	5'-TTTCTTCATTA-3'	5'-GTAATGAAGA-Dye
P2	5'-TTATCTACATA-3'	5'-TATGTAGATC-Dye
P3	5'-TTATGAATCTA-3'	5'-GTAGATTCAT-Dye
P4	5'-TTTCAATGTAT-3'	5'-CATACATTGA-Dye
P5	5'-TTAATTAGGAT-3'	5'-CATCCTAATT-Dye
P6	5'-TTAATTGAGTA-3'	5'-GTACTCAATT-Dye
P7	5'-TTTATATTGAC-3'	5'-CGTCAATATA-Dye
P8	5'-TTATGTTAATG-3'	5'-CCATTAACAT-Dye
P9 (10 nt)	5'-TTTCTTCATTAC-3'	5'-GTAATGAAGA-Dye
P10 (10 nt)	5'-TTGATCTACATA-3'	5'-TATGTAGATC-Dye
P11 (10 nt)	5'-TTATGAATCTAC-3'	5'-GTAGATTCAT-Dye

P12 (10 nt)	5’-TTAATTAGGATG-3’	5’-CATCCTAATT-Dye
P13 (10 nt)	5’-TTATGTTAATGG-3’	5’-CCATTAACAT-Dye
P14 (10 nt)	5’-TTAATTGAGTAC-3’	5’-GTACTCAATT-Dye
P15	5’-TTATAGTGATT-3’	5'-GAATCACTAT-Dye
P16 (10 nt)	5’-TTATACATCTAG-3’	5'-CTAGATGTAT-Dye
P17 (10 nt)	5’-TTTTAGGTAAAG-3’	5'-CTTTACCTAA-Dye
P18	5’-TTATAGTGATTC-3’	5'-GAATCACTAT -Dye

Table 6. *Antibodies used in this study*

Target	**Antibody**	**Species**
AcetylTubulin	Invitrogen (32-2700)	Mouse
AlphaTubulin	ThermoFisher(MA1-80017)	Rat
Bassoon	Abcam (ab82958)	Mouse
Beta3Tubulin	ThermoFisher (MA1-19187)	Mouse
Chx10	ThermoFisher (PA1-12566)	Sheep
Cone arrestin	Millipore (AB15282)	Rabbit
Gephyrin	SynapticSystem (147108)	Human
GFAP	Invitrogen (13-0300)	Rat
GFAP	Encor (MCA-5C10-AP)	Mouse
GFP/YFP	Invitrogen (PA5-22688)	Rabbit
HER2	Dako #A0485	Rabbit
MAP2	SantaCruz (sc5359)	Goat
pNFH	EnCor (CPCA-NF-H)	Chicken
SMA	Dako #M0851	Mouse
SV2	DSHB	Mouse
SynapsinI	Abcam (ab8)	Rabbit
SynapsinI/II	SynapticSystem (106004)	Guinea Pig
Synaptophysin	SynapticSystem (101004)	Guinea Pig

Tom20	SantaCruz (sc11415)	Rabbit
vGAT	SynapticSystem (131004)	Guinea Pig
Vimentin	Encor (CPCA-Vim)	Chicken
Vimentin	Biolegend (Poly29191)	Chicken

Table 7. *Antibodies and conjugated DNA docking strands for multiplexed diffraction-limited imaging in primary neuron culture*

Target	DNA conjugates	Docking strand	Target	DNA Conjugates	Docking strand
SynapsinI	anti-rabbit secondary antibody	P11	GFAP	primary mouse antibody	P18
vGAT	anti-guinea pig secondary antibody	P12	MAP2	anti-goat secondary antibody	P13
pNFH	anti-chicken secondary antibody	P14	AlphaTubulin	anti-rat secondary antibody	P10
AcetylTubulin	primary mouse antibody	P15	Gephyrin	anti-human secondary antibody	Alexa488

Table 8. *Antibodies and conjugated DNA docking strands for multiplexed diffraction-limited imaging in retina sections*

Target	DNA conjugates	Docking strand	Target	DNA conjugates	Docking strand
SV2	primary mouse antibody	P16	GFAP	anti-rat secondary antibody	P10
Cone arrestin	anti-rabbit secondary antibody	P11	Chx10	anti-sheep secondary antibody	P13

Vimentin	anti-chicken secondary antibody	P14	Synapsin	anti-guinea pig secondary antibody	P12

Table 9. *Antibodies and conjugated DNA docking strands for multiplexed diffraction-limited imaging in breast tumor sections*

Target	DNA conjugates	Docking strand	Target	DNA conjugates	Docking strand
HER2	anti-rabbit secondary antibody	P11	SMA	anti-mouse secondary antibody	P9

Table 10. *Antibodies and conjugated DNA docking strands for multiplexed SIM imaging*

Target	DNA conjugates	Docking strand	Target	DNA conjugates	Docking strand
alphaTubulin	anti-rat secondary antibody	P10	betaTubulin	anti-mouse secondary antibody	P9
Tom20	anti-rabbit secondary antibody	P11	Vimentin	anti-chicken secondary antibody	P17

Table 11. *Antibodies and conjugated DNA docking strands for multiplexed STED imaging*

Target	DNA conjugates	Docking strand	Target	Dna conjugates	Docking strand
SynapsinI	anti-rabbit secondary antibody	P11	Bassoon	anti-mouse secondary antibody	P9
pNFH	anti-chicken secondary	P14	GFAP	anti-rat secondary	P10

	antibody			antibody	

Table 12. *Antibodies and conjugated DNA docking strands for multiplexed super-resolution PAINT imaging*

Target	**DNA conjugates**	**Docking strand**	**Target**	**DNA conjugates**	**Docking strand**
SynapsinI	anti-rabbit secondary antibody	P3	Bassoon	anti-mouse secondary antibody	P1
vGAT	anti-guinea pig secondary antibody	P5	Vimentin	anti-chicken Secondary antibody	P6
Tom20	anti-rabbit secondary antibody	P4	AlphaTubulin	anti-rat secondary antibody	P2
GFAP	primary mouse antibody	P18	AcetylTubulin	Primary mouse antibody	P7

Chapter IV

Highly multiplexed *in situ* protein imaging with signal amplification using Immuno-HCR and Immuno-SABER

This chapter contains contents from publication:

1. Wang, Y., Xie, W., Kohman, R.E. and Church, G.M. (2018). Multiplexed imaging using same species primary antibodies with signal amplification. bioRxiv, p.274456.

*2. Saka, S.K.**.§, Wang, Y., **.§ Kishi, J.Y., Zhu, A., Zeng, Y., Xie, W., Kirli, K., Yapp, C., Cicconet, M., Beliveau, B.J., Lapan, S.W., Yin, S., Lin, M., Boyden, E.S., Kaeser, P.S., Pihan, G., Church, G.M. and Yin, P. § (2018). Highly multiplexed in situ protein imaging with signal amplification by Immuno-SABER. bioRxiv, p.507566.*

4.1. Abstract

A key challenge for *in situ* protein detection using DNA-barcoded primary antibodies is lack of signal amplification that is typically achieved by indirect immunostaining with polyclonal secondary antibodies or enzyme-based methods such as tyramide signal amplification. Without signal amplification, the detection sensitivity is limited as low-copy number proteins are difficult to be observed. In addition, the imaging throughput is slowed down as longer imaging time per image frame is necessary to obtain high quality images. To address the issue, I simultaneously explored two DNA-based amplification strategies: Hybridization chain reaction (HCR) and Signal amplification by exchange reaction (SABER), and successfully achieved over 50-folds signal amplification using both methods. I also demonstrated highly multiplexed *in situ* protein detection by combining DEI and SABER. Finally, I achieved highly multiplexed, high sensitivity and super-resolution imaging by conjoining DEI, SABER and Expansion Microscopy.

4.2. Multiplexed imaging using same species antibodies with signal amplification using immuno-HCR

4.2.1. Reduction of non-specific binding of DNA-conjugated antibodies

In HCR, a single DNA initiator sequence will trigger an assembly of large linear DNA structure by iterative HCR hairpin opening[39,40,82,83] (**Figure 24a**). We directly conjugated HCR-initiator DNA sequences to primary antibodies through covalent chemical modification[63]. We first tested the labeling specificity of DNA-modified primary antibodies by staining the antibodies in cultured BSC-1 cells followed by HCR amplification. Surprisingly, we observed strong nonspecific signals, especially inside the nucleus (**Figure 24b**), which has not been observed previously using secondary antibodies conjugated with shorter DNA oligonucleotides for DEI[11,45]. This is possibly due to the HCR DNA sequences (36 nucleotides) is much longer than the DEI docking DNA sequences (12 nucleotides). We decided to optimize the antibody staining protocol to reduce nonspecific binding. Sheared sperm DNA has previously been used to block nonspecific binding of DNA-conjugated antibodies[84]. We showed that addition of 0.5mg/ml of sheared sperm DNA during blocking and antibody incubation could reduce but not completely abolish nonspecific nuclear signal (**Figure 24b and c**). In order to further suppress nonspecific signals, we tested the addition of dextran sulfate in the antibody incubation buffer (**Figure 24b and c**).

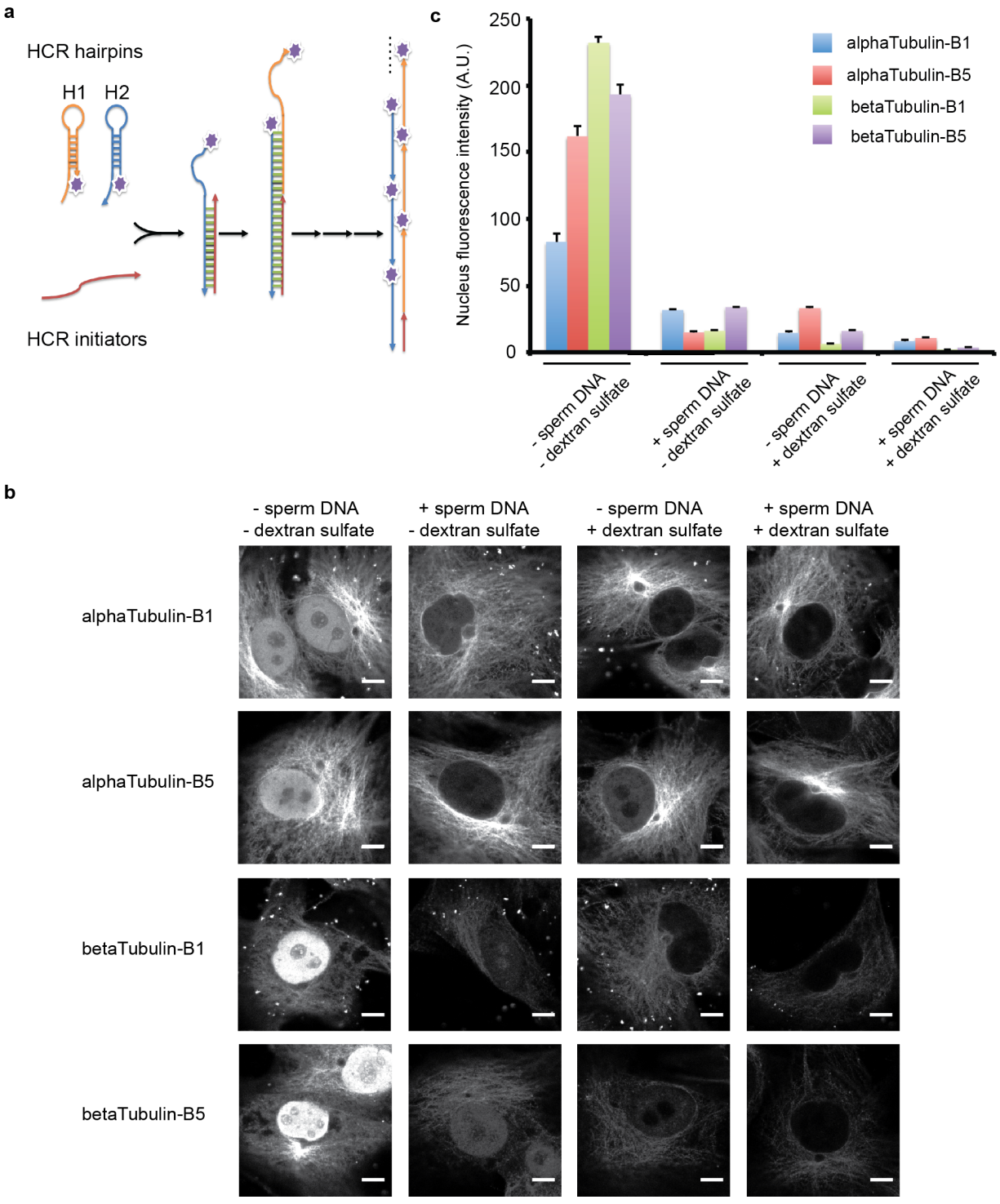

Figure 24. Reduction of Non-specific binding of DNA-conjugated antibodies. **a)** Schematic of HCR reaction. HCR initiator DNA sequence opens hairpin H1, which in turn opens hairpin H2. This exposes a new HCR initiator sequence, which triggers the next round of hairpin opening. **b)** Reduction of nonspecific signal by adding sperm DNA and dextran sulfate in the antibody incubation buffer. BSC-1 cells were fixed and stained with HCR B1- or B5-initiator conjugated anti-alphaTubulin or BetaTubulin antibodies in different incubation conditions. **c)** Quantification of nonspecific nuclear signals in different antibody incubation conditions.

High concentration (10% - 20%) of dextran sulfate has been used as a crowding reagent in DNA and RNA FISH experiments[85,86]. Empirically, we noticed that some primary antibodies failed to bind to their targets in 10% dextran sulfate solution (data not shown). We therefore performed a titration experiment to determine the minimal concentration of dextran sulfate. The result showed a good suppression of nonspecific nuclear signal could be achieved with as low as 0.02% dextran sulfate (**Figure 25**). We used 0.05% or 0.1% dextran sulfate plus 0.5mg/ml sheared sperm DNA for all following experiments.

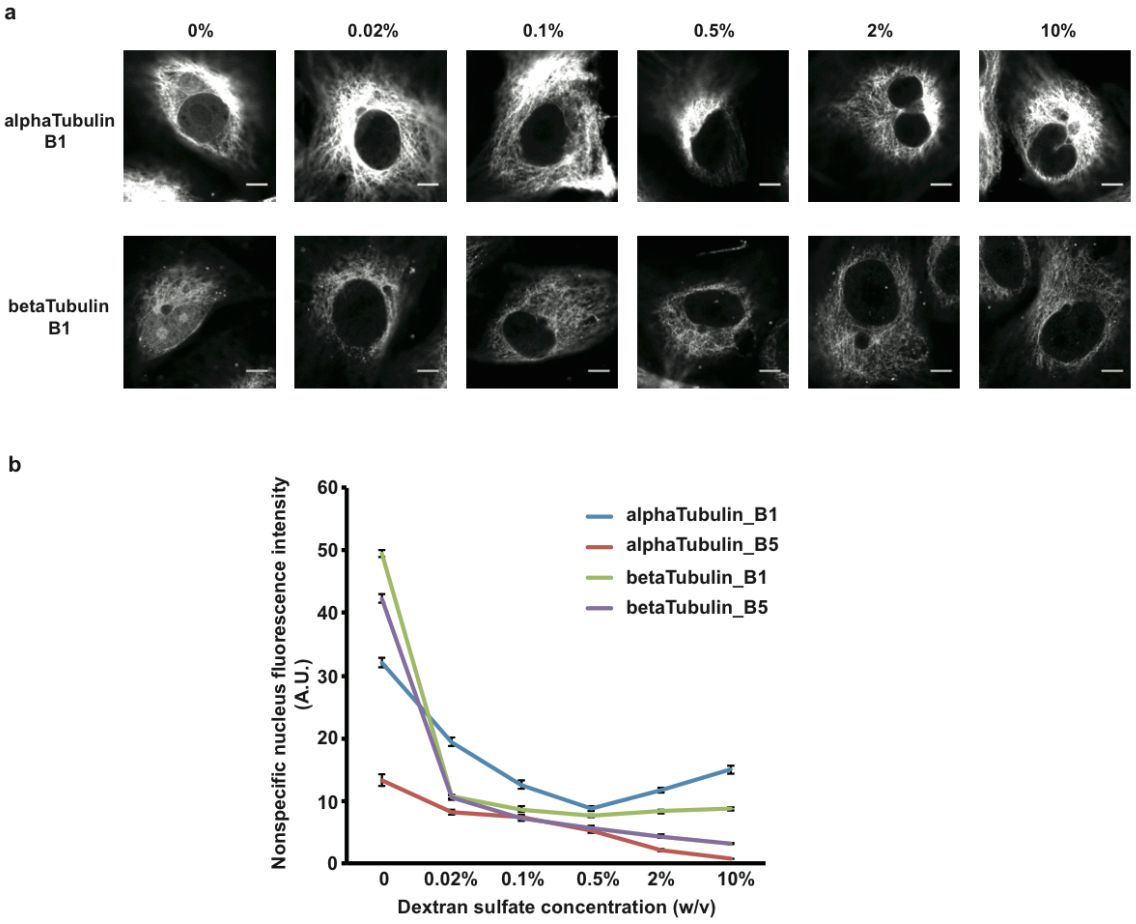

Figure 25. Optimization of the concentration of dextran sulfate in antibody incubation buffer to reduce nonspecific nucleus signals. BSC-1 cells were fixed and stained with HCR initiator DNA (B1 or B5) conjugated primary alphaTubulin and betaTubulin antibodies. Different concentrations of dextran sulfate (0% to 10%) in the antibody incubation buffer were tested. 0.5mg/ml sheared sperm DNA was added to all conditions. **a)** Demonstration of nonspecific nucleus signal in alphaTubulin-B1 and betaTubulin-B1 images. Scale bar: 10 μm. **b)** Quantification of nonspecific nucleus signals. (Error bar is SEM. n = 30)

Similar to conventional immunostaining, we also noticed for some antibodies the antibody concentration also had a modest effect on the nonspecific signal (**Figure 26**).

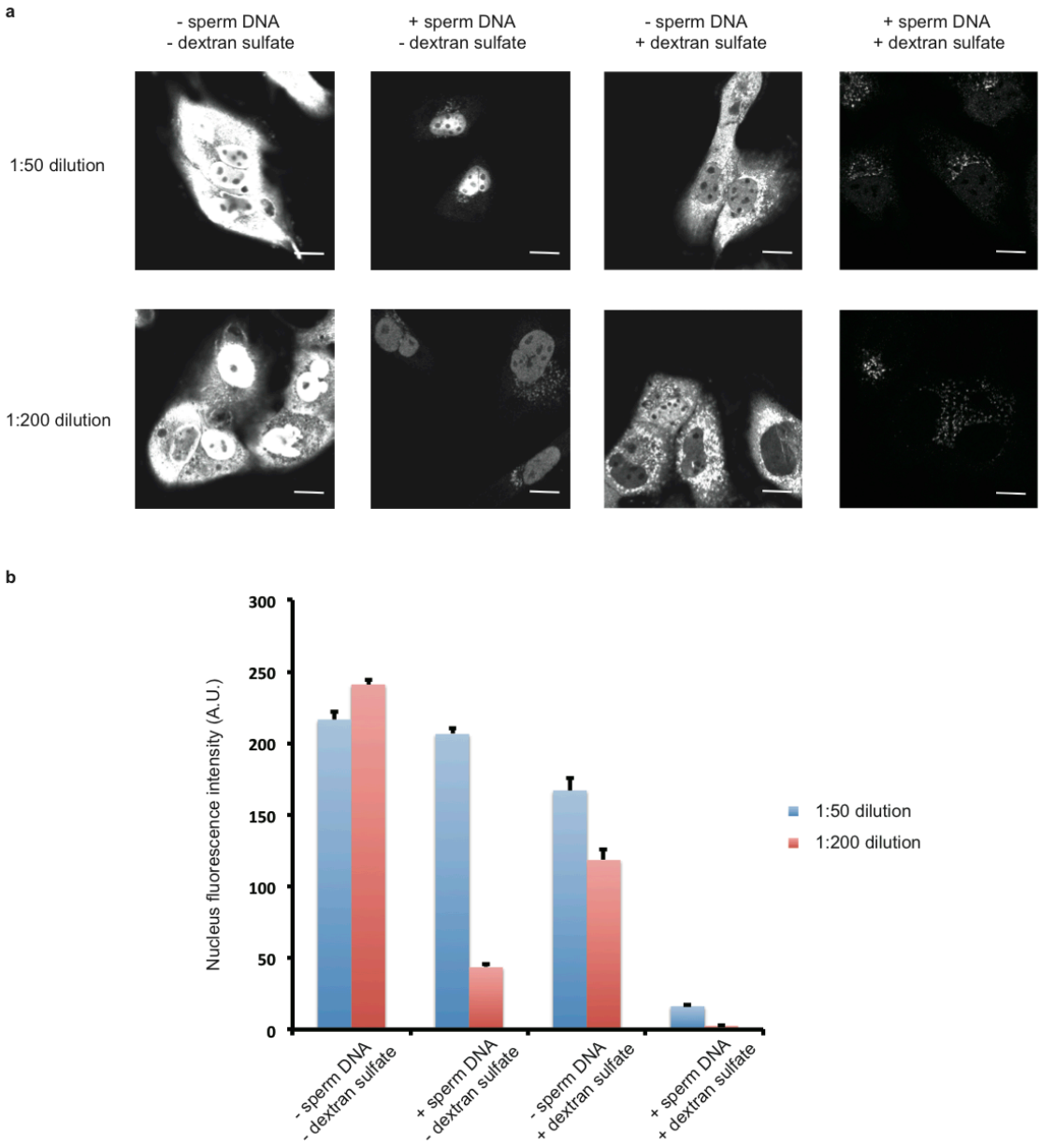

Figure 26. Reduction of non-specific nucleus signal by adjusting antibody incubation buffer composition and antibody concentration. a) BSC-1 cells were fixed and stained with HCR initiator (B3)-conjugated Golgi 97 antibodies. The antibodies were diluted in buffers containing with/without 0.5mg/ml sheared sperm DNA and with/without 0.05% dextran sulfate. Antibodies were diluted using 1:50 or 1:200 dilution factor. Scale bar: 20 μm. **b)** Quantification of nonspecific nucleus signals. Error bar is SEM and n = 100.

4.2.2. Signal amplification using immuno-HCR

We then quantified the signal amplified using HCR compared with the unamplified signal and the signal amplified using commercial fluorophore-conjugated secondary antibodies. We stained cultured BSC-1 cells or primary neurons with HCR initiator B1-conjugated alpha-tubulin antibodies, B5-conjugated alpha-tubulin or B5-conjugated GFAP antibodies (**Figure 27**). We were able to achieve as much as 89-fold increase of fluorescence signals for alpha-tubulin using HCR (**Figure 27**). More importantly, HCR outperformed commercial fluorophore-conjugated secondary antibodies and achieved better signal amplification. We noticed that the signal amplification fold was dependent on the targets (alpha-tubulin versus GFAP) and HCR sequences (B1 versus B5).

4.2.3. Multiplexed imaging with signal amplification using immuno-HCR

We finally performed multiplexed imaging using same species primary antibodies by conjugating orthogonal HCR initiator sequences to different antibodies. We first attached four mouse IgG (IgG1 subclass) primary antibodies against four distinct cellular structures (Golgi 97, Lamin B, Vimentin and Clathrin) with HCR initiators (B2 to B5). We then stained cultured BSC-1 cells with the four antibodies using our optimized staining protocol, followed by HCR signal amplification and confocal microscopy imaging. We were able to get high-quality images for all four targets (**Figure 28a**). We also performed multiplexed imaging in mouse retina tissue samples using four mouse IgG primary antibodies targeting Bassoon, SV2, pNFH (phosphorylated neurofilament heavy) and Calretinin. Bassoon and SV2 are two synaptic markers, and pNFH and Calretinin are two neuronal markers (**Figure 28b**). Bassoon is located in the active zone of synapses, and is in low abundance[52]. It can be seen that after HCR signal

amplification, Bassoon signals are clearly visible in 40 µm thick mouse retina sections (**Figure 28c**).

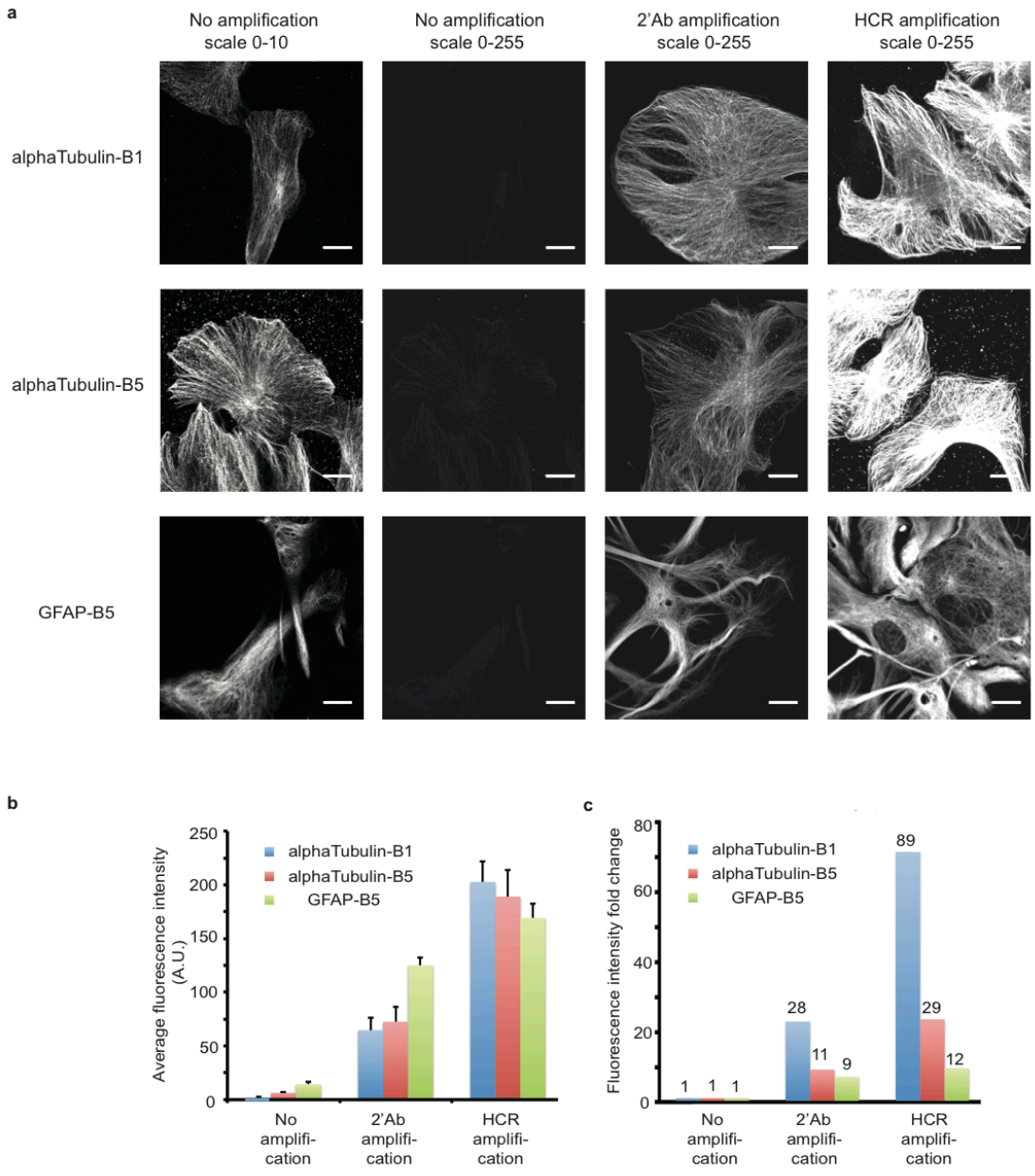

Figure 27. Quantification of fluorescence signal amplification by HCR. a) BSC-1 cells or primary mouse hippocampal neuron culture were fixed and stained with HCR initiator-conjugated antibodies against alphaTubulin and GFAP, respectively. In no amplification samples, the images were acquired using Alexa647-conjugated DNA strands that are complementary to the HCR initiator DNA sequences. Either Alexa647-conjugated secondary antibodies (2'Ab) or HCR hairpins were used to amplify the signals. The images were acquired at the same microscope setting. Scale bar: 20 μm. **b)** Quantification of image fluorescence intensity. Error bar is SEM and n = 12. **c)** Quantification of fluorescence intensity fold change based on average fluorescence intensity in b).

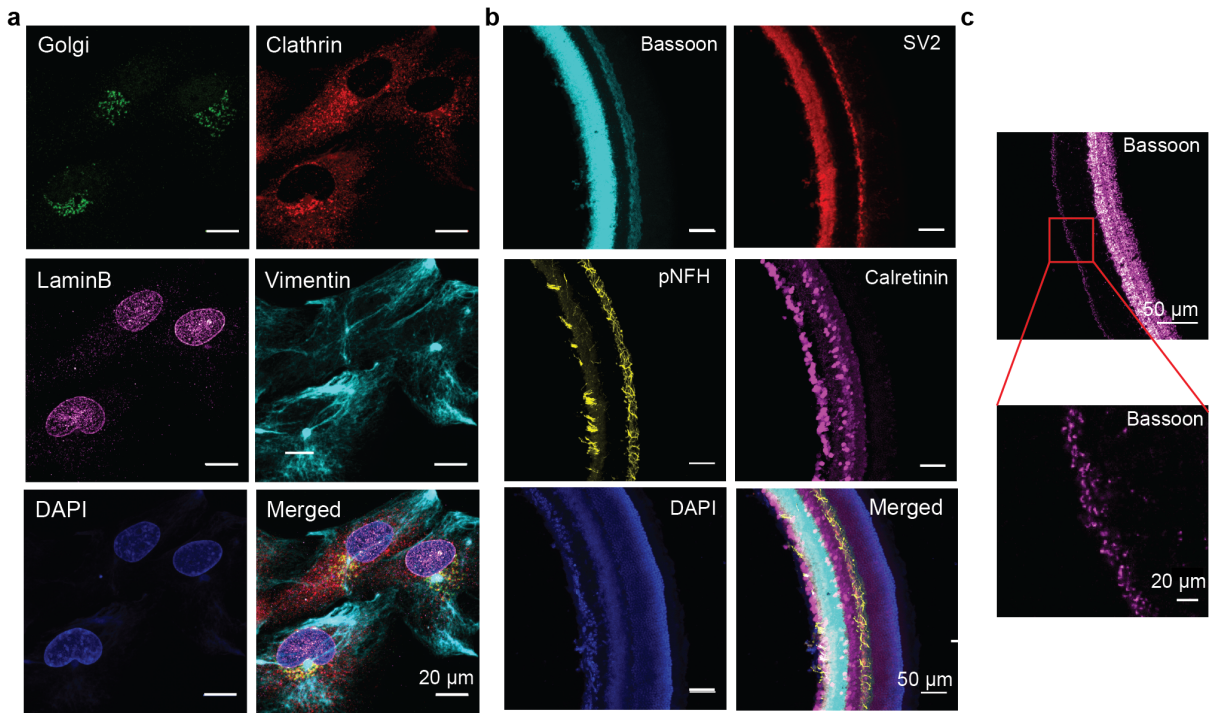

Figure 28. Multiplexed imaging using same species primary antibodies with signal amplification using immuno-HCR. a) Four-target imaging with all mouse IgG1 primary antibodies targeting cellular structures in BSC-1 cells. Four mouse IgG1 antibodies are conjugated with HCR-initiators (Golgi-B3, Clathrin-B2, LaminB-B4 and Vimentin-B5) and used to stain fixed BSC1 cells. DAPI was used to visualize the nucleus. **b)** Four target imaging using all mouse IgG primary antibodies targeting neuronal and synaptic proteins in mouse retina sections. 40 µm mouse retina sections were stained with HCR initiator-conjugated primary antibodies against targets as labeled (Bassoon-B1, SV2-B2, pNFH-B4 and Calretinin-B5). **c)** Magnified view of synapses in mouse retina sections marked by active zone protein Bassoon.

4.3. Highly multiplexed *in situ* protein detection using immuno-SABER

4.3.1. Concept of immuno-SABER

For *in situ* signal amplification, Immuno-SABER relies on a strategy entailing controlled *in vitro* synthesis of concatemers by Primer exchange reaction (PER), followed by programmed *in situ* assembly. PER utilizes a catalytic hairpin for controllable extension of a short primer sequence in an iterative manner (Figure **29a**)[87]**.** These concatemers provide controllable multiplexed signal amplification by acting as docking sites for multiple fluorophore-bearing DNA imager strands **(Figure 29b)**. We achieve rapid multiplexing through DNA-Exchange-Imaging as described above (**Figure 29c**).

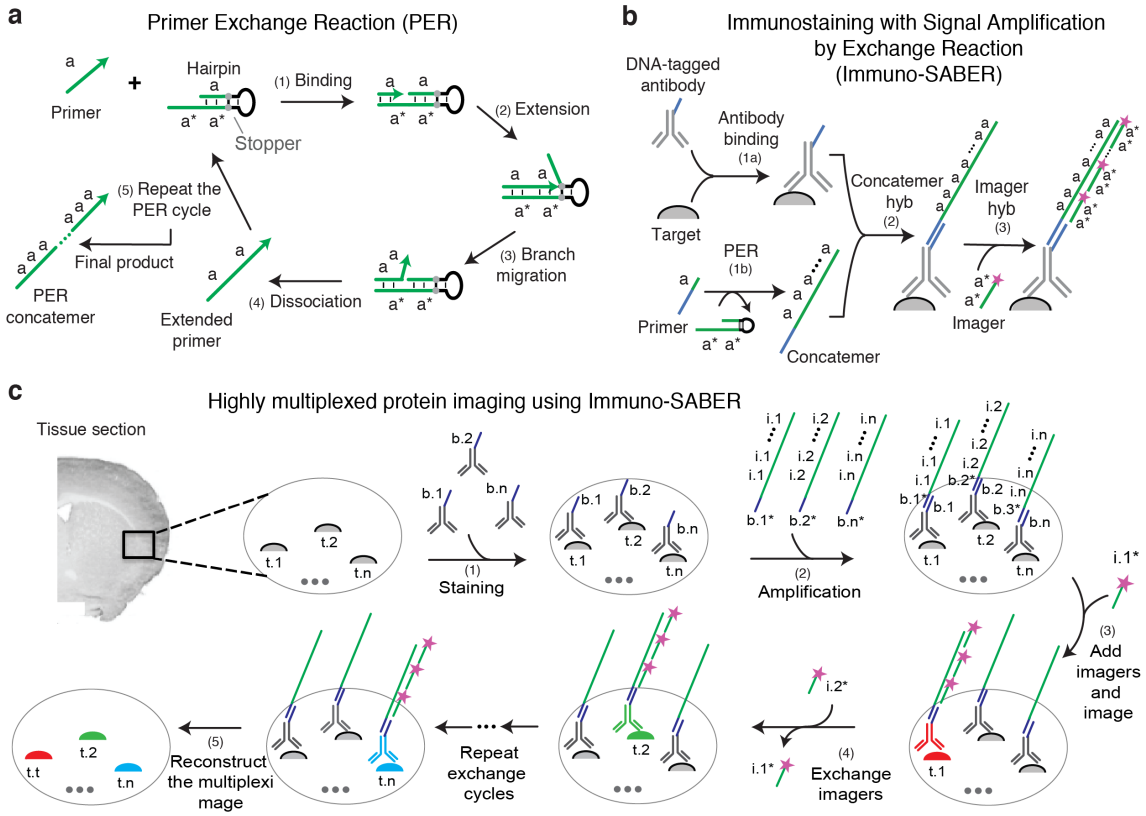

Figure 29. Immuno-SABER scheme. a) Mechanism of PER. (1) A 9-mer primer of sequence *a* binds to the single stranded *a** sequence on the hairpin. Asterisk denotes complementarity. (2) The primer is extended by a strand displacing polymerase (e.g. Bst) in an isothermal and autonomous manner. Each PER hairpin features a stopper sequence that halts polymerization and results in release of the polymerase. (3) The newly synthesized *a* segment is displaced from binding with the *a** segment of the hairpin through branch migration. (4) The extended primer and the intact hairpin autonomously dissociate. (5) Repetition of this copy-and-release process through repetitive reaction cycles produces a long concatemer of *a*. **b)** Schematic of Immuno-SABER: (1a) Antibodies are conjugated with DNA bridge strands (sequences) and used to stain targets in biological samples. (1b) Primer sequences (green line) are extended to a controlled length using PER. (2) The concatemers are hybridized to the bridge sequence (blue) on the antibody. (3) Fluorophore (depicted as purple star)-labeled 20-mer DNA "imagers" strands hybridize to the repeated binding sites on the long PER concatemers. Each imager is designed to bind to a dimer of the unit primer sequence. **c)** Schematic of highly multiplexed imaging using Immuno-SABER: (1) Different biological targets (t.1 to t.n) are labeled with corresponding antibodies conjugated with orthogonal DNA bridge strands (b.1 to b.n). (2) Orthogonal pre-extended concatemers are hybridized (via bridge complements b.1* to b.n*) to create simultaneous signal amplification. (3) The targets are visualized by hybridization of fluorophore-labeled DNA imaging strands (i.1* to i.n*) to their repeated binding sites (i.1 to i.n) on the orthogonal concatemers . (4) Multiple targets can be imaged by rapid exchange rounds, where orthogonal imagers are dehybridized and hybridized in multiple cycles. (5) The images are computationally aligned and pseudo-colorized to overlay different targets in the same sample.

4.3.2. Validation and quantification of signal amplification using Immuno-SABER

Using PER, we synthesized long DNA concatemers of desired lengths reaching >500 bases through modulation of reaction conditions such as reaction time, hairpin or dNTP concentration[79]. We first tested the suitability of these long DNA concatemers for *in situ* imaging in biological samples and quantified the amplification capability. To have a modular design for protein imaging, we utilized 42-nucleotide bridge sequences that would enable coupling of concatemers of choice to antibodies on demand. We provided the design criteria to create orthogonal bridge sequence libraries for probe barcoding previously[79]. We conjugated these 42mer single-stranded DNA (ssDNA) oligos to antibodies targeting lysine residues. The PER primers we utilize are similarly barcoded with complements of these bridge sequences. These primers are extended into concatemers via PER *in vitro*, and then applied onto cells and hybridized to the bridges *in situ*. For application of this *in vitro* extension and *in situ* assembly strategy on biological specimens there main considerations are: i) specificity of the labeling, ii) ability to label dense targets (due to potential interference of the probe size), iii) penetration and access to targets in highly crosslinked or thick tissue samples, and iv) efficient amplification for diverse targets.

To validate our approach and mitigate these potential considerations we have performed several demonstrations, and in each case included controls for a case where the same antibody was used without amplification or a conventional staining was performed with fluorophore-conjugated secondary antibodies **(Figure 30a)**. First, to evaluate the specificity and preservation of morphology upon labeling with the linear concatemers, we performed Immuno-SABER staining in cultured cells for microtubules as a test case for a densely arranged structural protein target. We have observed specific staining, clear tubular morphology and similar staining pattern

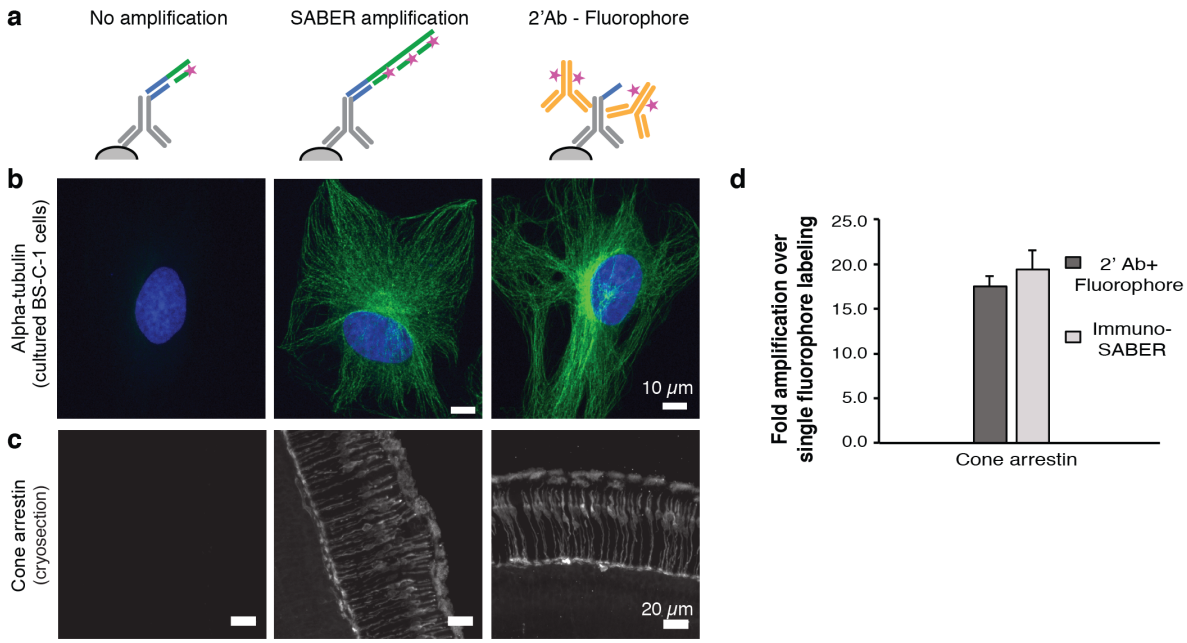

Figure 30. Validation of immuno-SABER in cell culture and tissue sections. a) Schematic of the experiment. **b)** Cultured BS-C-1 cells were immunostained for alpha-tubulin and three conditions were prepared for comparison: Unamplified condition, where (i) unextended primers with single binding site for imager (with Alexa647) was hybridized to the bridge on the antibody, (ii) the extended concatemer was hybridized for signal amplification (linear amplification), (iii) conventional antibody staining was performed with Alexa647-conjugated secondary antibodies. **c)** Cone arrestin staining in mouse retina cryosections. The experiment setup is same as (b). **e)** Level of signal amplification by Immuno-SABER was quantified by measuring the background-subtracted mean fluorescence for several regions of interest in the tissues and expressed as fold amplification over unamplified signal level. Conventional secondary antibody amplification was also quantified similarly and shown as reference. n = 6 images from 2 retina samples. Error bar indicates SEM.

to conventional immunostaining with fluorophore-conjugated secondary antibodies **(Figure 30b)**. For validation of the labeling strategy in tissue samples and quantification of the signal amplification capability of Immuno-SABER, we used 40 μm-thick mouse retina cryosections, similar to DEI (**Figure 30c and d**). Immuno-SABER yielded similar or slightly higher fluorescence signal than conventional fluorophore-conjugated secondary antibody staining using the same fluorophore. We quantified the signal amplification level using Immuno-SABER as 19.4-fold for cone arrestin. For comparison, conventional secondary antibody staining yielded 17.5-fold amplification **(Figure 30d)**. We note that the degree of *in situ* signal amplification

depends on multiple factors, including abundance and organization of targets, the antibodies (e.g. clonality, conjugation efficiency), the method of quantification (the unamplified signal level, thresholding, background subtraction), as well as the experimental conditions and properties of the SABER sequences (e.g. the length of SABER concatemer).

Despite the anticipated size of the long concatemers reaching >500 nucleotides, SABER concatemers can effectively penetrate relatively thick samples. We validated the penetration capability of the concatemers in whole-mount preparations of mouse retina by successfully staining for the Muller cell marker Vimentin and blood vessel marker Collagen IV, which both predominantly localize in the 100 μm region from nerve fiber layer to outer plexiform layer of the retina, as expected[88] **(Figure 31)**.

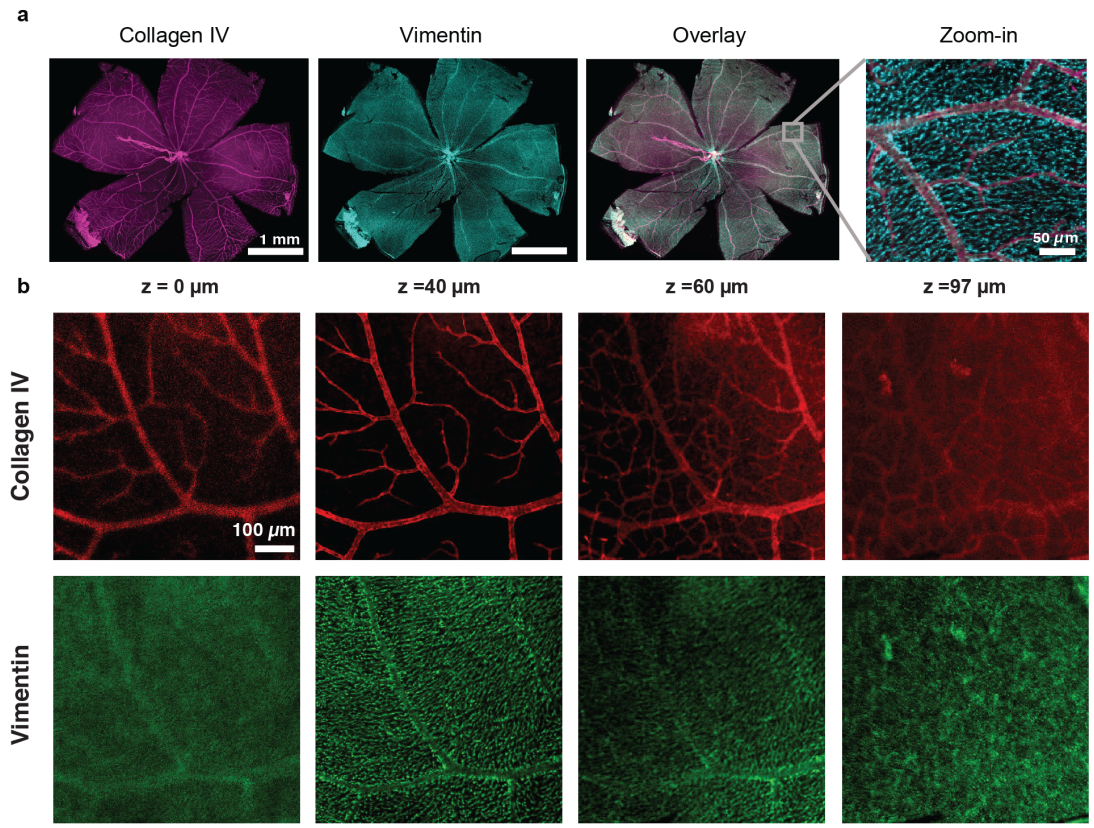

Figure 31. Validation of immuno-SABER in whole mount retina samples. a) Immuno-SABER was performed in whole-mount retina sections for collagen IV and vimentin. Maximum projections from confocal z-stacks are displayed. **b)** Selected confocal planes of a) are shown. Vimentin stains the Muller cells and Collagen IV stains the blood vessels, both of which are localized predominantly in the segments from nerve fiber layer to outer plexiform layer (~100 μm).

This high level of strand penetration may potentially be attributed to SABER concatemers being largely linear DNA structures designed in 3-letter code (made of only A, T, and C nucleotides) to be devoid of secondary structures (that may be otherwise stabilized by G-C pairings).

4.3.3. Enhancement of signals through branched-SABER

Although the amplification obtained through Immuno-SABER is substantial, further enhancement of the signal can be desirable for proteins of lower abundance, or to further improve the throughput of imaging (by allowing shorter exposure times through signal amplification). For this purpose, we developed a sequential amplification strategy where independently extended secondary concatemers can be branched off the primary concatemer to create more binding sites for fluorescent imagers (termed as 'branched SABER'). This can be achieved by a sequential round of concatemer hybridization as depicted in **Figure 32a**. We have performed similar tests to check the effect of an additional amplification round in mouse retina cryosections (**Figure 32 b and c**). With one round of branching, we obtained additional 8.4-fold amplification for cone arrestin in cryosections over single round Immuno-SABER detection (**Figure 32c**). Immuno-SABER allows further improvement of sensitivity by performing multiple hybridization rounds (termed as Iterative SABER) (**Figure 32d**). We applied this strategy in mouse retina cryosections, and performed 3 sequential rounds of SABER amplification following primary antibody staining to visualize synaptic marker SV2. Iterative-SABER yielded ~80-fold amplification over unamplified control (**Figure 32d**). For such high levels of amplification, catalyzed reporter deposition-based TSA is considered a gold-standard, which was reported to achieve 10-1000-fold sensitivity improvement under different assay types

and comparison conditions[26,89-92]. This can be further improved 2-10 fold by using poly-HRP

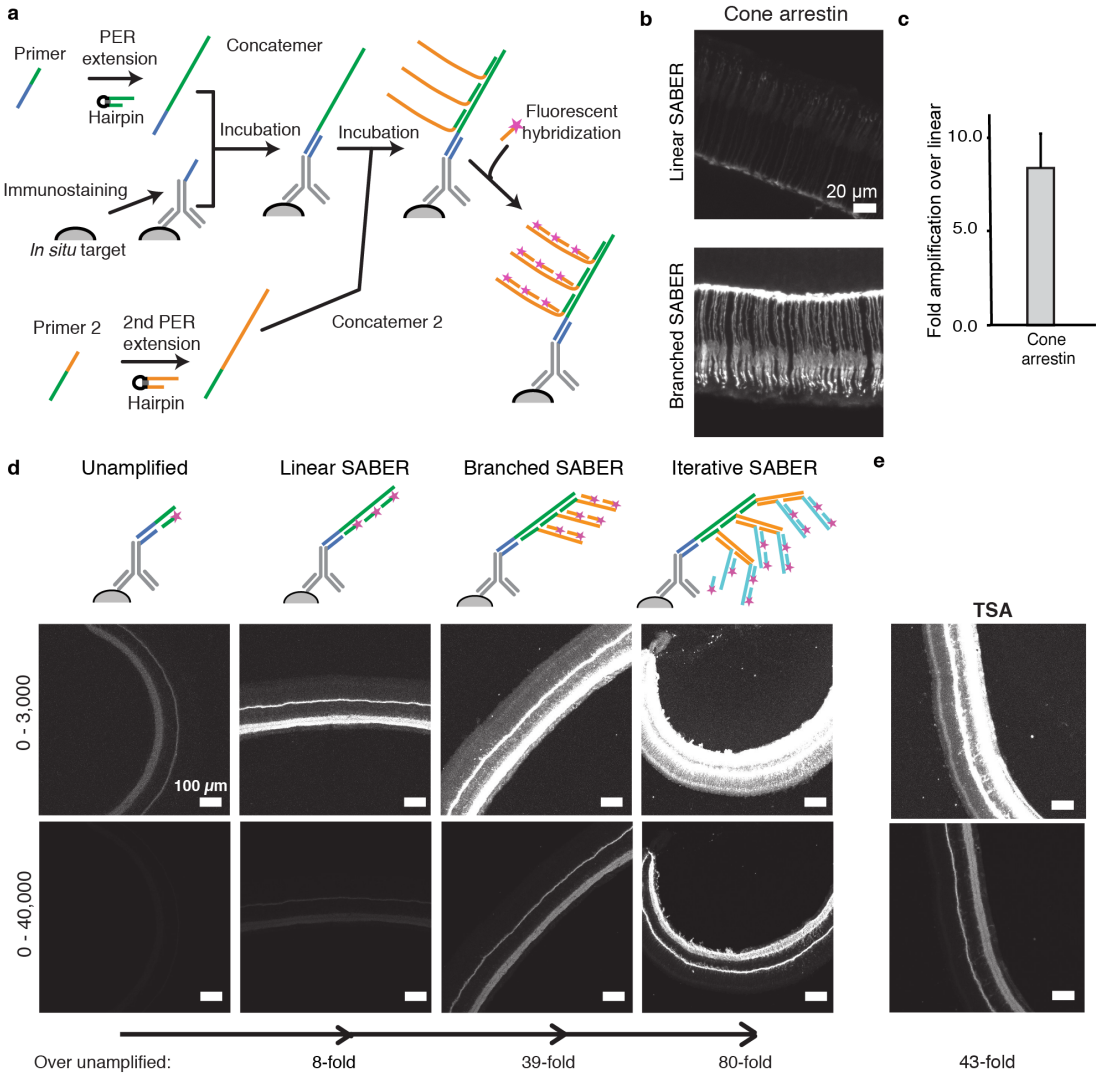

Figure 32. Signal amplification using branched-SABER. a) Schematic of branched-SABER. Primary PER concatemers can be targeted by secondary concatemers to form a branched structure which amplifies the signal further by presenting additional binding sites for the imagers. **b)** Comparison of signal amplification using linear and branched SABER on mouse retina sections targeting cone arrestin. **c)** Quantification of signals in (b). **d)** Comparison of signal amplification using linear SABER, branched SABER and iterative SABER and quantification of signal amplification over unamplified signals. **e)** Signal amplification using Tyramide signal amplification (TSA) compared with SABER in (d). The grayscale is adjusted as (d). The signal amplification fold is over signals in the unamplified images.

conjugated antibodies. However, due to lack of orthogonal chemistries TSA can only be applied to one target at a time, so to label multiple targets sequential antibody labeling and signal amplification with different fluorophores need to be performed with microwave-based removal

of antibodies after each round[27-29]. In addition, the amplification level in TSA is difficult to control and it is not ideal for high-resolution imaging due to spreading of the fluorescent tyramide molecules to nearby areas (reaction products have been shown to spread over a ~1 μm radius[32]). To investigate how Immuno-SABER performs in comparison to TSA, we first utilized the conventional TSA Kit from ThermoFisher that used mono-HRP conjugated secondary antibodies and -Alexa647-tyramide (i.e. signals were amplified both by secondary antibodies and by TSA). Although only DNA-conjugated primary antibodies were used, we found that iterative SABER could amplify signals to a higher level than TSA with secondaries (**Figure 32d and e**).

4.3.4. Validating sequences for multiplexing Immuno-SABER

PER has little inherent restrictions in sequence design outside of preferred single strandedness of the concatemer. We previously developed a computational pipeline to design orthogonal PER primer-hairpin pairs with maximum extension efficiency and minimum crosstalk by utilizing *in silico* simulations using NUPACK[66] and designed 50 orthogonal sequences to enable multiplexed imaging[79]. Here, we tested the performance to 32 SABER sequences to extend into long DNA concatemers using an *in vitro* gel-shift assay. **Figure 33a** displays long concatemers extended from 32 primers up to 600 to 700-nucleotide lengths (which is the range we use for primary SABER concatemers), visualized with SybrGold staining on denaturing PAGE gels. Since extension efficiency is sequence-dependent, reaction conditions were optimized by modulating the hairpin concentration and reaction time for each primer to obtain concatemers of similar lengths. All sequences in our test library succeeded to produce concatemers in the desired length range. All of the tested primers extended into long concatemers, with 31 out of 32

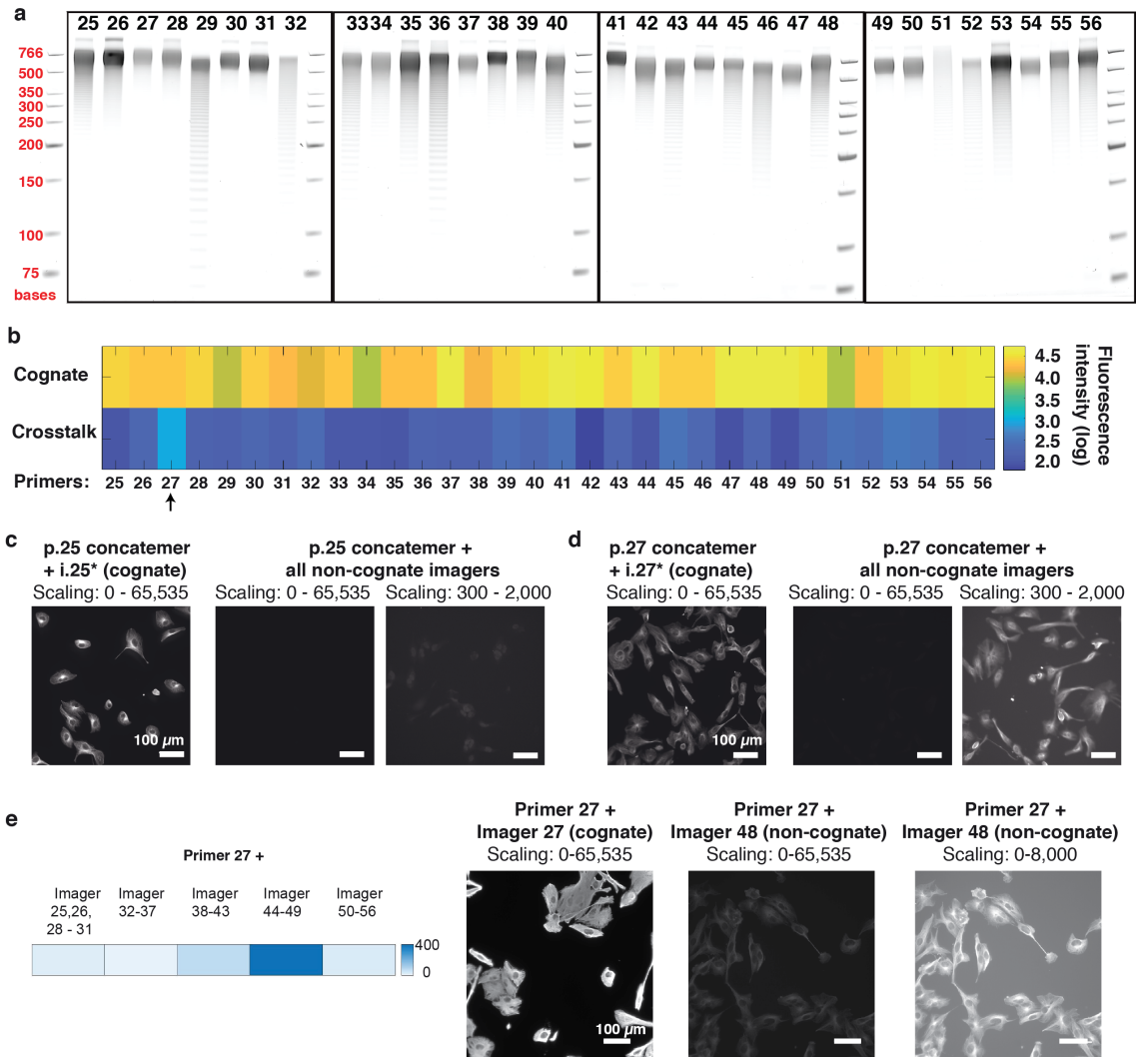

Figure 33. Sequence validation for highly multiplexed Immuno-SABER. a) 32 SABER sequences were extended to ~650 bases *in vitro* and examined by gel shift assay on a 6% denaturing PAGE gel. The 500 and 766 base ladder bands are displayed for reference. **b)** *In situ* performance and crosstalk analysis of SABER sequences. BSC1 cells were stained with bridge DNA-conjugated antibodies targeting α-Tubulin on a 96-well plate. Concatemers extended from each primer were hybridized to the bridges creating an array of wells labeled with primer sequences p.25-p.56. For each primer (e.g. p.25), both cognate and crosstalk wells were prepared by either applying the corresponding Alexa647-imager (e.g. i.25* for the concatemer extended from p.25) or by applying all the imagers except the cognate one (e.g. -i.26* to i.56* for p.25 concatemer). Images were captured in 16-bit (0-65,535). The fluorescence signals were quantified and plotted in the log scale and displayed as a heatmap. Non-negligible crosstalk signal was only detected for Primer 27 concatemer (indicated by the arrow). **c-d)** Representative images are shown for Primer 25 (p.25) and Primer 27 (p.27) concatemers. Crosstalk images are displayed with two different intensity scales to render the crosstalk signal visible. **e)** Crosstalk of Primer 27 was further evaluated and it was found that it weakly cross-talked with imager 48.

sequences (except #51) yielding a predominant long concatemer band at the desired target length, albeit some heterogeneity in the distribution of shorter reaction products **(Figure 33a)**.

After *in silico* design and *in vitro* validation of SABER sequences, we evaluated the *in situ* performance and orthogonality of detection (crosstalk check) through an imaging-based multi-well plate assay (**Figure 33b-e)**. DNA-conjugated antibodies targeting α-Tubulin were used to stain microtubules in fixed BSC1 cells, followed by hybridization of each DNA concatemer in separate wells. We divided the wells stained with the series of concatemers into two groups: (i) cognate group to be incubated with the corresponding imager strands, and (ii) crosstalk group where we added mixtures of imagers except the cognate imager strand. We were able to observe microtubule staining for all 32 sequences. Consistent with the *in vitro* gel shift assay, sequences that had lower extension efficiency (particularly primers 5, 8, 10 and 27) tended to yield less fluorescence signal compared to sequences that that extend with higher efficiency. We only observed minor crosstalk (crosstalk signal / cognate signal = 4%) for primer 27 (p.27) (**Figure 33d**). In the follow-up experiments, we determined the strand responsible for crosstalk as imager strand 48 (i.48*), which is excluded from the library for further multiplexed imaging (**Figure 33e**).

4.3.5. Highly multiplexed Immuno-SABER imaging in mouse retina cryosections

We validated highly multiplexed Immuno-SABER in thick (40 μm) cryosections of mouse retina and demonstrated ten-target in situ protein imaging. We first screened antibodies against a list of targets that have defined staining patterns, including cone arrestin, SV2, VLP1 (Visinin-like protein 1), Rhodopsin, Calretinin, PKα (Protein kinase C alpha), GFAP (Glial fibrillary acidic protein), Vimentin, Collagen IV, Calbindin. VLP1, Calretinin and Calbindin are all

calcium-binding proteins[93,94]. Calretinin labels a subset of amacrine and ganglion cells. Although it has been suggested that calbindin also exists in amacrine cells and ganglion cells, the antibody targeting calbindin we used mostly labels horizontal cells[94]. Rhodopsin is located in the rod photoreceptors. GFAP labels astrocytes, and Vimentin labels Muller cells[11]. Collagen IV marks blood vessels. PKCα labels blue cone cells and rod bipolar cells[94]. We then conjugated DNA bridge strands to those antibodies, and validated the specificity and affinity of DNA-conjugated antibodies by comparing the staining patterns from conventional staining using unmodified primary antibodies followed by fluorophore secondary antibodies **(Figure 34a)**.

As a control experiment for DNA-Exchange, we compared pre- and post-washing images for SV2, and found the imager strands were efficiently removed after washing (**Figure 34b**). To test whether the washing step causes sample damage or signal loss, we imaged SV2 for three rounds and found the correlation coefficient between images was above 0.95, suggesting the washing condition is sufficiently mild and non-disruptive (**Figure 34c**).

For highly multiplexed imaging, the 40 μm mouse retina section was first incubated with all DNA-conjugated antibodies simultaneously. All SABER concatemers were then added simultaneously to the sample and left at room temperature for overnight, followed by washing and microscopic imaging with sequential addition of fluorophore-attached imager strands. A z-stack of images was acquired for each target, and DAPI was imaged in every exchange cycle to monitor sample drift. The maximum projected images of each stack were computationally aligned using a sub-pixel registration algorithm using DAPI as the drift marker[11], and pseudo-colored for presentation **(Figure 35)**.

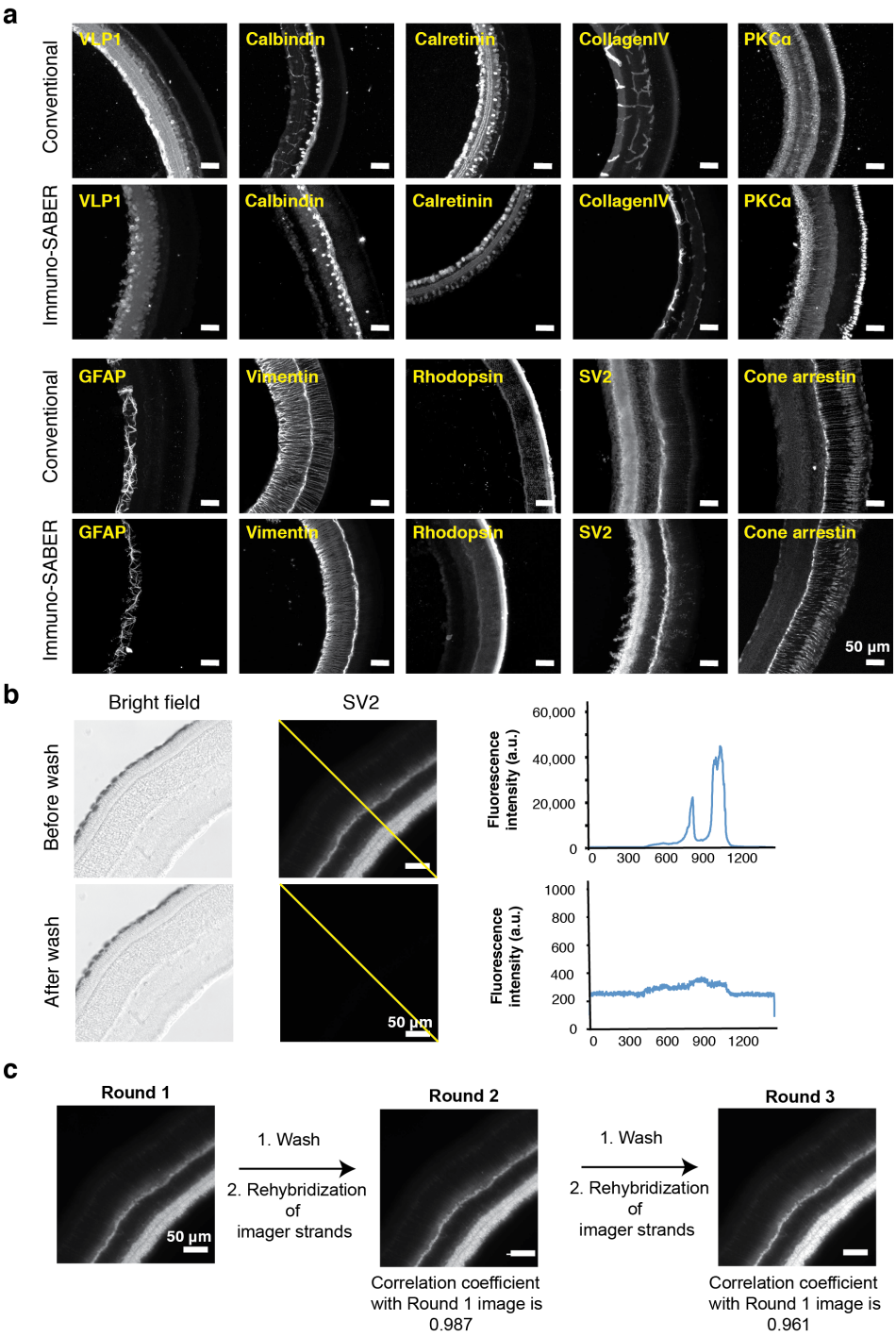

Figure 34. Control experiments for highly multiplexed imaging in mouse retina sections. (a) Comparison of antibody staining patterns before and after DNA conjugation. The images for unconjugated antibodies were taken using fluorophore-conjugated secondary antibody labeling, and the images for antibodies after conjugation were taken using primary antibody-Immuno SABER labeling. **(b)** Efficiency of washing to remove the imager strands. A 30 μm mouse retina section was stained with DNA-conjugated SV2 antibodies. Imager strands were washed using 0.1× PBS with 30% formamide at room temperature for 3×10 minutes. Before and after images were taken using the same imaging setting. The fluorescence intensity of indicated yellow line was measured using FIJI. **(c)** Washing conditions maintained sample integrity without signal loss. SV2 in mouse retina sections was imaged for three rounds and the correlation coefficient was calculated between the images.

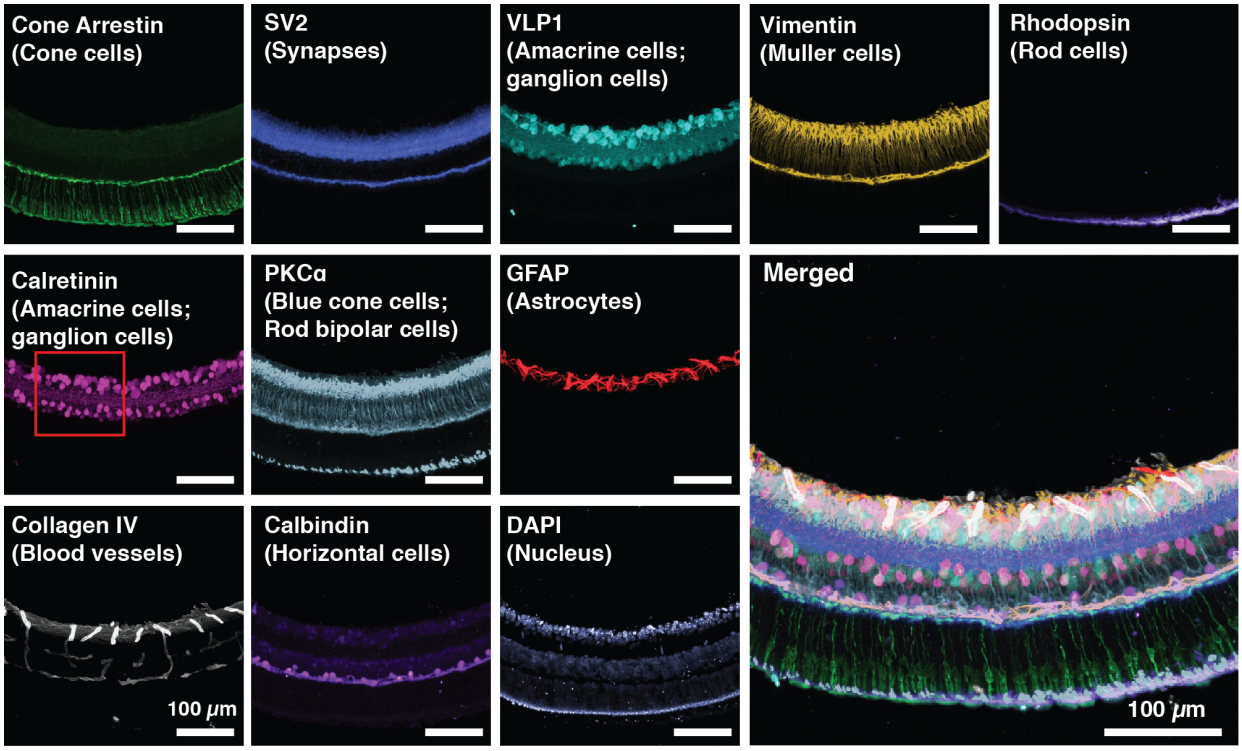

Figure 35. Highly multiplexed protein imaging using immuno-SABER in mouse retina cryo-sections. Ten protein targets labeling various retinal cell types as noted in the figure were visualized using immuno-SABER in a 40 μm mouse retina cryo-sections. The images were aligned using the DAPI channel computationally and pseudo-colorized for demonstration.

The highly multiplexed imaging result showed all targets were successfully captured using Immuno-SABER with expected staining patterns. Unexpectedly, we found that two calcium-binding proteins, VLP1 and Calretinin, together identify three populations of cells, $VLP1^{+}/Calretinin^{-}$, $VLP1^{-}/Calretinin^{+}$ and $VLP1^{+}/Calretinin^{+}$ **(Figure 36a)**. We confirmed these three cell types with conventional immunostaining using primary antibodies followed by fluorophore-conjugated secondary antibodies (**Figure 36b**). The antibody specificity was also validated by comparing the staining patterns of three different antibodies against the same target **(Figure 36c)**.

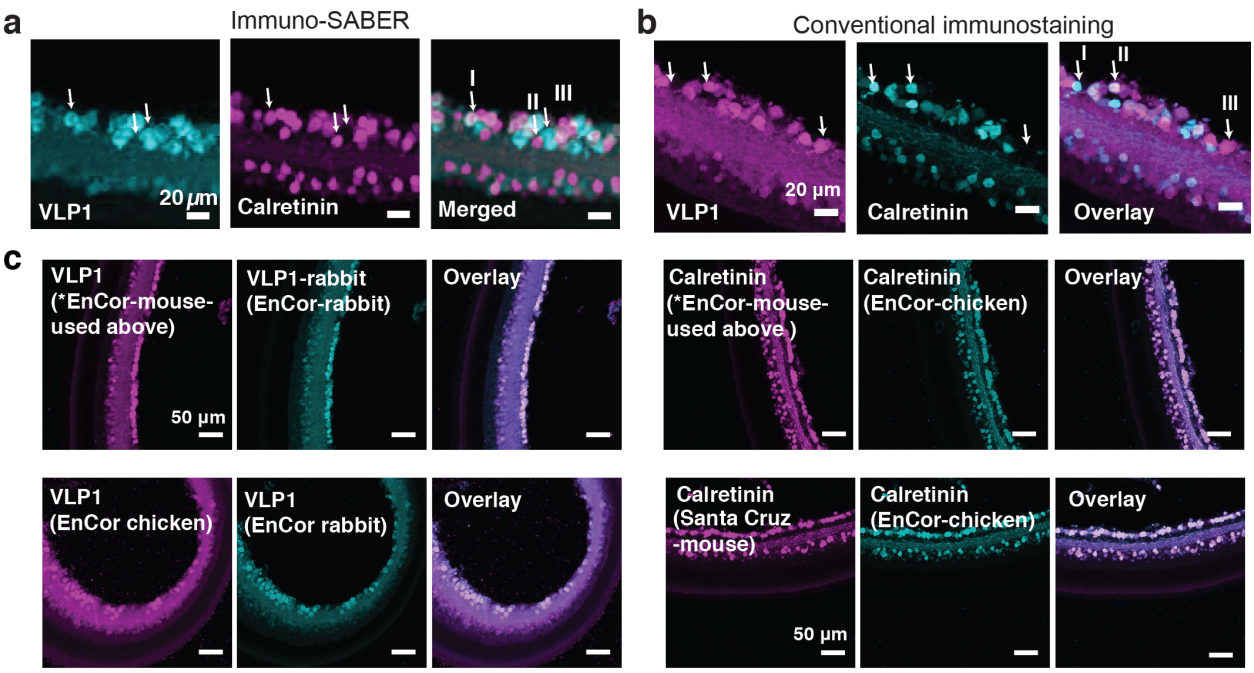

Figure 36. Cell type identification using highly multiplexed immuno-SABER. a) Three cell subtypes (marked with arrows, I: VLP1^{+} and Calretinin^{+}, II: VLP1^{-} and Calretinin^{+}, III: VLP1^{+} and Calretinin^{-}) can be differentiated based on VLP1 and Calretinin expression from data in **Figure 35. b)** Validation of three cell types using conventional immunostaining with primary antibodies followed by fluorophore conjugated secondary antibodies. **c)** Validation of specificity of antibodies used in (a) and (b). EnCor-mouse VLP1 and Encor-mouse Calretinin antibodies were used in the highly multiplexed imaging experiment. Additional two antibodies for each target, Encor-rabbit/chicken for VLP1 and Encor-chicken/SantaCruz-mouse for Calretinin, were used to test the specificity of the antibodies by colocalization.

4.4. Rapid, highly multiplexed super-resolution imaging combining immuno-SABER and Expansion Microscopy

The spatial resolution of conventional fluorescence microscopy is limited due to diffraction of light. A variety of super-resolution imaging methods, including Structure Illumination Microscopy (SIM), Stimulated Emission Depletion (STED), localization-based methods (e.g. STORM and PAINT) have been developed to overcome this limitation[95]. Recently, ExM, which improves the practical resolution by physically expanding hydrogel embedded samples, has been gaining popularity especially for imaging of tissues without specialized super-resolution instruments[96] (**Figure 37a**). Up to 20-fold expansion has been achieved, enabling ~25 nm spatial

resolution imaging[97]. However, a key challenge for ExM is that the physical expansion also dilutes fluorescence signals, creating a high need for signal amplification. Both secondary antibodies and HCR have been used to achieve higher signals in ExM with limited multiplexing capability[98]. A technique termed Magnified Analysis of the Proteome (MAP) was developed to achieve higher multiplexing by combining ExM with repeated antibody staining and retrieval[99]. Up to 7-rounds of sequential protein labeling was achieved with this method; however, due to the slow permeation of the antibodies into the thick expanded tissue samples, each round of primary and secondary antibody staining takes 2-9 days, making the approach slow and laborious for high-multiplexing.

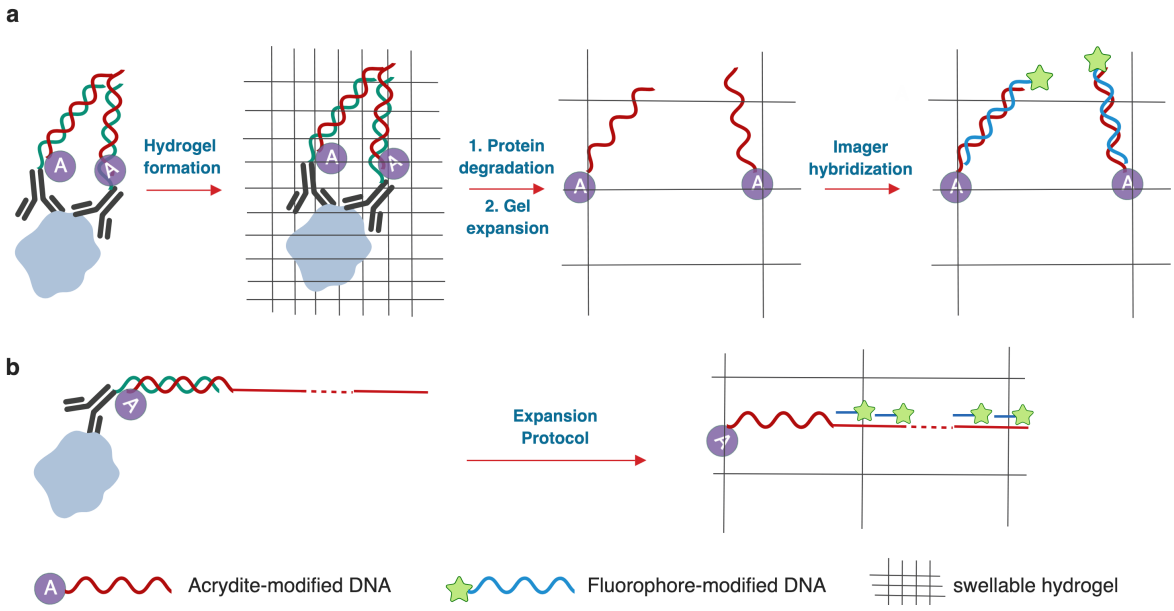

Figure 37. Schematic of Expansion Microscopy (ExM) and SABER-ExM. a) Expansion Microscopy. DNA-conjugated antibodies are used to label specific targets, followed by hybridization of complementary DNA oligonucleotides that are modified with acrydite groups. A swellable hydrogel (acrylamide + sodium acrylate) is formed to incorporate the acrydite groups. The sample then undergoes protease digestion, followed by hydrogel expansion. The expanded hydrogel is stabilized by re-embedding into a nonswellable hydrogel (non shown in the schematic) to prevent hydrogel shrinkage. Fluorophore-conjugated imager strands are then hybridized to the incorporated strands for microscopy imaging. **b)** SABER-ExM. Acrydite modified PER primer sequences are used to generate SABER concatemers, which are then used for hybridization as regular SABER protocol. The modified SABER concatemers are incorporated into the hydrogel and expanded along with the gel. Fluorophore modified imager strands are tiled on SABER sequences for signal amplified imaging.

We tested Immuno-SABER's applicability for ExM samples for rapid, highly multiplexed super-resolution imaging (**Figure 37b**). For this purpose, we modified the 5' end of the SABER concatemers with an acrydite moiety that could be incorporated into polyacrylate hydrogels. We first tested the protocol by staining mouse retina cryosections with DNA-conjugated SV2 antibodies **(Figure 38a)**. The result indicated ~ 3-fold expansion, which was consistent with the

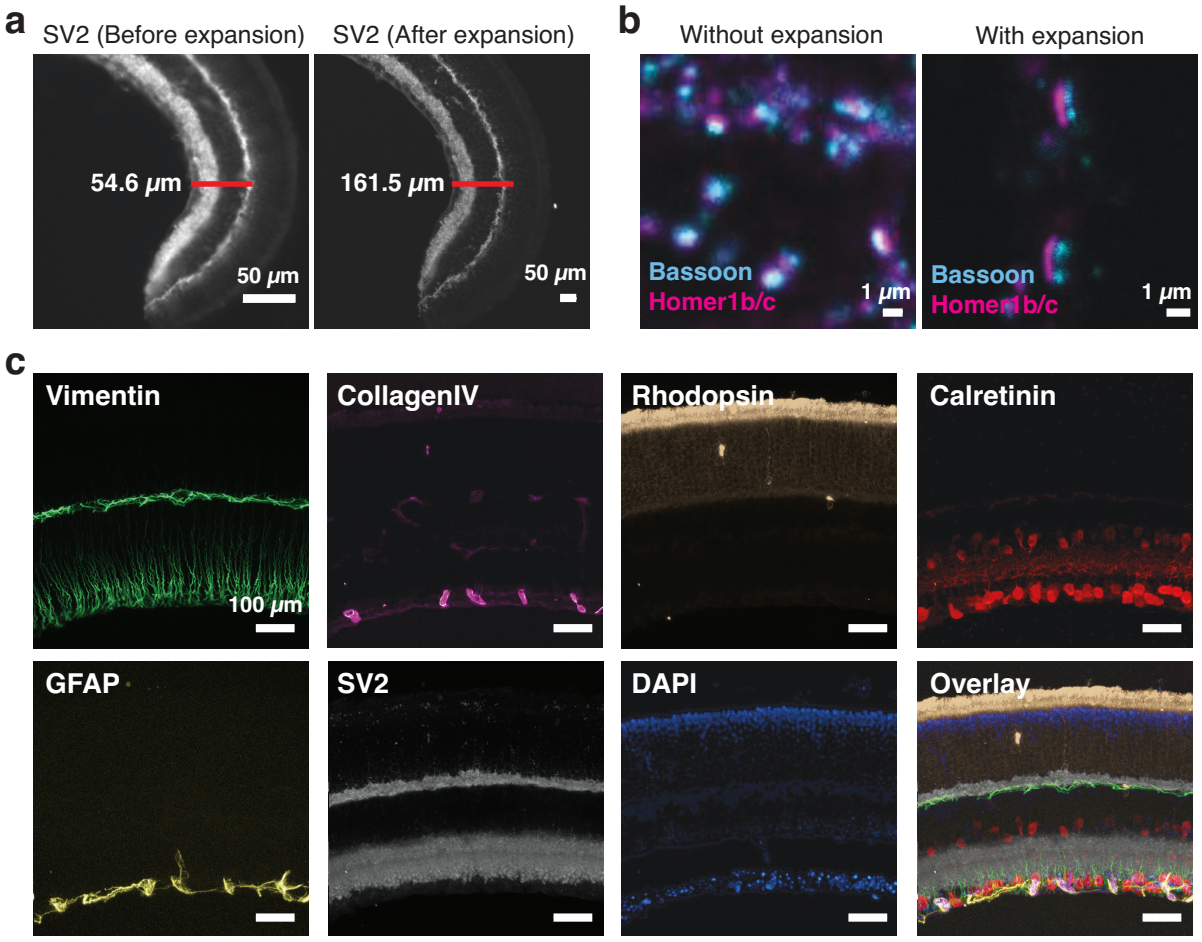

Figure 38. Highly multiplexed super-resolution imaging using Immuno-SABER Expansion Microscopy. a) Before and after expansion imaging of SV2 in mouse retina sections. **b)** Images of pre- and post-synaptic sites of neuronal synapses in a fixed primary mouse hippocampal neuron culture with and without expansion (different fields of view are shown). **c)** Super-resolution imaging of six protein targets in the originally 40 μm-thick mouse retina section (expanded ~3-folds). Two rounds of DNA-Exchange were performed to visualize all six targets. DAPI was imaged in both rounds to serve as a registration marker. The images were maximum projections of z-stacks. They were drift-corrected using DAPI channels, and pseudo-colored for presentation.

expansion factor achieved in the published exFISH protocol[100]. It was smaller than the expansion factor reported in the original expansion protocol (~4.5-fold) due to the shrinkage of the gel in the ionic gel re-embedding solution or in the imaging buffer with 0.5× PBS. To further evaluate Immuno-SABER for super-resolution imaging, we imaged a pre-synaptic marker, Bassoon, and a post-synaptic marker, Homer1b/c, in fixed primary mouse hippocampal neuron culture with and without expansion **(Figure 38b)**. While Bassoon and Homer1b/c were readily separated after expansion, they strongly overlapped without expansion. We next demonstrated multiplexed super-resolution imaging by visualizing six targets (Vimentin, Collagen IV, Rhodopsin, Calretinin, GFAP, SV2) in mouse retina cryosections **(Figure 38c)**.

Since the expanded sample was reaching ~350 μm in thickness, we increased both the incubation time and wash time for imagers (to 45 min and 1.5 h respectively) to achieve optimal imaging quality. Under these conditions, we were able to perform six-target imaging using two rounds of imager incubation in six hours, which is substantially faster than the MAP protocol that would take >3 days[99]. To further increase the speed, we incorporated an alternative fluorophore removal protocol that shortened the removal time from 1.5 h to only 10 min. In this alternative protocol, a disulfide bond was included in the imager strands between the fluorophore and DNA sequences. Hence, the fluorescence signal could be quickly displaced using reducing agents (e.g. TCEP)[67] (**Figure 39a** and **b**).

The DNA sequences and antibodies used for this study are listed in **Table 13 to 17**.

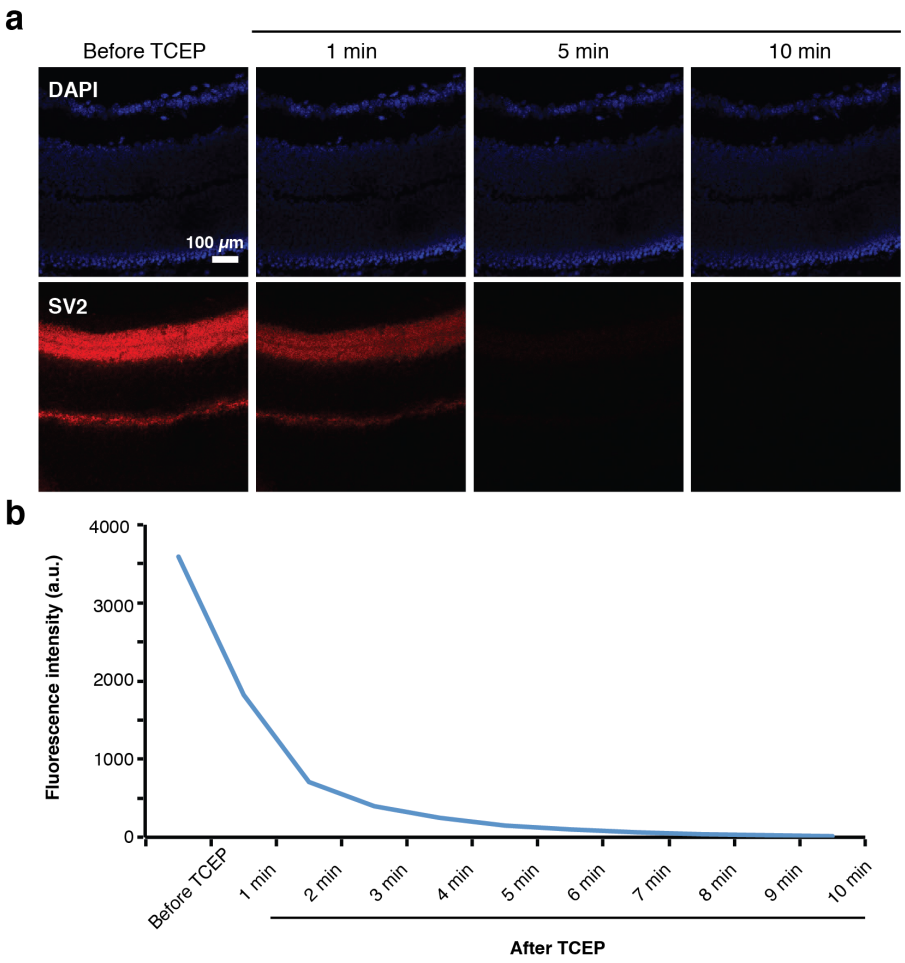

Figure 39. Removal of fluorescence signal in expanded samples using TCEP reduction. A mouse retina section stained with SV2 was expanded and visualized with disulfide bond modified imager strands. The fluorophores on the imager strands were cleaved using TCEP reduction. The fluorescence signal was monitored in a time course for 10 min. **b)** Quantification of fluorescence signals in (**a**) before and after TCEP reduction.

4.5. Methods

Immuno-HCR

Cultured cells preparation and staining

All animal procedures were in accordance with the National Institute for Laboratory Animal Research Guide for the Care and Use of Laboratory Animals and approved by the Harvard

Medical School Committee on Animal Care and the Massachusetts Institute of Technology Committee on Animal Care.

Primary mouse hippocampal neuron cultures were prepared from postnatal day 0 or 1 mice and plated on eight-well ibidi glass-bottom chambers with a density of 10,000 ~ 15,000 cells per well. Cells were grown for 14 days before fixation. BSC-1 cells were plated on eight-well ibidi glass-bottom chambers (10,000 cells per well) and grown for 24 hours.

Cells were fixed using 4% formaldehyde for 15 minutes at room temperature, followed by quenching in 50 mM NH_4Cl for 7 minutes. Cells were then permeabilized and blocked in 0.1% Triton X-100, 0.1% Tween20, 2% nuclease-free BSA (americanBIO, CAS 9048-46-8) and 0.5mg/ml sheared sperm DNA (ThermoFisher, AM96880) for 2 hours. Specimens were incubated with primary antibodies diluted in incubation buffer (0.05% Triton X-100, 0.05% Tween20, 2% nuclease-free BSA, 0.5mg/ml sheared sperm DNA and 0.1% or 0.05% dextran sulfate (Millipore, S4030)) overnight at 4 °C, and then washed with washing buffer (0.05% Triton X-100, 0.05% Tween20, 2% nuclease-free BSA) for five times (brief wash for the first two washes and 10 minute incubation for the other three washes). The samples were post-fixed using $BS(PEG)_5$ (ThermoFisher, 21581) for 1 hour, followed by quenching in 1x TBS for 10 minutes.

Mouse retina section preparation and staining

Animals were given a lethal dose of sodium pentobarbital (120 mg/kg) (MWI, 710101) and enucleated immediately. Eyes were removed and fixed in PFA for 15-30 min. Following dissection, retinas were immersed in 30% sucrose overnight prior to freezing in TFM (EMS, 72592) and cryosectioning at 40 μm. Eight-well ibidi glass-bottom chambers were treated with

poly-D-Lysine overnight, followed by 3 times 1xPBS washes. Retina sections were attached in ibidi chambers and stored at -20 °C. Sections were washed with 1x TBS + 0.3% Triton X-100 for three times with ten minutes per wash. They were then blocked and stained as above.

HCR amplification

Fluorophore-conjugated HCR hairpins were purchased from Molecular Instrument. Samples were blocked in amplification buffer (5x SSC buffer, 0.1% Tween 20 and 10% dextran sulfate) for 1 hour. Meanwhile, HCR hairpins were snap-cooled separately (heat hairpins at 95 °C for 90 seconds in a PCR machine, and then immediately put hairpins on ice for 5 minutes. The hairpins were then left at room temperature for 30 minutes). Hairpins were then mixed and diluted in amplification buffer to 60nM for each hairpin. Samples were incubated with HCR hairpins overnight at room temperature, and free hairpins were removed by three washes with 5x SSCT (5x SSC + 0.1% Tween 20). Hairpins sequences and attached fluorophores are listed in **Table 13**.

Confocal image acquisition

Samples were left in 5x SSC buffer during image acquisition. All images were acquired using a Zeiss Axio Observer with LSM 710 scanning confocal system with either 20x/0.8 NA dry objectives or 63x/1.46 NA oil-immersion objectives. The images were 512*512 pixels and acquired at acquisition speed 7. Each image was acquired by averaging 2 images. Alexa 488 was visualized using a 488nm laser; Alexa 514 was visualized using a 514nm laser; Alexa 546 was visualized using a 546nm laser; Alexa 594 was visualized using a 594nm laser; Alexa 647 was visualized using a 633nm laser.

Image analysis and quantification

All images were visualized and scaled using FIJI. For nonspecific nuclear signals, the fluorescence intensity of random regions of each nucleus was measured using FIJI. For signal amplification quantification, a binary mask was created for each image to represent the cellular structures using MATLAB, and the average fluorescence intensity (the sum of fluorescence signal within the binary mask / the total pixel number within the binary mask) was calculated. Background fluorescence intensity was calculated by averaging the fluorescence signal outside cells. The final fluorescence intensity was derived by subtracting the background fluorescence intensity from the average fluorescence intensity.

Antibodies

AlphaTubulin (ThermoFisher, MA1-80017), BetaTubulin (Sigma, T8328), BetaTubulin (HybridomaBank, E7), Golgi 97 (ThermoFisher, A-21270), LaminB (ThermoFisher, 33-2100), Clathrin (ThermoFisher, MA1-065), Vimentin (Sigma, V6389), GFAP (ThermoFisher, 13-0300), Bassoon (Enzo, ADI-VAM-PS003), SV2 (HybridomaBank), pNFH (EncorBio, MCA-AH1), Calretinin (EncorBio, MCA-6A9).

Antibody-DNA conjugation

The conjugation involves crosslinking of thiol-modified DNA oligonucleotidess to Lysine residues on antibodies. In brief, 250 uM 5' thiol-modified DNA oligonucleotides (Integrated DNA Technologies) were activated by 100 mM DTT for 2 hours at room temperature in dark and then purified using NAP5 columns (GE Healthcare Life Sciences, 17-0853-02) to remove

excessive DTT. Antibodies formulated in PBS only were concentrated using 0.5mL 50KDa Ambicon Ultra Filters (EMDMillipore, UFC510096) to 2 mg/ml and reacted with maleimide-PEG2-succinimidyl ester crosslinkers (ThermoFisher 22102) for 2 hours at 4 degree. Antibodies were then purified using 0.5ml 7kDA Zeba desalting columns (ThermoFisher, 89883) to remove excessive crosslinkers. Activated DNA oligonucleotides were incubated with antibodies (11:1 DNA: Antibody ratio) overnight at 4 °C. Final conjugated antibodies were washed using in 2ml 50KDa Ambicon Ultra Filters six times to remove non-reacted DNA oligonucleotides. Conjugated antibodies were kept at 4 °C.

Table 13. *HCR initiator and hairpin DNA sequences.* All sequences are 5' -> 3'.

Hairpin	Initiators sequence	Hairpin1 sequence	Hairpin2 sequence	Attached fluorophore
B1	gCATTCTTTC TTgAggAgggC AgCAAACggg AAgAg	CgTAAAggAAgACTC TTCCCgTTTgCTgCC CTCCTCgCATTCTTT CTTgAggAgggCAgC AAACgggAAgAg	gAggAgggCAgCAAACg ggAAgAgTCTTCCTTT ACgCTCTTCCCgTTTg CTgCCCTCCTCAAgA AAgAATgC	Alexa 647
B2	AgCTCAgTCC ATCCTCgTAA ATCCTCATC AATCATC	ggCggTTTACTggATg ATTgATgAggATTTA CgAggAgCTCAgTCC ATCCTCgTAAATCC TCATCAATCATC	CCTCgTAAATCCTCA TCAATCATCCAgTAA ACCgCCgATgATTgAT gAggATTTACgAggATg gACTgAgCT	Alexa 594
B3	AAAgTCTAA TCCgTCCCTg CCTCTATATC TCCACTC	CgggTTAAAgTTgAg TggAgATATAgAggC AgggACAAAgTCTA ATCCgTCCCTgCCTC TATATCTCCACTC	gTCCCTgCCTCTATAT CTCCACTCAACTTTA ACCCggAgTggAgATA TAgAggCAgggACggAT TAgACTTT	Alexa 514
B4	CACATTTAC AgACCTCAA CCTACCTCC AACTCTCAC	gAAgCgAATATggTg AgAgTTggAggTAggT TgAggCACATTTACA gACCTCAACCTACC	CCTCAACCTACCTCC AACTCTCACCATATT CgCTTCgTgAgAgTTgg AggTAggTTgAggTCTg	Alexa 546

		TCCAACTCTCAC	TAAATgTg	
B5	CACTTCATA TCACTCACT CCCAATCTC TATCTACCC	ATTggATTTgTAgggT AgATAgAgATTgggA gTgAgCACTTCATAT CACTCACTCCCAAT CTCTATCTACCC	CTCACTCCCAATCTC TATCTACCCTACAAA TCCAATgggTAgATAg AgATTgggAgTgAgTgA TATgAAgTg	Alexa 647 or Alexa 488

Immuno-SABER

PER sequences and preparation of SABER concatemers

In vitro extension of primers. Concatemer extensions were prepared as described previously[101]. Typically, 100 μl reactions were prepared in PBS with final concentrations of: 10 mM $MgSO_4$, 400-1000 units/ml of Bst LF polymerase (NEB M0275L or McLab BPL-300), 600 μM each of dATP/dCTP/dTTP (NEB #M0275L), 100 nM of Clean.G (5'-CCCCGAAAGTGGCCTCGGGCCTTTTGGCCCGAGGCCACTTTCG-3') hairpin[87], 50 nM-1.5 μM hairpin, and water to 90 μl. The Clean.G hairpin has a 5' stretch of C's. Pre-incubation with Clean.G helps to get rid of the impurities in the dHTP mixtures (made up of dATP, dTTP, and dCTP), which may have small amounts of dGTP contamination[87]. After incubation for 15 min at 37°C, 10 μl of 10 μM primer was added, and the reaction was incubated another 1-3 h at 37°C followed by 20 min at 80°C to heat inactivate the polymerase. Reaction products can be stored at -20°C for several months. In our demonstrations, PER products were diluted into concatemer hybridization solutions for binding to the bridge sequences. Alternatively, concatemers can be purified and concentrated using a MinElute (Qiagen #28004) kit with distilled water elution to reduce volume and salt concentration from the reaction condition. Primer sequences and details of the extension conditions utilized for **Figure 33** are listed in Table below. These primer sequences were presented as the 3' tail of the complements of the bridge strands given in Table

below**,** in the format: 5'- bridge*- tt (spacer nucleotides) - 9mer primer sequence - 3', where * denotes the reverse complement. For the extensions in **Figure 33**, the 25mer-tester* bridge was used for all the primers. The strands were obtained from IDT. Primers were synthesized and provided with standard desalting. Hairpins were ordered with 3' inverted dT modification to ensure they cannot be extended. Due to the modification, they were ordered with HPLC purification. Details of the primer and hairpin design criteria are described in our previous work[79,87]. For primary concatemers, we utilize concatemers reaching the 600-700 base based on empirical experience.

Gel electrophoresis. After extension, for internal quality control lengths of concatemers were evaluated by diluting 1 µl of *in vitro* reaction with 19 μl water. For quality controlling, samples were then run on 1-2% E-Gel EX agarose gels (Thermo Fisher #G402001) for 10 min on the E-gel apparatus (Invitrogen, iBase) alongside a 1 kb Plus DNA Ladder (Invitrogen) and imaged with the Sybr Gold channel on a Typhoon FLA 9000 scanner.

For the comparison gel in **Figure 33**, unpurified concatemers were run using 6% TBE-UREA PAGE gels (Thermo Fisher) at 55°C. The gel was pre-run for 1 h before loading the samples. 160 ng Quick-Load Purple Low Molecular Weight DNA Ladder (NEB #N0557S) was loaded as size reference. The reaction products were diluted 1:7 with 2× Urea-Loading Dye, and denatured at 95°C for 5 min. 9 μl from each sample was loaded on the gel. Both samples and the ladder were denatured. Samples were ran for 20 min at 75 V, and at 130 V for 1 h. Gels were stained with 1:10,000 SybrGold in 0.5× Tris-Borate-EDTA (TBE) for 30 min and scanned on a Typhoon FLA 9000 scanner.

Table 14. *Optimized concatemer extension conditions and sequences for the primer library for Figure 33*

Primer ID	Primer sequence	Hairpin ID	Hairpin sequence	Hairpin concentration	Time
p.25	CCAATAATA	h.25.25	ACCAATAATAGGGCCTTTTGGCCCTATTATTGGTTATTATTGG/3InvdT/	1.5 μM	3 h
p.26	ATAAACCTA	h.26.26	AATAAACCTAGGGCCTTTTGGCCCTAGGTTTATTTAGGTTTAT/3InvdT/	9 μM	3 h
p.27	CATCATCAT	h.27.27	ACATCATCATGGGCCTTTTGGCCCATGATGATGTATGATGATG/3InvdT/	0.75 μM	3 h
p.28	CAACTTAAC	h.28.28	ACAACTTAACGGGCCTTTTGGCCCGTTAAGTTGTGTTAAGTTG/3InvdT/	3 μM	2 h
p.29	TCTAAAATC	h.29.29	ATCTAAAATCGGGCCTTTTGGCCCGATTTTAGATGATTTTAGA/3InvdT/	15 μM	3 h
p.30	AATACTCTC	h.30.30	AAATACTCTCGGGCCTTTTGGCCCGAGAGTATTTGAGAGTATT/3InvdT/	5 μM	2 h
p.31	TTATTCACT	h.31.31	ATTATTCACTGGGCCTTTTGGCCCAGTGAATAATAGTGAATAA/3InvdT/	8.5 μM	2 h
p.32	CTTTTTTTC	h.32.32	ACTTTTTTTCGGGCCTTTTGGCCCGAAAAAAAGTGAAAAAAAG/3InvdT/	15 μM	3 h
p.33	CCTTCTATT	h.33.33	ACCTTCTATTGGGCCTTTTGGCCCAATAGAAGGTAATAGAAGG/3InvdT/	5 μM	2 h
p.34	CTCTACTAC	h.34.34	ACTCTACTACGGGCCTTTTGGCCCGTAGTAGAGTGTAGTAGAG/3InvdT/	4 μM	2 h
p.35	TAAAAACTC	h.35.35	ATAAAAACTCGGGCCTTTTGGCCCGAGTTTTTATGAGTTTTTA/3InvdT/	15 μM	3 h
p.36	AACTAATCT	h.36.36	AAACTAATCTGGGCCTTTTGGCCCAGATTAGTTTAGATTAGTT/3InvdT/	10 μM	2 h
p.37	TTTCTCTTC	h.37.37	ATTTCTCTTCGGGCCTTTTGGCCCGAAGAGAAATGAAGAGAAA/3InvdT/	8.5 μM	2 h
p.38	AACATACTA	h.38.38	AAACATACTAGGGCCTTTTGGCCCTAGTATGTTTTAGTATGTT/3InvdT/	5 μM	2 h
p.39	TTCATTTAC	h.39.39	ATTCATTTACGGGCCTTTTGGCCCGTAAATGAATGTAAATGAA/3InvdT/	10 μM	2 h
p.40	ATCCTACAA	h.40.40	AATCCTACAAGGGCCTTTTGGCCCTTGTAGGATTTTGTAGGAT/3InvdT/	9 μM	2 h
p.41	CAATCAAAA	h.41.41	ACAATCAAAAGGGCCTTTTGGCCCTTTTGATTGTTTTTGATTG/3InvdT/	4.5 μM	3 h
p.42	CTTACAAAC	h.42.42	ACTTACAAACGGGCCTTTTGGCCCGTTTGTAAGTGTTTGTAAG/3InvdT/	5 μM	2 h
p.43	ACAAATAAC	h.43.43	AACAAATAACGGGCCTTTTGGCCCGTTATTTGTTGTTATTTGT/3InvdT/	5 μM	2 h
p.44	TTTTCTACC	h.44.44	ATTTTCTACCGGGCCTTTTGGCCCGGTAGAAAATGGTAGAAAA/3InvdT/	4.5 μm	3h
p.45	CCCTTATTT	h.45.45	ACCCTTATTTGGGCCTTTTGGCCCAAATAAGGGTAAATAAGGG/3InvdT/	4 μM	3 h

p.46	TCTTTCATT	h.46.46	ATCTTTCATTGGGCCTTTTGGCCCAATGAAAGATAATGAAAGA/3InvdT/	4.5 μM	3 h
p.47	TTCTTACTC	h.47.47	ATTCTTACTCGGGCCTTTTGGCCCGAGTAAGAATGAGTAAGAA/3InvdT/	8.5 μM	1 h
p.48	CCATAAATC	h.48.48	ACCATAAATCGGGCCTTTTGGCCCGATTTATGGTGATTTATGG/3InvdT/	4 μM	3 h
p.49	CATTTATCC	h.49.49	ACATTTATCCGGGCCTTTTGGCCCGGATAAATGTGGATAAATG/3InvdT/	6.5 μM	1 h
p.50	ATACTTCAC	h.50.50	AATACTTCACGGGCCTTTTGGCCCGTGAAGTATTGTGAAGTAT/3InvdT/	4 μM	1 h
p.51	TACCTCTAA	h.51.51	ATACCTCTAAGGGCCTTTTGGCCCTTAGAGGTATTTAGAGGTA/3InvdT/	6 μM	3 h
p.52	CTCCTATTT	h.52.52	ACTCCTATTTGGGCCTTTTGGCCCAAATAGGAGTAAATAGGAG/3InvdT/	3 μM	2 h
p.53	CTATCCAAA	h.53.53	ACTATCCAAAGGGCCTTTTGGCCCTTTGGATAGTTTTGGATAG/3InvdT/	2 μM	3 h
p.54	ATCCCTATC	h.54.54	AATCCCTATCGGGCCTTTTGGCCCGATAGGGATTGATAGGGAT/3InvdT/	1 μM	3 h
p.55	TCATTACTT	h.55.55	ATCATTACTTGGGCCTTTTGGCCCAAGTAATGATAAGTAATGA/3InvdT/	6.5 μM	3 h
p.56	CTAAATCTC	h.56.56	ACTAAATCTCGGGCCTTTTGGCCCGAGATTTAGTGAGATTTAG/3InvdT/	3.5 μM	3 h
Test-primer	TCTCTTATT	h.test	ATCTCTTATTGGGCCTTTTGGCCCAATAAGAGATAATAAGAGA/3InvdT/	Not included in the gel assay	

Imagers. SABER imagers are 20mer DNA oligonucleotides with fluorophores on the 5' end and inverted dT modification on the 3' end. Imagers were designed to bind the dimers of the primer unit sequence to achieve stable but easily reversible binding that is necessary for DNA-exchange-imaging. Hence, format of the imager sequences are: 5' - Fluorophore- tt - primer* - t - primer* - t - Inverted dT - 3' (t's are spacer T nucleotides.). They were ordered from IDT with 5' fluorophore (Atto488, Atto565, Alexa647 or Alexa750), and 3' inverted dT modification, with HPLC purification. They are named as i.primerID#*. Sequences are listed in below.

Table 15. *Imager strands used for fluorescent visualization*

Imager ID	Imager sequence
i.25*	/Fluorophore/tt-TATTATTGG-t -ATTATTGG-t /3InvdT/
i.26*	/Fluorophore/tt-TAGGTTTAT-t-TAGGTTTAT-t /3InvdT/

i.27*	/Fluorophore/ tt-ATGATGATG-t-ATGATGATG-t 3InvdT/
i.28*	/Fluorophore/ tt-GTTAAGTTG-t-GTTAAGTTG-t/3InvdT/
i.29*	/Fluorophore/ tt-GATTTTAGA-t-GATTTTAGA-t/3InvdT/
i.30*	/Fluorophore/ tt-GAGAGTATT-t-GAGAGTATT-t/3InvdT/
i.31*	/Fluorophore/ tt-AGTGAATAA-t-AGTGAATAA-t/3InvdT/
i.32*	/Fluorophore/ tt-GAAAAAAAG-t-GAAAAAAAG-t/3InvdT/
i.33*	/Fluorophore/ tt AATAGAAGGt AATAGAAGG-t /3InvdT/
i.34*	/Fluorophore/ tt-GTAGTAGAG-t-GTAGTAGAG-t /3InvdT/
i.35*	/Fluorophore/ tt-GAGTTTTTA-t-GAGTTTTTA-t /3InvdT/
i.36*	/Fluorophore/ tt-AGATTAGTT-t-AGATTAGTT-t /3InvdT/
i.37*	/Fluorophore/ tt-GAAGAGAAA-t-GAAGAGAAA-t /3InvdT/
i.38*	/Fluorophore/ tt-TAGTATGTT-t-TAGTATGTT-t /3InvdT/
i.39*	/Fluorophore/ tt-GTAAATGAA-t-GTAAATGAA-t /3InvdT/
i.40*	/Fluorophore/ tt-TTGTAGGAT-t-TTGTAGGAT-t /3InvdT/
i.41*	/Fluorophore/ tt-TTTTGATTG-t-TTTTGATTG-t /3InvdT/
i.42*	/Fluorophore/ tt-GTTTGTAAG-t-GTTTGTAAG-t /3InvdT/
i.43*	/Fluorophore/ tt-GTTATTTGT-t-GTTATTTGT-t /3InvdT/
i.44*	/Fluorophore/ tt-GGTAGAAAA-t-GGTAGAAAA-t /3InvdT/
i.45*	/Fluorophore/ tt-AAATAAGGG-t-AAATAAGGG-t /3InvdT/
i.46*	/Fluorophore/ tt-AATGAAAGA-t-AATGAAAGA-t /3InvdT/
i.47*	/Fluorophore/ tt-GAGTAAGAA-t-GAGTAAGAA-t /3InvdT/
i.48*	/Fluorophore/ tt-GATTTATGG-t-GATTTATGG-t /3InvdT/
i.49*	/Fluorophore/ tt-GGATAAATG-t-GGATAAATG t /3InvdT/
i.50*	/Fluorophore/ tt-GTGAAGTAT-t-GTGAAGTAT t /3InvdT/
i.51*	/Fluorophore/ tt-TTAGAGGTA-t-TTAGAGGTA-t /3InvdT/
i.52*	/Fluorophore/ tt-AAATAGGAG-t-AAATAGGAG-t /3InvdT/

i.53*	/Fluorophore/ tt-TTTGGATAG-t-TTGGATAG-t /3InvdT/
i.54*	/Fluorophore/ tt-GATAGGGAT-t-GATAGGGAT-t /3InvdT/
i.55*	/Fluorophore/ tt AAGTAATGA-t-AAGTAATGA t /3InvdT/
i.56*	/Fluorophore/ tt GAGATTTAG-t-GAGATTTAG t /3InvdT/
Test-imager	/Fluorophore/ tt-AATAAGAGA-t-AATAAGAGA-t /3InvdT/

Branching primers. For stable hybridization of the secondary (branching) concatemers onto the primary concatemers, trimers of the unit repeat sequence were used as bridges, creating a 30-mer hybridization sequence. Hence, branching primers are designed in the format: 5'- p.1* - t -p.1* - t - p.1* - ttt (spacer) - p.2 - 3', where p.1 is the primer used for the primary concatemer, p.2 is the primer for the secondary concatemer, and t's are spacer T nucleotides. For secondary concatemers, we utilize extensions <500 bases based on empirical experience.

Similarly for iterative branching, the tertiary concatemer is designed to use the trimers of primer2 as the bridge, in the format: 5'- p.2* - t - p.2* - t - p.2* - ttt - p.3 - 3', where p.3 is the primer for the tertiary concatemer and t's are spacer T nucleotides. For tertiary concatemers. For the third round, we utilize extensions <300 bases based on empirical experience.

Antibody-DNA conjugation and purification

Conjugation. The conjugation involves crosslinking of thiol-modified DNA oligonucleotides to lysine residues on antibodies in a non-sequence-specific way. Briefly, 25 μl of 1 mM 5'-thiol-modified DNA oligonucleotides (Integrated DNA Technologies) were activated by 100 mM DTT (ThermoFisher #20291) for 2 h at room temperature in dark, and then purified using NAP5 columns (GE Healthcare Life Sciences #17-0853-02) to remove excessive DTT. Antibodies

formulated in PBS only (or with sodium azide) were concentrated using 0.5 mL 50 kDa Ambicon Ultra Filters (EMD Millipore #UFC510096) to 2 mg/ml and reacted with maleimide-PEG2-succinimidyl ester crosslinkers (ThermoFisher #22102) for 2 h at 4°C (100 μg antibodies: 3.75 μl of 1 mg/ml crosslinker). Antibodies were then purified using 0.5 ml 7 kDA Zeba desalting columns (ThermoFisher #89883) to remove excessive crosslinkers. Activated DNA oligonucleotides were incubated with antibodies (11:1, DNA: Antibody molar ratio) overnight at 4°C. Final conjugated antibodies were washed using 2 ml 50 kDa Ambicon Ultra Filters six times to remove non-reacted DNA oligonucleotides. The list of bridge sequences used for conjugation is provided in Table below. The list of antibodies and the corresponding bridge sequences used for each staining, as well as the capture and toehold strands for purification are provided in table below. Conjugated antibodies were diluted in the 1:50-1:200 for immunostaining.

Information note regarding antibody-DNA conjugations. Not all commercial antibodies are provided in a formulation readily available for conjugation (for example antibodies may be provided in unpurified whole serum form or formulated with stabilizers or protectors that interfere with conjugation). Hence customized formulation of antibodies may be required. In addition, we currently utilize non-specific conjugation to Lys residues and provide a simple protocol to prepare custom conjugation of antibodies[63]. Although multiple DNA oligos can be attached to each antibody molecule for further signal amplification, our reaction conditions are optimized to achieve 1-2 oligos per antibody, to prioritize conserving the antigen recognition capability upon conjugation. Alternatively, site-specific conjugation chemistries could be utilized, including click labeling of antibody gylcosyl residues (available as the SiteClick™ kit from

ThermoFisher). Independent of the conjugation method, we recommend testing of antibodies after conjugation to ensure functionality through comparison of the staining pattern with unconjugated antibody. As the high potential of DNA barcoding gains higher recognition and visibility, commercial antibody-DNA conjugation services and ready-to-use kits are also becoming available. Additionally, alternative recent probes (recombinant antibodies, nanobodies, aptamers, etc.) and probe labeling methods (such as unnatural amino acid incorporation or engineering of site-specific adaptor molecules) could facilitate new and highly-efficient means for standardized large-scale probe libraries as future resources.

Purification. To increase the staining efficiency, conjugated antibodies can be optionally purified using a DNA toehold-mediated affinity pull-down protocol. For this, 200 μl of high capacity streptavidin agarose (ThermoFisher #20357) was centrifuged down, washed 3 times using 500 μl PBS, and incubated with 10 μl 1 mM of biotin-labeled binding sequences in 300 μl PBS with 0.1% Triton X-100 for 30 min at room temperature. The agarose was then washed twice with PBS with 0.1% Triton X-100, followed by blocking with 250 μl blocking buffer (2% BSA + 0.1% Triton in PBS) for 1 h at room temperature with rotation. The agarose was then centrifuged and resuspended with 200 μl incubation buffer (1% BSA + 0.1% Triton in PBS) containing the DNA-conjugated antibodies, followed by rotation at 4°C for 1 h. The sample was centrifuged at 4°C and washed twice with 200 μl incubation buffer. The bound antibodies were recovered by adding 20 μl of 1 mM toehold strands (listed in below) in 200 μl incubation buffer. After centrifugation, the supernatant was collected and the agarose was washed three times with 300 μl washing buffer (PBS + 0.1% Triton), collecting supernatant for each time. The supernatant was pooled together and buffer exchanged using 2 ml 50 kDa Amicon Ultra Filters six times to

remove toehold DNA oligonucleotides. Binding sequences and toehold sequences were designed using NUPACK and are provided in table below.

Gel electrophoresis. To examine DNA antibody conjugation, antibodies were denatured in LDS sample buffer (ThermoFisher #NP0007) without reducing reagents (e.g. DTT or 2-ME) at 90 to 95°C for 3 min, and left to cool down to room temperature. The samples were run on 3 to 8% Tris-acetate PAGE gels (ThermoFisher #EA03752BOX) at 80 V for 30 min and 120 V for 3.5 h. The gels were stained with SimplyBlue™ safe stain (ThermoFisher #LC6060) according to the manufacturer's manual, and imaged using a Biorad Gel Doc™EZ imager system. It should be noted that BSA should be avoided in the purification step if the sample needs to be examined using PAGE gels.

Table 16. *Bridge sequences used for antibody conjugation*

Bridge sequence index	DNA sequence
bc42_0	AATTCTATGACACCGCCACGCCCTATATCCTCGCAATAACCC
bc42_1	ATTATCCCTACCGCCAAATCTCCGTGTCCTTAACCGACCTAT
bc42_2	CGTTATCGCCGCCTTATCCACTGTACGATCCTATTCCTCTCC
bc42_3	GTTTCCTATATTTAGCGTCCGTGTCGTTCTCCCGCGCAACAG
bc42_4	TATCTTAAGTCTTCGCGTGTTGTCTCGTCTGGGTATTGCGTT
bc42_5	TCCTGTCCCGACGATCCTACCCTTAAAGTTACTGCGCACCCT
bc42_6	CGGTGAGGTAGGAGTCGTGCGTATCGTTTCCTATATAGCCGT
bc42_7	AGTTCCTGTAGTATCCCGTCGCATAGTCGTACATTCACCGTC
bc42_8	AACAATTCAGCTCCGCCTTATACCGTCTTACCGCCAACATCG
bc42_9	GAATTTGGCCCGTTCTATGTCTAACTCGTGTTCCCGCTTGTA
bc42_10	GTCCTCGCTCTTTCCGCATTTTCCCGTATGCGCTTTGTATTA
bc42_11	TGTCTAAATTCTAATGCCGCCCTATGCCGCCGTTCCAACAAT
bc42_12	CCTTCCGCCGTATGAATTTGACCCGAAGCCCAACCCGACCCT
bc42_13	CAGTTCTTGTATCGCGTCACTTATCGGTTATTGTCCTCTCGC
bc42_14	CCAACCTCTCGTACCAAATTCCGCCACTCAAGCCGTATCAAA
bc42_15	GTTTCAAGAGTCCGTCGCAAATTCCACTACACGCTACGCCCA
25mer-tester	TATTTAGTGTTCGAATAGTTCGATCTAG

Table 17. *Antibodies used in SABER experiments, conjugated bridge sequences and respective SABER primers*

Antibody target	Source	Bridge sequence (for conjugation)	Capture and Toehold sequences for purification (if purified)	SABER primer sequences used in the experiments (+ denotes branching)
Conearrestin	Millipore #AB15282	25mer-tester	Capture: Biotin-GTTGCTGTCGTATGT-CTAGATCGAACTATTC Toehold: GAATAGTTCGATCTAG-ACATACGACAGCAAC	p.30 (Fig. 2) or p28 + p25 (Fig. 3) or test-primer (Fig. 6)
GFAP	ThermoFisher #13-0300	bc42_1	Capture: Biotin - GGGTAGGGTAGTGGT-ATAGGTCGGTTAAGGA Toehold: TCCTTAACCGACCTAT-ACCACTACCCTACCC	p.36 (Fig. 6 and Fig. 7)
PKCα	Novus #NB600-201	bc42_2	Binding sequence: Biotin - CGAGTGAGGTGGAAT-GGAGAGGAATAGGATC Toehold sequence: GATCCTATTCCTCTCC-ATTCCACCTCACTCG	p.25 (Fig. 6)
SV2	HybridomaBank	bc42_3	Capture: Biotin - CGAGTGGTAAGGCAT-CTGTTGCGCGGGAGAA Toehold: TTCTCCCGCGCAACAG-ATGCCTTACCACTCG	p.26 (Fig. 6, Fig.S6, Fig. 7 and Fig. S7); or p27 + p28 + p32 (Fig. S3)
Collagen IV	Novus #NB120-6586	bc42_4	Capture: Biotin - GAAATAGAATGAACG-AACGCAATACCCAGAC Toehold: GTCTGGGTATTGCGTT-CGTTCATTCTATTTC	p.27 (Fig. 6 and Fig.7)
Rhodopsin	EnCor Bio #MCA-A531	bc42_7	Capture: Biotin - GTTAAGGTGGAATGA-GACGGTGAATGTACGA Toehold: TCGTACATTCACCGTC-TCATTCCACCTTAAC	p.33 (Fig. 6 and Fig. 7)
Calbindin	EnCor Bio #MCA-5A9	bc42_8	Capture: Biotin - GGTGAGGTGTAGTGG-CGATGTTGGCGGTAAG Toehold: CTTACCGCCAACATCG-CCACTACACCTCACC	p.34 (Fig. 6)
Vimentin	Cell Signaling #5741S	bc42_9	Capture: Biotin - CGGAACAGATAAAGA-TACAAGCGGGAACACG	p.28 (Fig. 6 and Fig. 7)

			Toehold: CGTGTTCCCGCTTGTA-TCTTTATCTGTTCCG	
Calretinin	EnCor Bio #MCA3G9	bc42_10	Capture: Biotin - GCCAAATTCCACCGC-TAATACAAAGCGCATA Toehold: TATGCGCTTTGTATTA-GCGGTGGAATTTGGC	p.30 (Fig. 6 and Fig. 7)
VLP1	EnCor Bio #MCA-2D11	bc42_11	Capture: Biotin - CGGATGATGAGGGTG-ATTGTTGGAACGGCGG Toehold: CCGCCGTTCCAACAA-TCACCCTCATCATCCG	p.39 (Fig. 6)
Alpha-Tubulin	ThermoFisher #MA1-80017	bc42_0	Capture: Biotin - GTTGAGTGAGGTTGA-GGGTTATTGCGAGGAT Toehold: ATCCTCGCAATAACCC-TCAACCTCACTCAAC	p.30
Ki-67	Cell Signaling #9129 (formulated in PBS)	bc42_1	Capture: Biotin - GGGTAGGGTAGTGGT-ATAGGTCGGTTAAGGA Toehold: TCCTTAACCGACCTAT-ACCACTACCCTACCC	p.30 + p.28 + p.25 (Fig. 3e-j, S3h), or p.41 + p.34 (Fig. 5c), or p.30 or p.30 + p.28 (all other figures)
CD8a	Cell Signaling #85336 (formulated in PBS)	bc42_2	Capture: Biotin - CGAGTGAGGTGGAAT-GGAGAGGAATAGGATC Toehold: GATCCTATTCCTCTCC-ATTCCACCTCACTCG	p.40 + p.28 (Fig. 5c) or p.25 + p.31 (all other figures)
PD-1	Cell Signaling #43248 (formulated in PBS)	bc42_3	Capture: Biotin - CGAGTGGTAAGGCAT-CTGTTGCGCGGGAGAA Toehold: TTCTCCCGCGCAACAG-ATGCCTTACCACTCG	p.26 + p.39
IgA	Jackson #109-005-011	bc42_7	Unpurified	p.34 (Fig. 5a) or p.25 (Fig. 5c)
CD3e	Cell Signaling #85061 (formulated in PBS)	bc42_9	Capture: Biotin - CGGAACAGATAAAGA-TACAAGCGGGAACACG Toehold: CGTGTTCCCGCTTGTA-TCTTTATCTGTTCCG	p.27 + p.32
IgM	Jackson #709-006-073	bc42_11	Unpurified	p.39 (Fig. 5a) or p.35 (Fig. 5c)
Bassoon	Enzo ADI-VAM-#PS003	bc42_0 (conjugated onto the secondary antibody, Jackson ImmunoRese	Unpurified	p.30 (Fig.7 and Fig. S7)

		arch #715-005-151)		
Homer 1b/c	ThermoFisher #PA5-21487	bc42_3 (conjugated onto the secondary antibody, Jackson ImmunoResearch #711-005-052)	Unpurified	p.26 (Fig.7 and Fig. S7)
Anti-rabbit IgG (to detect Ki-67 indirectly)	Jackson # 711-005-152	bc42_3	Unpurified	p.30 + p.28 (Fig. 3h-j, S3i)

Antibodies used to validate colocalization of VLP1 and Calretinin in Fig. **S6d-f**: Calretinin (SantaCruz #SC-365956; EnCor Bio #CPCA-Calret; EnCor Bio #MCA-3G9 AP), VLP1 (EnCor Bio #RPCA-VLP1; EnCor Bio #CPCA-VLP1; EnCor Bio #MCA-2D11).

Fluorophore-conjugated secondary antibodies used for reference imaging: anti-rat-Alexa647 (ThermoFisher #A-21472), anti-rabbit-Alexa488 (ThermoFisher #A-21206), anti-rabbit-Atto488 (Rockland #611-152-122S), anti-mouse-Alexa647 (ThermoFisher #A-31571).

Microtubule staining in cell culture

Staining. BS-C-1 cells were plated on eight-well ibidi glass-bottom μ-slides (ibidi #80826) and grown until 50-60% confluency. Cells were fixed with 4% paraformaldehyde (PFA) for 45 min, and quenched with 100 mM NH_4Cl in PBS for 20 min and washed with PBS for 5 min. Cells were then permeabilized and blocked in 2% nuclease-free BSA (AmericanBIO, CAS 9048-46-8) + 0.1%-Triton in PBS for 30 min. Samples were incubated with DNA-conjugated primary antibodies diluted in the incubation buffer made of 0.1% Triton X-100, 2% nuclease-free BSA, 0.2 mg/ml sheared salmon sperm DNA, 0.05% Dextran sulfate (Millipore #S4030), 4 mM EDTA

in PBS overnight at 4°C, and then washed with PBS with 0.1% Triton X-100 and 2% BSA for 3 times for 10 min each. Samples were then washed with PBS twice for 5 min and post-fixed using 5 mM $BS(PEG)_5$ (ThermoFisher #21581) in PBS for 30 min, followed by quenching in 100 mM NH_4Cl in PBS for 5 minutes. The incubation with the primary concatemer was performed at 37°C in 20% formamide (deionized, Ambion #AM9342), 10% Dextran sulfate (Millipore #S4030) and 0.1% (v/v) Tween-20 in 2× SSC with 0.2 mg/ml sheared salmon sperm DNA for 3 h. 650 base long primary concatemers prepared *in vitro* by PER were diluted in this buffer at 133 nM final primer concentration (primer concentration in the PER mix is considered a proxy for the concatemer concentration after the reaction, since all primers are expected to be extended by the catalytic hairpins that are provided in excess). After concatemer hybridization the samples were washed for 5 min at RT with 45% formamide in PBS and three times for 10 min each with PBS + 0.1% Triton X-100 at 37°C. Branching hybridization was performed at 37°C in 30% formamide, 10% Dextran sulfate and 0.1% (v/v) Tween-20 in 2× SSC with 0.2 mg/ml sheared salmon sperm DNA for overnight at 133 nM final concentration of the 450 base long secondary concatemers. Samples were washed for 5 min at room temperature with 45% formamide in PBS and three times for 10 minutes each with PBS + 0.1% Triton X-100 at 37°C. Imagers were hybridized at 1-1.5 μM final concentration in PBS + 0.1% Triton X-100 for 1 h at room temperature (hybridization duration with the imagers can be significantly decreased for faster preparation), followed by a 5 min wash with PBS + 0.1% Triton X-100 and two times 5 min wash with PBS. Samples were stained with 1 µg/ml DAPI (Invitrogen #D1306) in PBS for 10 min and washed twice for 1 min with PBS. Imaging was performed in SlowFade with DAPI (Invitrogen #S36938) embedding medium.

Preparation, staining, SABER application and quantification on mouse retina cryosections

Sample preparation. All animal procedures were in accordance with the National Institute for Laboratory Animal Research Guide for the Care and Use of Laboratory Animals and approved by the Harvard Medical School Committee on Animal Care. Animals were given a lethal dose of sodium pentobarbital (120 mg/kg) (MWI, 710101) and enucleated immediately. Eyes were removed and fixed in PFA for 15 to 30 min. Following dissection, retinas were immersed in 30% sucrose overnight prior to freezing in TFM (EMS, 72592) and cryosectioning at ~30-40 μm. Eight-well ibidi glass-bottom μ-slides were treated with 0.3 mg/ml poly-D-Lysine for at least 30 minutes, followed by 3 times PBS washes. Retina sections were immobilized onto the glass and stored at -20°C. Sections were washed with Tris-buffered saline (TBS) + 0.3% Triton X-100 for three times with 10 min per wash. They were then blocked and stained as above, except that BSA was replaced by 5% donkey serum and 0.1% Tween-20 was replaced by additional 0.2% Triton X-100.

Immuno-SABER application. PER extensions were diluted in 1:7.5 to 1:20 (depending on the target density) in incubation buffers. Two different concatemer hybridization buffers were used: buffer 1 is 40% formamide + 10% Dextran sulfate + 0.1% Triton X-100 + 0.02% sodium azide + 5mM EDTA in PBS, and buffer 2 is 30% formamide + 10% Dextran sulfate + 0.1% Triton X-100 + 0.02% sodium azide + 5 mM EDTA in PBS. Buffer 1 was used for incubation with primary concatemers and buffer 2 was used for branching concatemers. The samples were left at room temperature overnight in a humidified chamber. The samples were washed with 45% formamide + 0.1 % Triton X-100 + 5mM EDTA in PBS for 30 minutes and twice with 30% formamide + 0.1 % Triton X-100 + 5mM EDTA in PBS for 30 min at room temperature. For

branched conditions, 45% formamide was replaced with 40% formamide for the first wash. For multiplexed imaging experiment, all primary concatemers were incubated simultaneously. Bridge and primer sequences for each target and experiment are given in table above.

To quantify linear SABER amplification for cone arrestin, the amplification samples were incubated with SABER concatemers extended from 25mer-tester*-tt-p.28 (CTAGATCGAACTATTCGAACACTAAATA-tt-CAACTTAAC). The unamplified samples were hybridized with the unextended primer 25mer-tester*-tt-p.28-a-p.28 (CTAGATCGAACTATTCGAACACTAAATA-tt-CAACTTAAC-a-CAACTTAAC), which carries one imager binding site (equivalent to two repeats of the primer sequence) instead of the extended concatemer (at the same final concentration).

For quantification of branched SABER for cone arrestin, the branching sample was first incubated with the primary concatemers extended from 25mer-tester*-tt-p.28, followed by incubation with secondary concatemers extended from 28*-t-28*-t-28*-ttt-p.25 primer (GTTAAGTTG-t-GTTAAGTTG-t-GTTAAGTTG-ttt-CCAATAATA).

For iterative SABER quantification for SV2, the unamplified sample was hybridized with unextended primer bc42_3*-tt-p.27-a-p.27 (CTGTTGCGCGGGAGAACGACACGGACGCTAAATATAGGAAAC-tt-CATCATCAT-a-CATCATCAT); the linear amplified sample was hybridized with the primary concatemer extended from bc42_3*-tt-p.27 (CTGTTGCGCGGGAGAACGACACGGACGCTAAATATAGGAAAC-tt-CATCATCAT). The branching sample additionally hybridized with the secondary concatemer 27*-t-27*-t-27*-ttt-p.28 (ATGATGATG-t-ATGATGATG-t-ATGATGATG-ttt-CAACTTAAC); the iterative

amplification sample was additionally hybridized the tertiary concatemer extended from 28*-t-28*-t-28*-ttt-p.32 (GTTAAGTTG-t-GTTAAGTTG-t-GTTAAGTTG-ttt-CTTTTTTTC).

Fluorescence Imaging. Fluorophore-labeled imager strands were diluted in 0.1% Triton X-100 in PBS to ~250 nM-1 μM, and incubated with samples for 30 min, followed by washing using 0.1% Triton X-100 in 0.5× PBS for three times. Samples were left in PBS during image acquisition.

For 10-color multiplexing, the entire experiment was done using five rounds of buffer exchange with an average of 1.5 h per round that included 30 min for imager hybridization, 15 min for excessive imager strands removal, 15 min for imaging and 30 min for imager strands removal. It should be noted that the duration for each step is sample dependent with thicker samples requiring longer time to ensure complete penetration and signal removal. To ensure the best signal and simplify the multiplexed experimental design, we allowed excessive time for each step, however it is possible to shorten incubation and washing times upon optimization.

All images for mouse retina sections were acquired using a Zeiss Axio Observer with LSM 710 scanning confocal system with a 20×/0.8 NA air objective. The images were 512×512 pixels or 1024×1024 pixels and acquired at acquisition speed 7. Each image was acquired by averaging 2 images. Atto488 was visualized using a 488 nm laser; Atto565 was visualized using a 546 nm laser; Alexa647 was visualized using a 633 nm laser. To remove imager strands, samples were washed three times with 30% formamide + 0.1% Triton X-100 in 0.1× PBS. The samples were left in PBS during imaging. Acquired images were scaled and colorized for display using FIJI[102] and Photoshop.

Tyramide signal amplification. For retina cryosections, Alexa Fluor 647 TSA™ Kit #6 with HRP–goat anti-mouse IgG (Life Technologies #T20916) was used following manufacturer's recommendations, without the optional pre-bleaching step and with 7.5 min tyramide incubation.

Quantification. For quantification of signal amplification in retina samples (SV2 and cone arrestin), the mask regions were selected manually using FIJI and mean fluorescence intensity was calculated. The background was calculated by averaging the fluorescence signal of six randomly selected regions outside the retinas. The final fold-amplification values were obtained by subtracting the background value from the average signal value for the condition and normalizing that by the unamplified or by the linear condition.

Preparation, staining, SABER application on whole mount retina samples

Sample preparation and staining. Whole mount retina samples were prepared as free-floating samples, which allowed reagents to penetrate from both sides of retinas. The thickness of whole mount retina samples are typically ~160 to 180 μm. The samples preparation was conducted with a similar protocol as above but with longer incubation and wash times. DNA-conjugated primary antibodies were incubated for 40 h at 4°C, and washed for 3 × 1 h. DNA extensions were incubated for 40 h at room temperature, and washed for 3 × 1 h. Fluorescent oligos were incubated for 2 h at room temperature, followed by 3 × 30 min. Retinas were flattened by creating 4 incisions and mounted on a glass slide. Bridge and primer sequences for each target are given in table above.

Imaging. The images were acquired using a Zeiss Axio Observer with LSM 710 scanning confocal system with a 10×/0.45 NA air objective. A z-stack of 98 sections with 1 μm spacing was taken for each target. It should be noted that although the entire whole mount retina is about ~180 μm, the signal from vimentin and collagen IV are typically located in half of the retina section from the nerve fiber layer to the outer plexiform layer.

PER sequence crosstalk analysis

BS-C-1 cells were grown in glassbottom 96-well plate (Ibidi #89626) with 5,000 cells per well. Cells were fixed with 4% PFA for 15 minutes, and quenched with 50 mM NH_4Cl in PBS for 7 min. Cells were then permeabilized and blocked in 0.1% Triton X-100, 0.1% Tween20, 2% nuclease-free BSA (AmericanBIO, CAS 9048-46-8) and 0.2 mg/ml sheared salmon sperm DNA (ThermoFisher #AM9680) in PBS for 1 h. Samples were incubated with DNA-conjugated primary antibodies diluted in incubation buffer (0.05% Triton X-100, 0.05% Tween20, 2% nuclease-free BSA, 0.2 mg/ml sheared salmon sperm DNA, 0.05% Dextran sulfate (Millipore #S4030), 5 mM EDTA in PBS) overnight at 4°C, and then washed with washing buffer (0.05% Triton X-100, 0.05% Tween-20, 2% nuclease-free BSA, 5 mM EDTA in PBS) for five times (1-2 min for the first two washes and 10 min incubation for the other three washes). Samples were washed with PBS twice and post-fixed using 5 mM $BS(PEG)_5$ (ThermoFisher #21581) in PBS for 1 h, followed by quenching in TBS for 10 min. Concatemer and imager hybridizations were performed as described in Section 5 for the retina cryosections.

For cognate wells, 20 nM corresponding imager strands were incubated, while for crosstalk wells, all other imager strands were incubated with 20 nM for each imager strand. The samples were imaged using Zeiss Axio Observer Z1 with a 20×/0.8 air objective. For signal

quantification, the bright field images were acquired and used to create masks in MATLAB. Average fluorescence signals were calculated within the mask region. The background was calculated as the average fluorescence signals outside the cells. The final fluorescence intensity was average fluorescence intensity within cell masks minus background intensity.

Expansion microscopy

The PER primer sequences were modified with acrydite at the 5'-end (Integrated DNA Technologies), and extended as above. Mouse retina samples were stained with DNA-conjugated antibodies, followed by SABER extension incubation. After washing away excessive SABER extension, a layer of expandable gel was formed according to the original expansion microscopy protocol[96]. In brief, samples were incubated monomer solution (1x PBS, 2 M NaCl, 8.625% (w/v) sodium acrylate, 2.5% (w/v) acrylamide, 0.15% (w/v) N,N'-methylenebisacrylamide) with ammonium persulfate (APS) and teramethylethylenediamine (TEMED) on ice with open air for 20 minutes. A gelation chamber was then constructed by placing a No.1 coverglass on each side of the tissue section and covering with a No.1 coverglass. The specimens were transferred to a humidified incubator and left at 37°C for 2 h. The samples were then digested using Proteinase K (New England BioLabs, Cat.No: P8107S) at 1:100 dilution in digestion buffer (50 mM Tris (pH 8), 1 mM EDTA, 0.5% Triton X-100, 0.8 M guanidine HCl) at 37 °C overnight. The digested samples were then expanded in excess volumes of de-ionized water. To prevent expanded samples from shrinkage, they were re-embeded in a nonexpandable gel (3% acrylamide, 0.15% N,N′-Methylenebisacrylamide with 0.05% APS, 0.05% TEMED). The gel was placed on a bind-silane treated No.1.5 coverglass and immersed in the gel solution on ice for 20 minutes, followed by gelation at 37°C for 1.5 h. To coat coverglass with bind-silane, wash the coverglass with

ddH_20 followed by 100% ethanol. Dilute 5 µl of Bind-Silane reagent (GE #GE17-1330-01) into 8 ml of ethanol, 1.8 ml of ddH_2O and 200 µl of acetic acid. After re-embedding, the samples were imaged as above in regular retina tissue section imaging.

For the primary neuron culture, the culture was grown on a 12 mm diameter round #1 coverslips, and stained with Bassoon and Homer1b/c antibodies, followed by DNA-conjugated anti-mouse and rabbit secondary antibodies. The expandable gel (19% (w/v) sodium acrylate, 10% (w/v) acrylamide, 0.05% (w/v) N,N'-methylenebisacrylamide in PBS) was formed by placing the coverslip against a parafilm sheet with 20 µl of expansion gel solution in between. The gel was then digested and expanded as above. The gel was transferred to a coverslip dish (ibidi #81148) and was incubated with the imager strands (Atto488-i.30* and Atto565-i.26*) in 0.5× PBS without re-embedding and left in 0.5× PBS during confocal imaging, which gave a similar expansion factor of ~3 fold. Fluorescence imaging was performed as described in Section 5 for the retina cryosections.

Chapter V

Discussion and Conclusion

Mapping molecular heterogeneity at single cell level is of great interest, and a number of large-scale collaborative projects, such as the Human Cell Atlas Project and the Human BioMolecular Atlas Program, have been launched to develop technologies for such efforts[103,104]. In the past few years, advancement of single cell DNA/RNA sequencing of dissociated cells has enabled researchers to discover new cell types and analyze cell population change. However, the loss of spatial information makes it difficult to understand how different cell types interact with each other to realize biological functions. Hence, *in situ* analysis with highly multiplexed microscopy imaging methods such as Fluorescence *in situ* Sequencing (FISSEQ)[105], Multiplexed Error-robust FISH (MERFISH)[67,106], Sequential Barcoding FISH (seqFISH)[43,107], Spatially-resolved Transcript Amplicon Readout Mapping (STARmap)[108] and ClampFISH[109] are poised to recover the molecular identities of cells in their spatial context by allowing high levels of multiplexing. For RNA molecules, amplification with high-multiplexing has been attained via combinatorial barcoding or amplicon-supported *in situ* sequencing[105,107,108,110]. However, these capabilities have not translated similarly for multiplexed amplification of protein targets, owing to differences in their cellular organization. Unlike RNA transcripts, which are sparsely organized and mostly found as discrete spots, proteins are spatially overlapping and are organized in clusters with high densities of multiple other targets. This makes the combinatorial or sequencing based readout of barcodes in multiplexed fashion very challenging.

5.1 Summary of the evolution of DNA-Exchange-Imaging and Immuno-SABER

In this thesis, we focused on highly multiplexed *in situ* protein imaging, an application that is relatively less developed and in high need of new innovations. We previously reported Exchange-PAINT, a technique that allows highly multiplexed single molecule localization based

super-resolution imaging using DNA-barcoded antibodies. To obtain better DNA-conjugated labeling probes, we first developed a chemical method to covalently attach single stranded DNA oligonucleotides to lysine residues of antibodies/nanobodies. Compared with the "antibody-biotin-streptavidin-biotin-DNA sandwich" method used previously, this method has two major advantages: 1) covalent conjugation prevents the detachment of DNA oligonucleotides from antibodies, which otherwise causes loss of signals and cross-contamination of signals between antibodies; 2) shorter crosslinker between antibodies and DNA oligonucleotides reduces linkage errors and improves imaging accuracy. With those improved probes, we demonstrated eight-target super-resolution Exchange-PAINT imaging in fixed cell culture samples.

Exchange-PAINT has a few key drawbacks: slow imaging speed, limited sample depth and requirement for high signal-to-noise microscopy. To develop a more universal platform for highly multiplexed imaging, we developed DNA-Exchange-Imaging (DEI). Instead of transient binding between imager and docking DNA duplex, DEI uses semi-transient or stable binding between imager and docking DNA duplex. Semi-transient has the benefit of fast imager exchange, but it has lower signal-to-noise compared with stable binding, making the stable binding scheme a preferred method for later technique development. Using DEI, we successfully applied the DNA-Exchange scheme to diffraction confocal and super-resolution SIM/STED imaging platforms to achieve rapid, highly multiplexed *in situ* protein imaging.

The key challenge for the initial DEI method is that lack of signal amplification limits the imaging quality and detection sensitivity. To solve the problem, we introduced two DNA-based signal amplification methods, HCR and SABER. Both methods can successfully amplify the signal about 5-80 folds, depending on the targets, sample types and protocol used. HCR utilizes small DNA hairpins so that the penetration of HCR hairpins are faster compared with the long

DNA concatemers used in SABER. However, the current design of HCR only has five orthogonal hairpin pairs, limiting the number of protein targets that can be simultaneously detected. In addition, the current design of HCR has fluorophores conjugated to the DNA hairpins and hence it is not compatible with DEI. We have been working on developing a new generation of HCR that has more orthogonal hairpin pairs and is also compatible with DEI. The work has not been finalized and therefore is not included in the thesis. On the other hand, SABER enables highly multiplexed *in situ* detection with high sensitivity. It is naturally compatible with DEI for rapid signal addition and removal. To design orthogonal SABER sequences, we relied on a 3-letter code (where G nucleotides are avoided in the primer sequence) and an efficient and non-leaky stopper for the polymerase to achieve controlled signal amplification through PER. We performed *in situ* testing of a pool of 32 from our 50 *in silico* designed sequences, where we detected minor crosstalk for only 1 of the 1024 pairs (32×32) under our experimental conditions. Owing to the simplicity of sequence design and minimal sequence constraints PER requires, it is straightforward to scale up the orthogonal sequence pool size and reach much higher multiplexing levels for detailed protein maps. Despite of the long concatemers (600~700 nucleotides) used in SABER, we saw no significant penetration issue in thick whole mount samples (~100 μm thick from each side). We hypothesize that it is attributed to the 3-letter code used for SABER sequence design that minimized secondary structures of the concatemers. One requirement for using SABER is long incubation time to allow SABER concatemers to penetrate samples. For 5 μm FFPE sample, one-hour incubation is sufficient to generate strong signals. For 40 μm mouse retina cryosections, we usually leave the incubation overnight at room temperature. For ~160 μm whole mount retina samples, we incubate the sample with SABER concatemers for ~40 hours at room temperature. Higher incubation

temperature can accelerate concatemers penetration but also increase the risk of sample dehydration, making a humidified chamber a necessity. Using Immuno-SABER, we demonstrated 10-target protein imaging using all primary conjugated antibodies in mouse retina sections. Interestingly, we found three cell types identified by VLP1 and Calretinin colocalization. It shows the usefulness of highly multiplexed imaging as VLP1 is less well studied and hypothesis-driven research would likely not to exam the colocalization of these two markers.

With the high multiplexing and high sensitivity capabilities of Immuno-SABER, we combined it with super-resolution expansion microscopy (ExM). Compared with other super-resolution imaging platforms, expansion microscopy is unique as it does not require specialized microscopy and a regular confocal microscopy is adequate. As a result, it enables fast scanning and deep sample imaging, which is critical for large-scale complex tissue mapping such as whole brain scanning. A key challenge for ExM is that the physical expansion of samples dilutes fluorescence signals as a function of the expansion factor. SABER compensates the signal loss by signal amplification. Using SABER-ExM, we demonstrated 6 targets imaging in tissue samples expanded ~3-fold in three dimensions within six hours in contrast to ~4-5 days using previously published protocols such as MAP[99]. With the alternative protocol using TCEP reduction, the experimental time can be further reduced to 3 hours.

5.2 Remaining challenges for highly multiplexed *in situ* protein imaging using DNA-barcoded antibodies

The methods of using DNA-barcoded antibodies for highly multiplexed *in situ* protein imaging have rapidly evolved during the past few years owing to the efforts both from our lab

and from other labs[111-116]. One element, however, has not fundamentally changed and is becoming the bottleneck for the technology. That is the antibody. All developed methods rely on high quality antibodies to bring DNA barcodes to specific cellular targets. Although numerous antibody companies are in the market with tens of thousands of commercialized antibodies, it, unfortunately, cannot fulfill the requirement for highly multiplexed imaging because 1) Not all targets have available antibodies, particularly for membrane proteins, proteins without known functions and post-translational modifications. In the case of existing antibodies, not all antibodies work for immunostaining purposes. This limits which target can be imaged and analyzed using highly multiplexed *in situ* protein imaging. 2) Antibodies are costly reagents with 100 μg typically selling for more than $300. Our DNA conjugation protocol uses at least 100 μg antibodies as the input material with a yield of less than 50%. With the goal of achieving 30-target *in situ* protein imaging, the starting cost for antibodies will easily go beyond $10,000, which is not practical for most research laboratories. In addition, the majority of commercial antibodies are in a formulation with BSA or glycerol for long-term storage. The formulation is not compatible with the conjugation chemistry, and customization of antibody formulation from commercial companies is exceedingly expensive. 3) For a certain target that is widely studied, multiple antibodies are usually developed by different antibody companies. Considering the cost of antibodies, testing all antibodies to find out the best antibody is unrealistic for individual laboratories. In addition, it poses challenges for reproducibility of the results because different antibodies may give rise to different staining results due to their affinity and specificity. 4) With the current non-specific DNA antibody labeling technique, we have experienced a significant variation regarding the number of conjugated DNA per antibody and the sites for DNA conjugation, which occasionally lead to the failure of antibodies to recognize targets after DNA

conjugation. Information such as protein sequences can be helpful to guide conjugation optimization. However, such information is not open to the public.

To address this antibody challenge, we have proposed to establish an open-access recombinant antibody database. Open access allows scientists to obtain and share knowledge freely. Recombinant antibodies enable long-term low cost storage of antibody information as computer files, as well as customized antibody engineering and production. This project contains two major components: recombinant antibody development and validation. It is a community-driven project, which means both development and validation will not be done by a single research entity. Instead, the work will be disseminated to the entire community of researchers who are using antibodies as research tools. Groups with antibody development expertise, such as Neuromab in UC Davis and Institute for Protein Innovation in Harvard, can lead the effort for antibody generation. The products can be validated for specific application (e.g. immunostaining, Western blot or immunoprecipitation) by individual laboratories that are interested in the target. A centralized internet-based platform, similar to Protein Data Bank, can be developed for knowledge deposition and sharing. To motivate scientists to develop and validate antibodies, technologies such as blockchain could be used to assign credits to scientists who contribute to the database. I believe this database will become a tremendously valuable resource for the community.

5.3 Concluding remarks

Since the invention of immunofluorescence imaging for *in situ* protein detection in 1930s, the technique has evolved dramatically and has become one of most widely used techniques in

research and clinical laboratories. In this thesis, I presented simple and effective methods for highly multiplexed, high sensitivity and high/super optical resolution *in situ* protein detection. The method is valuable for a wide spectrum of potential applications including tissue atlases, tumor/disease profiling, pathology analysis and biomarker screening/discovery. It will greatly contribute to the next-generation *in situ* 'omics' analysis and broaden our knowledge about how complex biological systems are functioning.

Appendix A

Invited Review: From Designing the Molecules of Life to Designing Life: Future Applications Derived from Advances in DNA Technologies

From Designing the Molecules of Life to Designing Life: Future Applications Derived from Advances in DNA Technologies

Richie E. Kohman[1,+], Aditya M. Kunjapur[2,+], Eriona Hysolli[2,+], Yu Wang[1,2,+,] and George M. Church[1,2,*]

1. Wyss Institute for Biologically Inspired Engineering, Harvard University, Boston, MA, USA
2. Department of Genetics, Harvard Medical School, Boston, MA, USA

+ These authors contributed equally to this work.

Since the elucidation of its structure, DNA has been at the forefront of biological research. In the past half century, an explosion of DNAbased technology development has occurred with the most rapid advances being made for DNA sequencing. In parallel, dramatic improvements have also been made in the synthesis and editing of DNA from the oligonucleotide to the genome scale. In this Review, we will summarize four different subfields relating to DNA technologies following this trajectory of smaller to larger scale. We begin by talking about building materials out of DNA which in turn can act as delivery vehicles in vivo. We then discuss how altering microbial genomes can lead to novel methods of production for industrial biologics. Next, we talk about the future of writing whole genomes as a method of studying evolution. Lastly, we highlight the ways in which barcoding biological systems will allow for their three-dimensional analysis in a highly multiplexed fashion.

DNA Nanotechnology

International Edition: DOI: 10.1002/anie.201707976
German Edition: DOI: 10.1002/ange.201707976

From Designing the Molecules of Life to Designing Life: Future Applications Derived from Advances in DNA Technologies

*Richie E. Kohman[+], Aditya M. Kunjapur[+], Eriona Hysolli[+], Yu Wang[+], and George M. Church**

Keywords:
DNA nanotechnology · DNA synthesis · genome engineering · genome recoding · synthetic biology

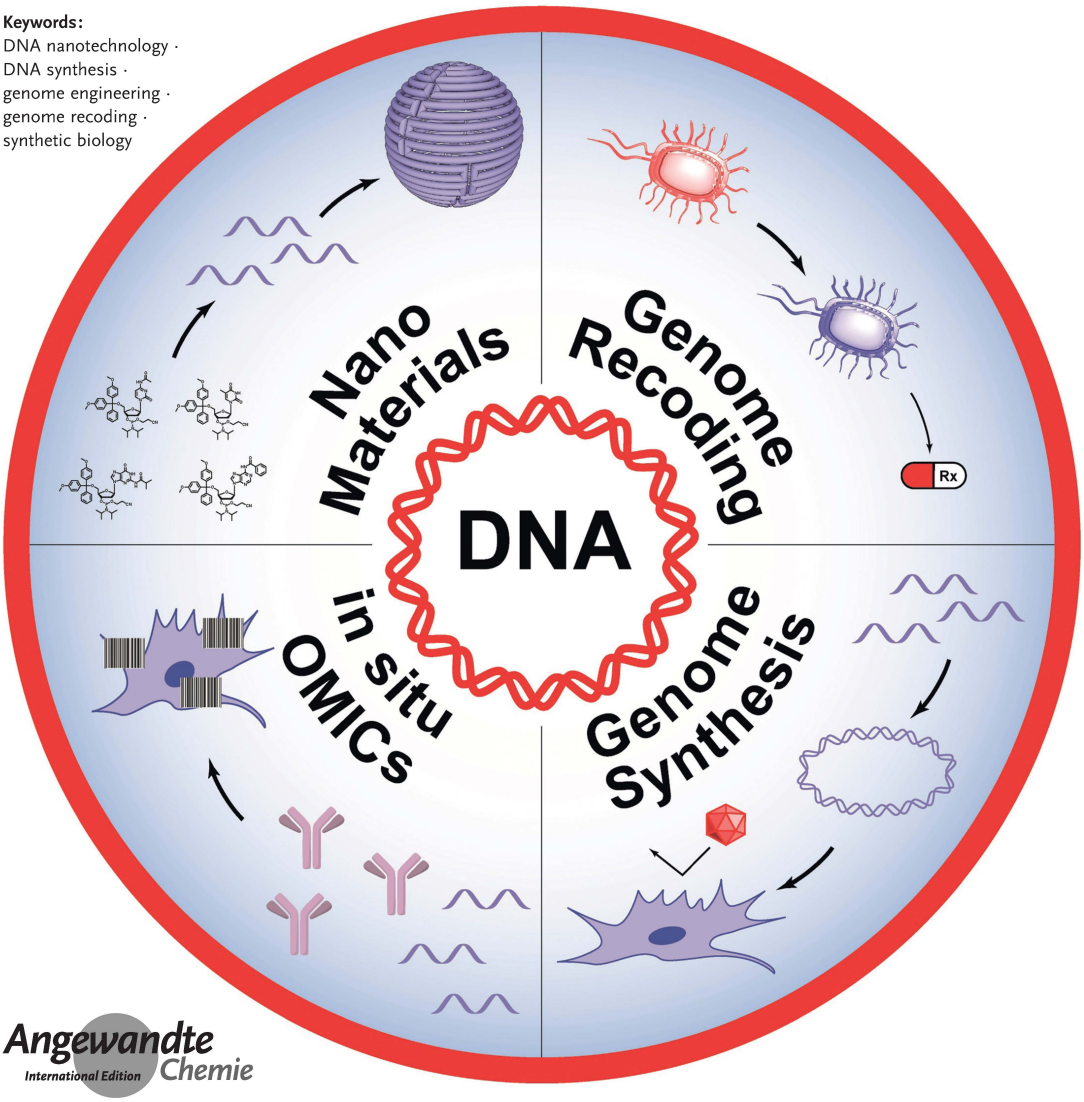

Selected section written by myself:

The use of DNA as information carriers for *in situ* 'omics' analysis

With the capability of engineering and generating more and more complex organisms, we need better tools to investigate and understand the biological processes underlying their functions. Both natural and synthetic biological systems typically consist of a large number of distinct molecular species that coordinate with each other to realize certain biological functions. By investigating only a portion of the system, limited information can be acquired, which may be inconclusive or misleading in some cases. Technological advances, especially in the fields of DNA sequencing and mass spectrometry, have enabled us to measure different molecular species from cells in an unbiased and comprehensive manner[117]. The resulted system-level 'omics' data have greatly expanded our understanding of complex biological systems[118]. However, most currently available technologies can only perform in-bulk analysis[119]. Recently developed single-cell DNA/RNA sequencing can work for cells in suspension that are obtained naturally (e.g. blood cells), or from mechanical/enzymatic dissociation[119,120]. Given that complex biological systems are spatially well organized, the loss of positional information of individual cells makes it challenging to trace the data back to their original location in order to generate physiologically relevant interpretation. Therefore, developing technologies for spatially resolved omics or so-called *in situ* omics is of great importance and broad interest. Here, we summarize some past and ongoing work from our lab and other labs on using DNA for *in situ* omics analysis.

Beyond its role as the building blocks for genome, DNA can be viewed simply as a string of 4-letter code. It has enormously large design space with its diversity increasing exponentially (4^N) as a function of the length of DNA. This information-rich property of DNA has been

utilized to archive digital data, such as books and movies[121-125]. DNA can also be repurposed to serve as molecular barcodes. We envision that if we can label each molecule species with a specific DNA barcode *in situ*, we can obtain the positional and quantitative information of each targeted molecule by simply reading out the corresponding DNA barcode (**Figure**). A library of orthogonal barcodes can be curated and used to label diverse types of molecules (e.g. DNA, RNA, protein, metabolites etc.) to generate the *in situ* 'omics'.

A variety of methods can be used for decoding DNA *in situ*, and we herein will focus on two most widely used methods, Fluorescence *in situ* Sequencing (FISSEQ) and sequential hybridization with complementary fluorescent DNA probes (**Figure**). Both methods utilize fluorescence microscopy as the readout platform. FISSEQ, previously developed by our lab, is an *in situ* DNA sequencing method, wherein DNA sequences can be directly read out in biological samples such as tissue sections without DNA/RNA extraction[126-128].Unbiased *in situ* RNA sequencing with FISSEQ has been demonstrated in fixed human fibroblasts[127]. In a simulated injury model FISSEQ could successfully capture the gene expression profile change between fibroblasts close to and further from the wound sites[127]. Nilsson et al. used FISSEQ to perform highly multiplexed targeted RNA detection[129]. In their study, 39 different mRNA species were simultaneously measured in fresh-frozen breast cancer tissue sections, and the result revealed heterogeneity in the localization pattern across the tissue and the number of signals for different mRNA transcripts. The second strategy for decoding DNA sequences *in situ* is to perform sequential hybridization with complementary fluorescent DNA probes. Compared to FISSEQ, the technical requirement for sequential hybridization is lower; however the multiplexing capability of this method also decreases. By reiterative probe hybridization and signal removal using photobleaching, Guo et al. demonstrated seven RNA targets imaging in

single Hela cells[130]. Combinatorial DNA barcoding strategy was introduced to enhance the multiplexing capability of sequential hybridization methods[131-134]. Zhuang and her colleagues have developed Multiplexed Error-Robust Fluorescence *In Situ* Hybridization (MERFISH) to detect hundreds of different RNA species *in situ*[133]. In MERFISH, each RNA species is labeled with a combination of multiple (N) readout DNA sequences, resulting in a total of 2^N-1 barcodes. The actual barcode library is smaller than 2^N-1 for the purpose of error detection and correction. MERFISH has been applied to detect RNA expression profile in both fibroblast cell cultures and mouse brain samples[133,135,136]. A key requirement for *in situ* detection is sufficient signal-to-noise (S/N) ratio. In FISSEQ, rolling circle amplification is used to generate hundreds of copies of the same signal in order to achieve a reasonable S/N ratio[126-128]. MERFISH relies on labeling the same RNA molecule with multiple FISH probes with the same DNA barcodes. As a result, it sets the limit for the minimal length of RNA can be detected using MERFISH (i.e. small RNAs like microRNA cannot be detected using this method). To increase S/N ratio, Cai et al. integrated a signal amplification method called hybridization chain reaction (HCR) with multiplexed RNA FISH[107,137-141]. This allows the researchers to perform highly multiplexed RNA detection in thick tissue samples[107,141].

The same strategy can also be applied to DNA and protein to achieve highly multiplexed DNA or protein analysis *in situ*. Yin et al. have developed DNA-Exchange-Imaging, a highly multiplexed *in situ* protein detection method in which DNA barcode-conjugated antibodies are used to label different protein targets inside biological samples[63,142-144]. By simple buffer exchange to introduce and remove fluorophore-conjugated complementary DNA probes, the researchers have shown rapid multiplexed protein detection in both cell cultures and tissue samples. More interestingly, by tuning the binding affinity between fluorophore-conjugated

DNA probes to the DNA barcodes on antibodies, the researchers can achieve highly multiplexed super-resolution imaging that is critical to resolve fine cellular structures (e.g. neuronal synapses)[63,142,144]. A related work employing a different sequential hybridization strategy (i.e. toehold displacement rather than buffer exchange in DNA-Exchange-Imaging) also proved that highly multiplexed protein detection could be readily accomplished using DNA-barcoded antibodies[145]. More recently, DNA barcodes have also been introduced into neuron projections and individual synapses, which can provide a potential strategy for high throughput neuron projectome and connectome analysis[146-148]. We anticipate that using DNA barcodes for *in situ* 'omics' can be integrated into an even broader number of systems to study questions that cannot be easily tackled with before.

A few challenges, however, still remain to be solved in order to achieve a more comprehensive *in situ* 'omics' analysis. One is spatial crowding when a large number of molecules are labeled and imaged. A potential solution is to combine it with expansion microscopy, a technique that physically expands samples using swellable hydrogel[53,97,100,149,150]. Another challenge is lack of specific and high-affinity labeling probes to target proteins and metabolites. Commercially available antibodies are costly and unable to be engineered (e.g. to specific formulation for DNA conjugation). We have recently initiated a multi-institute effort to generate an open-access antibody database that deposits DNA sequences of antibodies obtained from in-house selection or hybridoma sequencing. We believe this open-access antibody database will greatly benefit the research community beyond the use for *in situ* 'omics' analysis we present here.

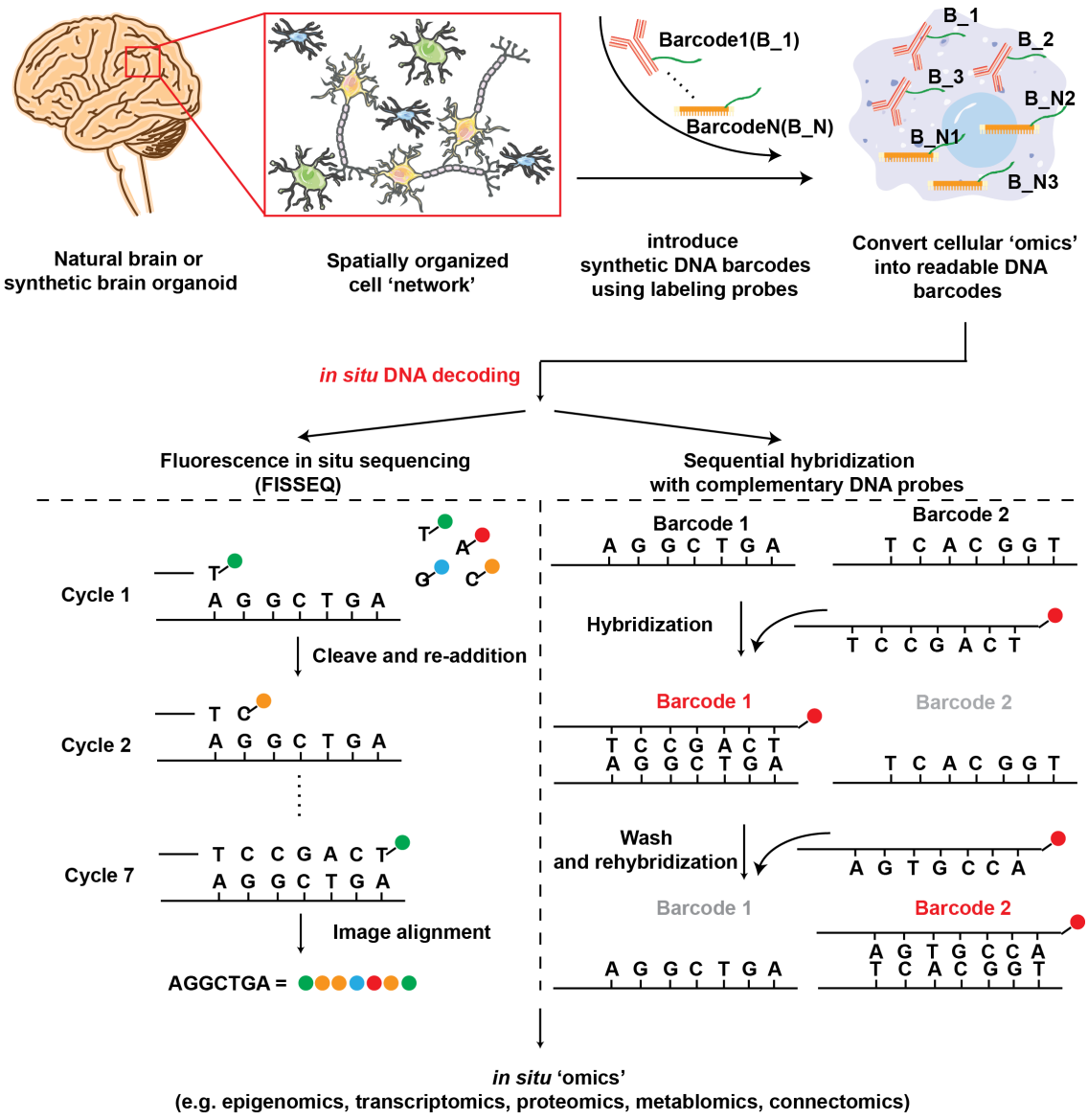

Figure. The use of DNA as information carrier for *in situ* 'omics' analysis. Complex biological systems, such as natural brain or synthetic brain organoid, are built from a spatially well-organized network of different types of cells. Labeling probes, such as antibodies and fluorescence *in situ* hybridization (FISH) probes, that are conjugated with synthetic DNA barcodes are introduced to biological samples to convert their molecular information to readable DNA barcodes. It is followed by *in situ* DNA decoding using either fluorescence *in situ* sequencing (FISSEQ) or sequential hybridization with complementary DNA probes. In FISSEQ, each type of four nucleotides (A,T,C,G) is labeled with a spectrally-distinct fluorophore. Iterative addition and cleavage of fluorophore-conjugated nucleotides is performed in conjunction with fluorescent image acquisition. The DNA sequence can be obtained by computational image alignment to register the fluorescent signal back to the position of corresponding DNA barcode. Sequential hybridization method uses iterative hybridization and removal of fluorophore-labeled complementary DNA probes. The DNA sequences are designed to be orthogonal to minimize crosstalk between different barcodes.

Appendix B

Open science :Proposal for a “Next-Generation” Scientific Publication System

Proposal for a "Next-Generation" Scientific Publication System

Yu Wang[1,2] and George M. Church [1,2]

1. Wyss Institute for Biologically Inspired Engineering, Harvard University, Boston, Massachusetts, USA
2. Department of Genetics, Harvard Medical School, Boston, Massachusetts, USA

Correspondence: Yu Wang (yuwang01@fas.harvard.edu) and George M. Church (gchurch@genetics.med.harvard.edu)

The idea of 'open science' is gaining attraction among the scientific community, with an increasing number of journals becoming open-access. However, open science is not only about the negotiation between scientists and publishers, but also about how "open" scientists should be before their scientific work is published on journals. One key challenge we see in the journal-based system is that competition between scientists for publication in high-profile journals impedes open and rapid sharing of scientific work. In order to generate novel but also significant results that can meet the criteria for high-profile journals, researchers typically spend years in one project to follow a specific hypothesis and generate a compelling scientific 'story'. As a result, it is not uncommon to see phenomena like keeping project as confidential for years, irreproducible results with biased experiment design and data interpretation to favor certain hypotheses, and researchers stressed out with the concern of getting 'scooped'. In an attempt to alleviate publication pressure for researchers and build an e-network among scientists to promote collaboration, we propose an online scientific data and results sharing system that complements the current journal-based system. Our system is inspired by the Gordon conference

and Github. The ultimate goal of this system is to build a community in which researchers with similar interest collaboratively solve scientific questions, just as the Human Genome Sequencing Project.

Publicly sharing scientific data and results is essential for promoting the research community as a whole by offering opportunities for engagement with peer scientists throughout the world. Academic journals are traditionally the mainstream approach to publish scientific work. It is undeniable that publication on scientific journals has become one of the most critical factors to evaluate a researcher's scientific achievement and capability, which directly affects their career advancement. It also appears that researchers are more likely to be acknowledged by publishing their work in high profile journals.

It becomes problematic being that high profile journals are limited. With an increasing number of scientific works being generated nowadays, those journals have to keep raising the bar and be more selective about the work they publish. This naturally creates a competition among researchers who are involved in the system. Sadly, many of us have started to do science in a way that it is more likely to be published in high profile journals, instead of being driven by pure scientific interest. We are constantly exposed to the pressure of getting positive, novel and significant results in order to make a compelling "story." Unfortunately, the nature of science determines that we only get negative or positive yet incremental results. Worse still, we have to keep our work confidential until it is close to publication or has been published, which could take months or even years.

This has led to several issues. Firstly, in order to complete a project for publication on scientific journals within a reasonable amount of time, researchers are more likely to be biased

on experimental design and data interpretation that favors their original hypotheses. Worse case scenario, some researchers may even falsify data to get expected results. Secondly, even though researchers hold a fair attitude towards their work, science is complicated and sensitive to the technologies, methods and reagents used in the experiments. There is a chance that experiment results are pure artifacts that cannot be reproduced by others labs. This can be from contaminated cell lines or wrong antibodies used in the project, or lack of expertise in skill-demanding fields such as statistic and microscopy. A good example is the use of p-values for statistical significance tests in biological experiments, which has been heavily criticized by statisticians and even banned by several journals[151,152]. Unfortunately, because the scientific work is hidden for confidential purposes, some of these artifacts may not be realized for years depending on when the work is published. Thirdly, even in the case that everything is on the right track, researchers may worry their work can be 'scooped' by other researchers. This can be devastating for researchers because most high profile journals list novelty as one of their major criteria for publication. Finally, not only can this publication pressure lead to scientific irreproducibility, but also contribute to scientists' mental health issues that have recently gained a high level of awareness.

In order to alleviate this publication pressure and promote collaboration among researchers, we need a faster but also reliable scientific data and results sharing system that can complement the current journal-based publication system. Inspired by the Gordon conference, Github, and many other open science platforms, we here propose a new publication scheme that takes advantage of fast-developing Internet platforms, with the goal to build a scientifically rigorous and socially joyful research community.

The proposed system consists of two inter-connected components: an online open-access data/results deposition platform (e.g. Pubpub, Biorxiv) as well as an online networking system (e.g. an integrated system from Researchgate, Facebook and Google Scholar) (**Figure**). One key difference of our proposed system from the current publication system is that we encourage researchers to publish project milestones instead of complete scientific 'stories.' Project milestones can be scientific ideas or experiment results that have been rigorously validated at any length. The format of published milestones can be short communications, including a brief introduction for background or project rationale, results, and more importantly, detailed methods and original data that are the key for quality check and result reproduction. The online networking system is used to facilitate the sharing of scientific work and encourage peer scientists to evaluate and give feedback on the work. In this online platform, researchers can establish their own profiles with real identity, and directly communicate with peer scientists by following each other's profiles. Moreover, researchers are allowed to select their research interest as tags to form research circles. Each published project milestone will be labeled with keywords as tags by the authors. The online system will match the tags and automatically send the milestone to all researchers who have the same tag. Each published milestone will also come with a publicly trackable interactive discussion board where authors and peer scientists can leave and reply to feedback on the work. In contrast to the current peer-review system that depends on opinions from one to three reviewers. This system enables a cloud based peer review that obtains opinions from thousands of peer scientists with similar interest from around the world. When

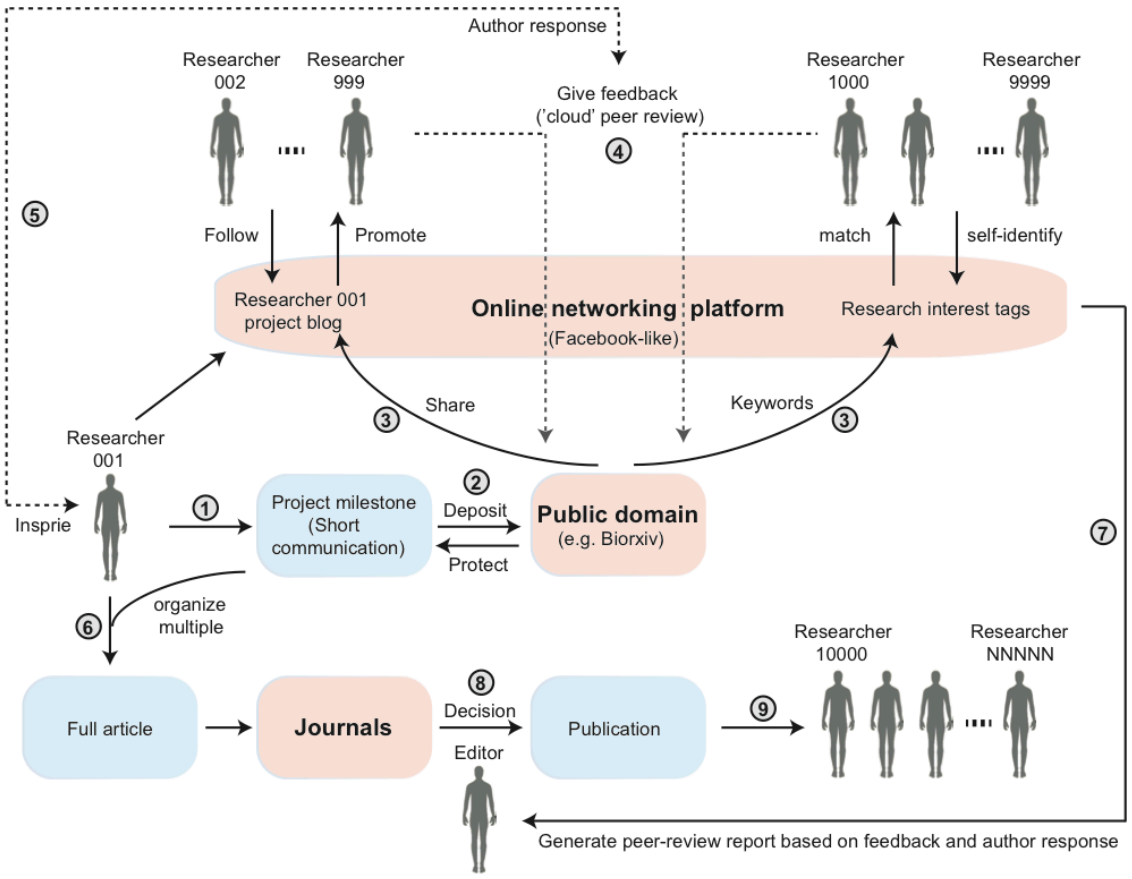

Figure. Schematic of Proposed Scientific Data and Result Sharing System. **Step1**: Researcher 001 finishes a project milestone and writes it as a short communication. **Step2**: The short communication is deposited on public domains such as Pubpub and Biorxiv. The public appearance serves to protect the author's intellectual property. **Step3**: The short communication is shared to other researchers through two ways: one is via posting by Researcher 001 on his/her scientific project blog on the Online networking platform to the project followers; the other is via keywords matching by the system to scientists who share the same research interest. **Step4**: Peer researchers give feedback on the work through an online interactive discussion board, functioning as a 'cloud' peer review system. **Step5**: Researcher 001 responds to the feedback and gets inspired to carry on the project. **Step6**: Researcher 001 organizes multiple related project milestones into a full article and submits it to a journal. **Step7**: Researcher 001 requests a report of the cloud peer review generated by the system to be sent to the journal editor. **Step8**: The journal editor makes a decision on the publication based on the cloud peer review. **Step9**: The full article gets accepted by the journal and released to the entire research community.

finished, researchers can organize multiple deposited milestones into a more whole article and submit it to their favorite scientific journals. This online system will automatically generate a report including the metrics and the 'cloud' peer review, which can be used by journal editors to make a fast decision on the manuscript.

This proposed system is motivated to build an online platform that mimics Gordon conference where researchers are encouraged to share scientific thoughts and results openly and comfortably. A few features of the system should be noted: firstly, releasing project milestones instead of full-length articles will greatly accelerate the process of scientific results sharing. Researchers do not have to spend years to follow a specific hypothesis and prove it 'right and significant.' Negative and incremental results can be written as project milestones and published. In addition, by sharing results early in a project, researchers can get prompt feedback from peer scientists. This can help researchers to quality-check their current research as well as to develop future research plans. Secondly, unlike Gordon conference where unpublished results are only shared based on the trust between scientists within the same research field. This proposed system utilizes public domains, such as Pubpub, to serve as time records to protect researchers' intellectual properties. This potentially enables even more open discussion among a wider range of scientists. Thirdly, with the increasing trend of interdisciplinary research, it has become more difficult to find reviewers who have the expertise in all aspects of a paper. The 'cloud' peer review includes opinions from peer scientists with different backgrounds, allowing a more thorough evaluation of the paper. Although it might be arguable, we believe that this 'cloud' peer review should be less biased in contrast to the current system where editors based on suggestions from authors choose anonymous reviewers. Lastly, this proposed system still allows researchers to organize multiple milestones into a full-length article to submit to scientific journals. We include this component mainly because the journal-based publication system is so deeply ingrained in the research community that it is challenging to change it completely at once. It, in our perspective, is also the reason that open science initiatives have hitherto not been very

successful. We hope this proposed system can function as an intermediate stage to allow funding agencies, career committees and scientists to gradually transition to open science.

With fast-developing Internet technologies, we consider that there is no significant technical barrier for this proposed system. In fact, most of the components in the proposed system are already available (e.g. Pubpub, Biorxiv, Researchgate, Google scholar article alert). In our opinion, different open science platforms should coordinate with each other to construct a single integrated system that provides researchers the most convenience, instead of forcing researchers to shuffle between different platforms. In addition, to make researchers more willing to openly share their work, funding agencies and career committees should examine beyond publication on journals. This system could potentially generate metrics based on researchers' activities to provide additional references for funding agencies and career committees to evaluate. With a joint effort between academia (i.e. thousands of researchers who are actively engaged in the publication system, and funding agencies) and technology companies (e.g. Facebook, Google and Microsoft), this proposed system and other open science systems would greatly benefit the entire scientific research community, by making it scientifically rigorous but also socially joyful.

Lastly, we have been actively discussing this proposed system with our colleagues, including established faculties, young investigators, postdocs and graduate students, and encountered some frequently asked questions. We have listed them and put our thoughts as a Q&A section here:

1. *If we deposit our milestones in public, how can we prevent other labs from 'stealing' the idea to perform similar experiments and get them published in scientific journals before we do?*

We think this is the key element that drives the entire publication pressure. That is, scientific journals are the only way for researchers to protect their intellectual properties. It is also the key problem we are trying to address in our proposed system. Deposition in public domains such as Pubpub can serve as a time stamp for original authors to claim credits. In addition, the milestones will be automatically sent to thousands of scientists with the same interest. It will very likely cover most of researchers who work in the same field with original authors. This will quickly establish the idea among the scientific community that those original authors make the initial discovery, which is more important than just publishing in specific journals.

In addition, the initial motivation for developing this new system is to encourage our research community to be more collaborative and less competitive. Competition in science is less valuable when compared to the competition in business. Once we make the initial discovery and deposit it into the online system, we should encourage peer scientists to follow up our work and make a joint effort to decipher the science behind the discovery. One potential way to promote collaboration is to describe current or proposed work for the project at the end of the deposited milestone. By doing this, authors can potentially get feedback from peer scientists on the direction of the project. Meanwhile, other scientists can avoid doing the same work.

From a practical perspective, a significant amount of follow-up work can be done during the preparation of milestone papers. The 'pirates' will actually run the risk of getting 'scooped' by follow-up milestones from original authors. In addition, this online networking system allows faster and wider communication throughout the entire research community. This also means any dishonest behaviors such as releasing work with false

information to prevent others to follow up the work or stealing others' work can be quickly and easily recognized.

2. *How can we prevent the system from abuse to claim credits by publishing ill-performed studies?*

We agree this could potentially be a downside for open sharing of scientific results before significant peer review. However, the system comes with a quality check mechanism, that is, the 'cloud' peer review. We encourage researchers to include detailed methods and original data along with the deposited milestone for evaluation. Any ill-performed studies (e.g. manipulating or even falsifying data) will soon be flagged, and the authors run the risk of losing their reputation by publishing ill-performed studies. In addition, scientific credits will not be simply given to someone just because they published first. Assignment of scientific credits has to be carefully justified and broadly acknowledged.

3. *The comment section for papers has existed for journals and preprint service (e.g. Biorxiv) for a long time. However, it has not been well used. How are you going to promote this 'cloud' peer review idea?*

We have also noted this phenomenon. Although we have anecdotally heard of authors' papers published on Biorxiv receiving comments through emails, it is not sufficient for the 'cloud' peer review. We think the underlying reason for missing useful comments in

the current system is that researchers do not have the motivation to leave and respond to comments publicly. Papers that are deposited in Biorxiv are mostly full articles that are likely under review or soon-to-be reviewed at peer-review journals. Paper authors will likely only take comments from journal reviewers seriously. As a result, leaving comments publicly on Biorxiv by peer scientists will not gain much attention from authors. On the contrary, in our proposed system, the feedback on deposited milestones from peer scientists may directly affect downstream experiments. Therefore, it is critical for authors to have an active discussion with peer scientists. In addition, we encourage journal editors to take this 'cloud' peer review into consideration when they make a decision for publishing. This will encourage peer scientists to leave comments in the system as well as somewhat 'nudge' authors to respond to comments. We think once more researchers get used to the open discussion platform, it will become a habit without further motivation.

4. *What is the relationship between this proposed system and the current journal-based system? Will it replace the current journal-based system?*

We think this proposed system complements the current journal-based system. We don't foresee it replacing the current system for some time. However, it may modify the current one. For example, the 'cloud' peer review may replace the close-door anonymous peer-review, which may actually expedite the entire paper publication process.

In our opinion, scientific journals, especially high profile journals, have a broad range of audience from different backgrounds. Therefore, it can serve as a good "advertising"

platform to bring scientific work to a larger number of researchers who do not share the same scientific interest tags.

5. *How is this system different from other open science platforms that allow scientists to openly share lab notebooks?*

Openly sharing lab notebooks is one of the ultimate goals of 'open science initiative'. However, it may not be feasible for every researcher at current stage. In addition, a key challenge we see in openly sharing lab notebooks is that lack of organized information makes peer-review from other scientists challenging. It should still be coupled with releasing work in a 'paper-like' format.

Acknowledgement

We acknowledge members in Dr. George Church's and Dr. Peng Yin's laboratories, Dr. Constance Cepko, Dr. Bernardo Sabatini, Dr. Wayne Marasco for fruitful discussion. We acknowledge Justin Granchelli and Noah Donoghue for their comments on the manuscript.

Appendix C

List of Publication

Disclosure: The thesis contains contents from the following publications:

Primary Research Article:

1. Agasti, S.S.*, Wang, Y.*, Schueder, F., Sukumar, A., Jungmann, R. § and Yin, P. § (2017). DNA-barcoded labeling probes for highly multiplexed Exchange-PAINT imaging. *Chemical science*, 8(4), pp.3080-3091. (* indicates co-first authors; § indicates co-corresponding authors)

2. Wang, Y., Woehrstein, J.B., Donoghue, N., Dai, M., Avendaño, M.S., Schackmann, R.C.J., Zoeller, J.J., Wang, S.S.H., Tillberg, P.W., Park, D., Lapan, S.W., Boyden, E.S., Brugge, J.S., Kaeser, P.S., Church, G.M., Agasti, S.S. §, Jungmann, R. § and Yin, P. § (2017). Rapid sequential *in situ* multiplexing with DNA exchange imaging in neuronal cells and tissues. *Nano letters*, 17(10), pp.6131-6139. (§ indicates co-corresponding authors)

3. Wang, Y., Xie, W., Kohman, R.E. and Church, G.M. (2018). Multiplexed imaging using same species primary antibodies with signal amplification. *bioRxiv*, p.274456.

4. Saka, S.K.**,§, Wang, Y., **,§ Kishi, J.Y., Zhu, A., Zeng, Y., Xie, W., Kirli, K., Yapp, C., Cicconet, M., Beliveau, B.J., Lapan, S.W., Yin, S., Lin, M., Boyden, E.S., Kaeser, P.S., Pihan, G., Church, G.M. and Yin, P. § (2018). Highly multiplexed *in situ* protein imaging with signal amplification by Immuno-SABER. *bioRxiv*, p.507566. (** indicates co-first authors that are ordered alphabetically; § indicates co-corresponding authors)

Review Article:

1. Kohman, R.E.*, Kunjapur, A.M.*, Hysolli, E.*, Wang, Y.* and Church, G.M. (2018). From Designing the Molecules of Life to Designing Life: Future Applications Derived from Advances in DNA Technologies. *Angewandte Chemie International Edition*, 57(16), pp.4313-4328. (* indicates co-first authors)

Others:

1. Kishi, J.Y.*, Beliveau, B.J.*, Lapan, S.W.*, West, E.R., Zhu, A., Sasaki, H.M., Saka, S.K., Wang, Y., Cepko, C.L. § and Yin, P. § (2018). SABER enables highly multiplexed and amplified detection of DNA and RNA in cells and tissues. *bioRxiv*, p.401810. (* indicates co-first authors; § indicates co-corresponding authors)

2. Wang, Y., Church, G.M. (2018). Proposal for a 'next-generation' scientific publishing system. Pubpub, Church lab. https://church.pubpub.org/

Reference

1 Hoffman, W., Lakkis, F. G. & Chalasani, G. B Cells, Antibodies, and More. *Clin J Am Soc Nephrol* **11**, 137-154, doi:10.2215/CJN.09430915 (2016).

2 Lippow, S. M., Wittrup, K. D. & Tidor, B. Computational design of antibody-affinity improvement beyond in vivo maturation. *Nat Biotechnol* **25**, 1171-1176, doi:10.1038/nbt1336 (2007).

3 Muyldermans, S. Nanobodies: natural single-domain antibodies. *Annu Rev Biochem* **82**, 775-797, doi:10.1146/annurev-biochem-063011-092449 (2013).

4 Lakhin, A. V., Tarantul, V. Z. & Gening, L. V. Aptamers: problems, solutions and prospects. *Acta Naturae* **5**, 34-43 (2013).

5 Chakravarty, R., Goel, S. & Cai, W. Nanobody: the "magic bullet" for molecular imaging? *Theranostics* **4**, 386-398, doi:10.7150/thno.8006 (2014).

6 Coons, A. H. The beginnings of immunofluorescence. *J Immunol* **87**, 499-503 (1961).

7 Matos, L. L., Trufelli, D. C., de Matos, M. G. & da Silva Pinhal, M. A. Immunohistochemistry as an important tool in biomarkers detection and clinical practice. *Biomark Insights* **5**, 9-20 (2010).

8 Marrack, J. Nature of antibodies. *Nature* **133**, 2 (1934).

9 Coons, A. H. The demonstration of pneumococcal antigen in tissues by the use of fluorescent antibody. *J Immunol* **45** (1942).

10 Mullins, J. M. Overview of fluorophores. *Methods Mol Biol* **34**, 107-116, doi:10.1385/0-89603-285-X:107 (1994).

11 Wang, Y. *et al.* Rapid Sequential in Situ Multiplexing with DNA Exchange Imaging in Neuronal Cells and Tissues. *Nano Lett* **17**, 6131-6139, doi:10.1021/acs.nanolett.7b02716 (2017).

12 Angelo, M. *et al.* Multiplexed ion beam imaging of human breast tumors. *Nat Med* **20**, 436-442, doi:10.1038/nm.3488 (2014).

13 Levenson, R. M., Borowsky, A. D. & Angelo, M. Immunohistochemistry and mass spectrometry for highly multiplexed cellular molecular imaging. *Lab Invest* **95**, 397-405, doi:10.1038/labinvest.2015.2 (2015).

14 Akter, K. *et al.* Antimicrobial and antioxidant activity and chemical characterisation of Erythrina stricta Roxb. (Fabaceae). *J Ethnopharmacol* **185**, 171-181, doi:10.1016/j.jep.2016.03.011 (2016).

15 Giesen, C. W., H. A. O.; Schapiro, D.; Zivanovic, N.; Jacobs, A.; Hattendorf, B.; Schüffler, P. J.; Grolimund, D.; Buhmann, J. M.; Brandt, S.; Varga, Z.; Wild, P. J.; Günther, D.; Bodenmiller, B. . Highly multiplexed imaging of tumor tissues with subcellular resolution by mass cytometry. *Nature Methods* **11**, 417-425 (2014).

16 Schulz, D. *et al.* Simultaneous Multiplexed Imaging of mRNA and Proteins with Subcellular Resolution in Breast Cancer Tissue Samples by Mass Cytometry. *Cell Syst* **6**, 25-36 e25, doi:10.1016/j.cels.2017.12.001 (2018).

17 Wei, L. *et al.* Super-multiplex vibrational imaging. *Nature* **544**, 465-470, doi:10.1038/nature22051 (2017).

18 Gerdes, M. J. *et al.* Highly multiplexed single-cell analysis of formalin-fixed, paraffin-embedded cancer tissue. *Proc Natl Acad Sci U S A* **110**, 11982-11987, doi:10.1073/pnas.1300136110 (2013).

19 Lin, J. R., Fallahi-Sichani, M. & Sorger, P. K. Highly multiplexed imaging of single cells using a high-throughput cyclic immunofluorescence method. *Nat Commun* **6**, 8390, doi:10.1038/ncomms9390 (2015).

20 Lin, J.-R. *et al.* Highly multiplexed immunofluorescence imaging of human tissues and tumors using t-CyCIF and conventional optical microscopes. *eLife* **7**, doi:10.7554/eLife.31657 (2018).

21 Waters, J. C. Accuracy and precision in quantitative fluorescence microscopy. *J Cell Biol* **185**, 1135-1148, doi:10.1083/jcb.200903097 (2009).

22 Rich, R. M. *et al.* Elimination of autofluorescence background from fluorescence tissue images by use of time-gated detection and the AzaDiOxaTriAngulenium (ADOTA) fluorophore. *Anal Bioanal Chem* **405**, 2065-2075, doi:10.1007/s00216-012-6623-1 (2013).

23 Saka, S. K. *et al.* Highly multiplexed in situ protein imaging with signal amplification by Immuno-SABER. *bioRxiv*, 507566 (2018).

24 Wang, Y., Xie, W., Kohman, R. E. & Church, G. M. Multiplexed imaging using same species primary antibodies with signal amplification. *BioRxiv*, 274456 (2018).

25 Bobrow, M., Litt, G. J., Shaughnessy, K. J., Mayer, P. C. & Conlon, J. The use of catalyzed reporter deposition as a means of signal amplification in a variety of formats. *Journal of Immunological Methods* **150**, 145-149 (1992).

26 Buki, A., Walker, S. A., Stone, J. R. & Povlishock, J. T. Novel Application of Tyramide Signal Amplification (TSA): Ultrastructural Visualization of Double-labeled Immunofluorescent Axonal Profiles. *J Histochem Cytochem* **48**, 153-161, doi:10.1177/002215540004800116 (2000).

27 Yarilin, D. *et al.* Machine-based method for multiplex in situ molecular characterization of tissues by immunofluorescence detection. *Sci Rep* **5**, 9534, doi:10.1038/srep09534 (2015).

28 Stack, E. C., Foukas, P. G. & Lee, P. P. Multiplexed tissue biomarker imaging. *J Immunother Cancer* **4**, 9, doi:10.1186/s40425-016-0115-3 (2016).

29 Stack, E. C., Wang, C., Roman, K. A. & Hoyt, C. C. Multiplexed immunohistochemistry, imaging, and quantitation: a review, with an assessment of Tyramide signal amplification, multispectral imaging and multiplex analysis. *Methods* **70**, 46-58, doi:10.1016/j.ymeth.2014.08.016 (2014).

30 Schweitzer, B. *et al.* Immunoassays with rolling circle DNA amplification: a versatile platform for ultrasensitive antigen detection. *Proc Natl Acad Sci U S A* **97**, 10113-10119, doi:10.1073/pnas.170237197 (2000).

31 Nagendran, M., Riordan, D. P., Harbury, P. B. & Desai, T. J. Automated cell-type classification in intact tissues by single-cell molecular profiling. *Elife* **7**, doi:10.7554/eLife.30510 (2018).

32 Chen, Y. *et al.* TSA-Seq Mapping of Nuclear Genome Organization. *bioRxiv*, doi:doi: 10.1101/307892 (2018).

33 Deng, R. Z., K.; Wang, L.; Sun, Y.; LI, J. DNA-Sequence-Encoded Rolling Circle Amplicon for Single-Cell RNA Imaging. *CHEM* **4**, 1373–1386 (2018).

34 Kern, D. *et al.* An enhanced-sensitivity branched-DNA assay for quantification of human immunodeficiency virus type 1 RNA in plasma. *J Clin Microbiol* **34**, 3196-3202 (1996).

35 Pachl, C. T., J. A.; Kern, D. G.; Sheridan, P. J.; Fong, S. J.; Stempien, M.; Hoo, B.; Besemer, D.; Yeghiazarian, T.; Irvine, B.; Kolberg, J. . Rapid and precise quantification of HIV-1 RNA in plasma using a branched DNA signal amplification assay. *JAIDS Journal of Acquired Immune Deficiency Syndromes* **8**, 446 (1995).

36 Player, A. N., Shen, L. P., Kenny, D., Antao, V. P. & Kolberg, J. A. Single-copy gene detection using branched DNA (bDNA) in situ hybridization. *J Histochem Cytochem* **49**, 603-612, doi:10.1177/002215540104900507 (2001).

37 Wang, F. *et al.* RNAscope: a novel in situ RNA analysis platform for formalin-fixed, paraffin-embedded tissues. *J Mol Diagn* **14**, 22-29, doi:10.1016/j.jmoldx.2011.08.002 (2012).

38 Battich, N., Stoeger, T. & Pelkmans, L. Image-based transcriptomics in thousands of single human cells at single-molecule resolution. *Nat Methods* **10**, 1127-1133, doi:10.1038/nmeth.2657 (2013).

39 Dirks, R. M. & Pierce, N. A. Triggered amplification by hybridization chain reaction. *Proc Natl Acad Sci U S A* **101**, 15275-15278, doi:10.1073/pnas.0407024101 (2004).

40 Choi, H. M., Beck, V. A. & Pierce, N. A. Next-generation in situ hybridization chain reaction: higher gain, lower cost, greater durability. *ACS Nano* **8**, 4284-4294, doi:10.1021/nn405717p (2014).

41 Choi, H. M. T. *et al.* Third-generationin situhybridization chain reaction: multiplexed, quantitative, sensitive, versatile, robust. *Development* **145**, dev165753, doi:10.1242/dev.165753 (2018).

42 Trivedi, V., Choi, H. M. T., Fraser, S. E. & Pierce, N. A. Multidimensional quantitative analysis of mRNA expression within intact vertebrate embryos. *Development* **145**, doi:10.1242/dev.156869 (2018).

43 Shah, S. *et al.* Single-molecule RNA detection at depth by hybridization chain reaction and tissue hydrogel embedding and clearing. *Development* **143**, 2862-2867, doi:10.1242/dev.138560 (2016).

44 Sylwestrak, E. L., Rajasethupathy, P., Wright, M. A., Jaffe, A. & Deisseroth, K. Multiplexed Intact-Tissue Transcriptional Analysis at Cellular Resolution. *Cell* **164**, 792-804, doi:10.1016/j.cell.2016.01.038 (2016).

45 Lin, R. *et al.* A hybridization-chain-reaction-based method for amplifying immunosignals. *Nat Methods*, doi:10.1038/nmeth.4611 (2018).

46 Wang, Y., Xie, W., Kohman, R. E. & Church, G. M. Multiplexed imaging using same species primary antibodies with signal amplification. *bioRxiv*, doi:doi: 10.1101/274456 (2018).

47 Thorley, J. A., Pike, J. & Rappoport, J. Z. in *Fluorescence Microscopy* 199-212 (Elsevier, 2014).

48 Huang, B., Bates, M. & Zhuang, X. Super-resolution fluorescence microscopy. *Annu Rev Biochem* **78**, 993-1016, doi:10.1146/annurev.biochem.77.061906.092014 (2009).

49 Dai, M., Jungmann, R. & Yin, P. Optical imaging of individual biomolecules in densely packed clusters. *Nature nanotechnology* **11**, 798 (2016).

50 Balzarotti, F. *et al.* Nanometer resolution imaging and tracking of fluorescent molecules with minimal photon fluxes. *Science* **355**, 606-612 (2017).

51 Jungmann, R. *et al.* Multiplexed 3D cellular super-resolution imaging with DNA-PAINT and Exchange-PAINT. *Nature methods* **11**, 313 (2014).

52 Jungmann, R. *et al.* Quantitative super-resolution imaging with qPAINT. *Nature methods* **13**, 439 (2016).

53 Chen, F., Tillberg, P. W. & Boyden, E. S. Optical imaging. Expansion microscopy. *Science* **347**, 543-548, doi:10.1126/science.1260088 (2015).

54 Gao, R. *et al.* Cortical column and whole-brain imaging with molecular contrast and nanoscale resolution. *Science* **363**, eaau8302 (2019).

55 Ries, J., Kaplan, C., Platonova, E., Eghlidi, H. & Ewers, H. A simple, versatile method for GFP-based super-resolution microscopy via nanobodies. *Nature methods* **9**, 582 (2012).

56 He, Q. *et al.* The effect of PEGylation of mesoporous silica nanoparticles on nonspecific binding of serum proteins and cellular responses. *Biomaterials* **31**, 1085-1092, doi:10.1016/j.biomaterials.2009.10.046 (2010).

57 Dempsey, G. T., Vaughan, J. C., Chen, K. H., Bates, M. & Zhuang, X. Evaluation of fluorophores for optimal performance in localization-based super-resolution imaging. *Nat Methods* **8**, 1027-1036, doi:10.1038/nmeth.1768 (2011).

58 Bates, M., Huang, B., Dempsey, G. T. & Zhuang, X. Multicolor super-resolution imaging with photo-switchable fluorescent probes. *Science* **317**, 1749-1753, doi:10.1126/science.1146598 (2007).

59 Rothbauer, U. *et al.* Targeting and tracing antigens in live cells with fluorescent nanobodies. *Nat Methods* **3**, 887-889, doi:10.1038/nmeth953 (2006).

60 Mikhaylova, M. *et al.* Resolving bundled microtubules using anti-tubulin nanobodies. *Nat Commun* **6**, 7933, doi:10.1038/ncomms8933 (2015).

61 Haun, J. B., Devaraj, N. K., Hilderbrand, S. A., Lee, H. & Weissleder, R. Bioorthogonal chemistry amplifies nanoparticle binding and enhances the sensitivity of cell detection. *Nat Nanotechnol* **5**, 660-665, doi:10.1038/nnano.2010.148 (2010).

62 Kost, T. A., Condreay, J. P., Ames, R. S., Rees, S. & Romanos, M. A. Implementation of BacMam virus gene delivery technology in a drug discovery setting. *Drug Discov Today* **12**, 396-403, doi:10.1016/j.drudis.2007.02.017 (2007).

63 Agasti, S. S. *et al.* DNA-barcoded labeling probes for highly multiplexed Exchange-PAINT imaging. *Chem Sci* **8**, 3080-3091, doi:10.1039/c6sc05420j (2017).

64 Turner, C. E. Paxillin interactions. *J Cell Sci* **113 Pt 23**, 4139-4140 (2000).

65 Zhang, D. Y. & Seelig, G. Dynamic DNA nanotechnology using strand-displacement reactions. *Nature chemistry* **3**, 103 (2011).

66 Zadeh, J. N. *et al.* NUPACK: analysis and design of nucleic acid systems. *Journal of computational chemistry* **32**, 170-173 (2011).

67 Moffitt, J. R. *et al.* High-throughput single-cell gene-expression profiling with multiplexed error-robust fluorescence in situ hybridization. *Proc Natl Acad Sci U S A* **113**, 11046-11051, doi:10.1073/pnas.1612826113 (2016).

68 Jungmann, R. *et al.* Single-molecule kinetics and super-resolution microscopy by fluorescence imaging of transient binding on DNA origami. *Nano Lett* **10**, 4756-4761, doi:10.1021/nl103427w (2010).

69 Micheva, K. D., Busse, B., Weiler, N. C., O'Rourke, N. & Smith, S. J. Single-synapse analysis of a diverse synapse population: proteomic imaging methods and markers. *Neuron* **68**, 639-653, doi:10.1016/j.neuron.2010.09.024 (2010).

70 Cheng, C. L., Djajadi, H. & Molday, R. S. Cell-specific markers for the identification of retinal cells by immunofluorescence microscopy. *Methods Mol Biol* **935**, 185-199, doi:10.1007/978-1-62703-080-9_12 (2013).

71 Swaroop, A., Kim, D. & Forrest, D. Transcriptional regulation of photoreceptor development and homeostasis in the mammalian retina. *Nat Rev Neurosci* **11**, 563-576, doi:10.1038/nrn2880 (2010).

72 Kim, D. S. *et al.* Identification of molecular markers of bipolar cells in the murine retina. *J Comp Neurol* **507**, 1795-1810, doi:10.1002/cne.21639 (2008).

73 Yang, H., Standifer, K. M. & Sherry, D. M. Synaptic protein expression by regenerating adult photoreceptors. *J Comp Neurol* **443**, 275-288 (2002).

74 Zoeller, J. J., Bronson, R. T., Selfors, L. M., Mills, G. B. & Brugge, J. S. Niche-localized tumor cells are protected from HER2-targeted therapy via upregulation of an anti-apoptotic program in vivo. *NPJ Breast Cancer* **3**, 18, doi:10.1038/s41523-017-0020-z (2017).

75 Viegas, M. S., Martins, T. C., Seco, F. & do Carmo, A. An improved and cost-effective methodology for the reduction of autofluorescence in direct immunofluorescence studies on formalin-fixed paraffin-embedded tissues. *Eur J Histochem* **51**, 59-66 (2007).

76 Gustafsson, M. G. *et al.* Three-dimensional resolution doubling in wide-field fluorescence microscopy by structured illumination. *Biophys J* **94**, 4957-4970, doi:10.1529/biophysj.107.120345 (2008).

77 Guizar-Sicairos, M., Thurman, S. T. & Fienup, J. R. Efficient subpixel image registration algorithms. *Opt Lett* **33**, 156-158 (2008).

78 Beater, S., Holzmeister, P., Lalkens, B. & Tinnefeld, P. Simple and aberration-free 4color-STED--multiplexing by transient binding. *Opt Express* **23**, 8630-8638, doi:10.1364/OE.23.008630 (2015).

79 Kishi, J. Y. *et al.* SABER enables highly multiplexed and amplified detection of DNA and RNA in cells and tissues. *bioRxiv*, 401810 (2018).

80 Schueder, F. *et al.* Universal Super‐Resolution Multiplexing by DNA Exchange. *Angewandte Chemie International Edition* **56**, 4052-4055 (2017).

81 Behbod, F. *et al.* An intraductal human-in-mouse transplantation model mimics the subtypes of ductal carcinoma in situ. *Breast Cancer Res* **11**, R66, doi:10.1186/bcr2358 (2009).

82 Choi, H. M. *et al.* Programmable in situ amplification for multiplexed imaging of mRNA expression. *Nat Biotechnol* **28**, 1208-1212, doi:10.1038/nbt.1692 (2010).

83 Choi, H. M. *et al.* Mapping a multiplexed zoo of mRNA expression. *Development* **143**, 3632-3637, doi:10.1242/dev.140137 (2016).

84 Kazane, S. A. *et al.* Site-specific DNA-antibody conjugates for specific and sensitive immuno-PCR. *Proc Natl Acad Sci U S A* **109**, 3731-3736, doi:10.1073/pnas.1120682109 (2012).

85 Fluorescence in situ hybridization. *Nature Methods* **2**, 237, doi:10.1038/nmeth0305-237 (2005).

86 Matthiesen, S. H. & Hansen, C. M. Fast and non-toxic in situ hybridization without blocking of repetitive sequences. *PLoS One* **7**, e40675, doi:10.1371/journal.pone.0040675 (2012).

87 Kishi, J. Y., Schaus, T. E., Gopalkrishnan, N., Xuan, F. & Yin, P. Programmable autonomous synthesis of single-stranded DNA. *Nat Chem* **10**, 155-164, doi:10.1038/nchem.2872 (2018).

88 Slijkerman, R. W. *et al.* The pros and cons of vertebrate animal models for functional and therapeutic research on inherited retinal dystrophies. *Prog Retin Eye Res* **48**, 137-159, doi:10.1016/j.preteyeres.2015.04.004 (2015).

89 Speel, E. J., Hopman, A. H. & Komminoth, P. Amplification methods to increase the sensitivity of in situ hybridization: play card(s). *J Histochem Cytochem* **47**, 281-288, doi:10.1177/002215549904700302 (1999).

90 Garrigues, H. J., Rubinchikova, Y. E. & Rose, T. M. KSHV cell attachment sites revealed by ultra sensitive tyramide signal amplification (TSA) localize to membrane microdomains that are up-regulated on mitotic cells. *Virology* **452-453**, 75-85, doi:10.1016/j.virol.2014.01.006 (2014).

91 Bobrow, M. N., Harris, T. D., Shaughnessy, K. J. & Litt, G. J. Catalyzed reporter deposition, a novel method of signal amplification. Application to immunoassays. *J Immunol Methods* **125**, 279-285 (1989).

92 Clutter, M. R., Heffner, G. C., Krutzik, P. O., Sachen, K. L. & Nolan, G. P. Tyramide signal amplification for analysis of kinase activity by intracellular flow cytometry. *Cytometry A* **77**, 1020-1031, doi:10.1002/cyto.a.20970 (2010).

93 Bernstein, H. G. *et al.* Regional and cellular distribution of neural visinin-like protein immunoreactivities (VILIP-1 and VILIP-3) in human brain. *J Neurocytol* **28**, 655-662 (1999).

94 Haverkamp, S. & Wassle, H. Immunocytochemical analysis of the mouse retina. *J Comp Neurol* **424**, 1-23 (2000).

95 Sydor, A. M., Czymmek, K. J., Puchner, E. M. & Mennella, V. Super-Resolution Microscopy: From Single Molecules to Supramolecular Assemblies. *Trends Cell Biol* **25**, 730-748, doi:10.1016/j.tcb.2015.10.004 (2015).

96 Chen, F., Tillberg, P. W. & Boyden, E. S. Expansion microscopy. *Science* **347**, 543-548, doi:10.1126/science.1260088 (2015).

97 Chang, J. B. *et al.* Iterative expansion microscopy. *Nat Methods* **14**, 593-599, doi:10.1038/nmeth.4261 (2017).

98 Lin, R. *et al.* A hybridization-chain-reaction-based method for amplifying immunosignals. *Nat Methods* **15**, 275-278, doi:10.1038/nmeth.4611 (2018).

99 Ku, T. *et al.* Multiplexed and scalable super-resolution imaging of three-dimensional protein localization in size-adjustable tissues. *Nat Biotechnol* **34**, 973-981, doi:10.1038/nbt.3641 (2016).

100 Chen, F. *et al.* Nanoscale imaging of RNA with expansion microscopy. *Nat Methods* **13**, 679-684, doi:10.1038/nmeth.3899 (2016).

101 Kishi, J. Y. *et al.* in *BioRxiv* (2018).

102 Schindelin, J. *et al.* Fiji: an open-source platform for biological-image analysis. *Nat Methods* **9**, 676-682, doi:10.1038/nmeth.2019 (2012).

103 Regev, A. *et al.* The Human Cell Atlas. *eLife* **6**, doi:10.7554/eLife.27041 (2017).

104 HuBMAP. *The Human BioMolecular Atlas Program*, <<https://commonfund.nih.gov/hubmap>> (2018).

105 Lee, J. H. *et al.* Highly multiplexed subcellular RNA sequencing in situ. *Science* **343**, 1360-1363, doi:10.1126/science.1250212 (2014).

106 Chen, K. H., Boettiger, A. N., Moffitt, J. R., Wang, S. & Zhuang, X. RNA imaging. Spatially resolved, highly multiplexed RNA profiling in single cells. *Science* **348**, aaa6090, doi:10.1126/science.aaa6090 (2015).

107 Shah, S., Lubeck, E., Zhou, W. & Cai, L. In Situ Transcription Profiling of Single Cells Reveals Spatial Organization of Cells in the Mouse Hippocampus. *Neuron* **92**, 342-357, doi:10.1016/j.neuron.2016.10.001 (2016).

108 Wang, X. *et al.* Three-dimensional intact-tissue sequencing of single-cell transcriptional states. *Science* **361**, doi:10.1126/science.aat5691 (2018).

109 Rouhanifard, S. H. *et al.* ClampFISH detects individual nucleic acid molecules using click chemistry-based amplification. *Nat Biotechnol*, doi:10.1038/nbt.4286 (2018).

110 Gaspar, I. & Ephrussi, A. Strength in numbers: quantitative single-molecule RNA detection assays. *Wiley Interdiscip Rev Dev Biol* **4**, 135-150, doi:10.1002/wdev.170 (2015).

111 Goltsev, Y. *et al.* Deep profiling of mouse splenic architecture with CODEX multiplexed imaging. *Cell* **174**, 968-981. e915 (2018).

112 Schweller, R. M. *et al.* Multiplexed in situ immunofluorescence using dynamic DNA complexes. *Angewandte Chemie International Edition* **51**, 9292-9296 (2012).

113 Giedt, R. J. *et al.* Single-cell barcode analysis provides a rapid readout of cellular signaling pathways in clinical specimens. *Nature communications* **9**, 4550 (2018).

114 Stoeckius, M. *et al.* Simultaneous epitope and transcriptome measurement in single cells. *Nature methods* **14**, 865 (2017).

115 Peterson, V. M. *et al.* Multiplexed quantification of proteins and transcripts in single cells. *Nature biotechnology* **35**, 936 (2017).

116 Agasti, S. S., Liong, M., Peterson, V. M., Lee, H. & Weissleder, R. Photocleavable DNA barcode–antibody conjugates allow sensitive and multiplexed protein analysis in single cells. *Journal of the American Chemical Society* **134**, 18499-18502 (2012).

117 Horgan, R. P. & Kenny, L. C. 'Omic'technologies: genomics, transcriptomics, proteomics and metabolomics. *The Obstetrician & Gynaecologist* **13**, 189-195 (2011).

118 Ge, H., Walhout, A. & Vidal, M. Integrating 'omic' information: a bridge between genomics and systems biology. *Trends in Genetics* **19**, 551-560, doi:10.1016/j.tig.2003.08.009 (2003).

119 Crosetto, N., Bienko, M. & van Oudenaarden, A. Spatially resolved transcriptomics and beyond. *Nature reviews. Genetics* **16**, 57-66, doi:10.1038/nrg3832 (2015).

120 Wang, Y. & Navin, N. E. Advances and applications of single-cell sequencing technologies. *Molecular cell* **58**, 598-609, doi:10.1016/j.molcel.2015.05.005 (2015).

121 Church, G. M., Gao, Y. & Kosuri, S. Next-generation digital information storage in DNA. *Science (New York, N.Y.)* **337**, 1628, doi:10.1126/science.1226355 (2012).

122 Goldman, N. *et al.* Towards practical, high-capacity, low-maintenance information storage in synthesized DNA. *Nature* **494**, 77-80, doi:10.1038/nature11875 (2013).

123 Grass, R. N., Heckel, R., Puddu, M., Paunescu, D. & Stark, W. J. Robust chemical preservation of digital information on DNA in silica with error-correcting codes. *Angewandte Chemie (International ed. in English)* **54**, 2552-2555, doi:10.1002/anie.201411378 (2015).

124 Erlich, Y. & Zielinski, D. DNA Fountain enables a robust and efficient storage architecture. *Science (New York, N.Y.)* **355**, 950-954, doi:10.1126/science.aaj2038 (2017).

125 Shipman, S. L., Nivala, J., Macklis, J. D. & Church, G. M. CRISPR-Cas encoding of a digital movie into the genomes of a population of living bacteria. *Nature*, doi:10.1038/nature23017 (2017).

126 Shendure, J. *et al.* Accurate multiplex polony sequencing of an evolved bacterial genome. *Science (New York, N.Y.)* **309**, 1728-1732, doi:10.1126/science.1117389 (2005).

127 Lee, J. *et al.* Highly Multiplexed Subcellular RNA Sequencing in Situ. *Science* **343**, 1360-1363, doi:10.1126/science.1250212 (2014).

128 Lee, J. H. *et al.* Fluorescent in situ sequencing (FISSEQ) of RNA for gene expression profiling in intact cells and tissues. *Nature protocols* **10**, 442-458, doi:10.1038/nprot.2014.191 (2015).

129 Ke, R. *et al.* In situ sequencing for RNA analysis in preserved tissue and cells. *Nature Methods* **10**, 857-860, doi:10.1038/nmeth.2563 (2013).

130 Xiao, L. & Guo, J. Multiplexed single-cell in situ RNA analysis by reiterative hybridization. *Analytical Methods* **7**, 7290-7295 (2015).

131 Lubeck, E. & Cai, L. Single-cell systems biology by super-resolution imaging and combinatorial labeling. *Nat Methods* **9**, 743-748, doi:10.1038/nmeth.2069 (2012).

132 Lubeck, E., Coskun, A. F., Zhiyentayev, T., Ahmad, M. & Cai, L. Single-cell in situ RNA profiling by sequential hybridization. *Nat Methods* **11**, 360-361, doi:10.1038/nmeth.2892 (2014).

133 Chen, K., Boettiger, A. N., Moffitt, J. R., Wang, S. & Zhuang, X. Spatially resolved, highly multiplexed RNA profiling in single cells. *Science* **348**, doi:10.1126/science.aaa6090 (2015).

134 Coskun, A. F. & Cai, L. Dense transcript profiling in single cells by image correlation decoding. *Nat Methods* **13**, 657-660, doi:10.1038/nmeth.3895 (2016).

135 Moffitt, J. R. *et al.* High-performance multiplexed fluorescence in situ hybridization in culture and tissue with matrix imprinting and clearing. *Proceedings of the National Academy of Sciences of the United States of America* **113**, 14456-14461, doi:10.1073/pnas.1617699113 (2016).

136 Moffitt, J. R. *et al.* High-throughput single-cell gene-expression profiling with multiplexed error-robust fluorescence in situ hybridization. *Proceedings of the National Academy of Sciences of the United States of America* **113**, 11046-11051, doi:10.1073/pnas.1612826113 (2016).

137 Dirks, R. M. & Pierce, N. A. Triggered amplification by hybridization chain reaction. *Proceedings of the National Academy of Sciences of the United States of America* **101**, 15275-15278, doi:10.1073/pnas.0407024101 (2004).

138 Choi, H. M. *et al.* Programmable in situ amplification for multiplexed imaging of mRNA expression. *Nature biotechnology* **28**, 1208-1212, doi:10.1038/nbt.1692 (2010).

139 Choi, H. M., Beck, V. A. & Pierce, N. A. Next-generation in situ hybridization chain reaction: higher gain, lower cost, greater durability. *ACS nano* **8**, 4284-4294, doi:10.1021/nn405717p (2014).

140 Choi, H. M. *et al.* Mapping a multiplexed zoo of mRNA expression. *Development (Cambridge, England)* **143**, 3632-3637, doi:10.1242/dev.140137 (2016).

141 Shah, S. *et al.* Single-molecule RNA detection at depth by hybridization chain reaction and tissue hydrogel embedding and clearing. *Development (Cambridge, England)* **143**, 2862-2867, doi:10.1242/dev.138560 (2016).

142 Jungmann, R. *et al.* Multiplexed 3D cellular super-resolution imaging with DNA-PAINT and Exchange-PAINT. *Nat Methods* **11**, 313-318, doi:10.1038/nmeth.2835 (2014).

143 Schueder, F. *et al.* Universal Super-Resolution Multiplexing by DNA Exchange. *Angew Chem Int Ed Engl* **56**, 4052-4055, doi:10.1002/anie.201611729 (2017).

144 Wang, Y. *et al.* Rapid sequential in situ multiplexing with DNA-Exchange-Imaging. *bioRxiv*, 112227 (2017).

145 Schweller, R. M. *et al.* Multiplexed in situ immunofluorescence using dynamic DNA complexes. *Angewandte Chemie (International ed. in English)* **51**, 9292-9296, doi:10.1002/anie.201204304 (2012).

146 Marblestone, A. H. *et al.* Rosetta brains: a strategy for molecularly-annotated connectomics. *arXiv preprint arXiv:1404.5103* (2014).

147 Kebschull, J. M. *et al.* High-Throughput Mapping of Single-Neuron Projections by Sequencing of Barcoded RNA. *Neuron* **91**, 975-987, doi:10.1016/j.neuron.2016.07.036 (2016).

148 Peikon, I. D. *et al.* Using high-throughput barcode sequencing to efficiently map connectomes. *Nucleic acids research*, doi:10.1093/nar/gkx292 (2017).

149 Zhao, Y. *et al.* Nanoscale imaging of clinical specimens using pathology-optimized expansion microscopy. *Nat Biotechnol*, doi:10.1038/nbt.3892 (2017).

150 Tillberg, P. W. *et al.* Protein-retention expansion microscopy of cells and tissues labeled using standard fluorescent proteins and antibodies. *Nat Biotechnol* **34**, 987-992, doi:10.1038/nbt.3625 (2016).

151 Baker, M. Statisticians issue warning over misuse of P values. *Nature* **531**, 151, doi:10.1038/nature.2016.19503 (2016).

152 Nuzzo, R. Scientific method: statistical errors. *Nature* **506**, 150-152, doi:10.1038/506150a (2014).